



UNIVERSITY OF PRISTINA-FACULTY OF SCIENCES  
KOSOVSKA MITROVICA-REPUBLIC OF SERBIA

THE  
UNIVERSITY  
THOUGHT  
PUBLICATION IN NATURAL SCIENCES

**VOL. 8, N° 1, 2018.**

---

**ISSN 1450-7226 (Print)**

**ISSN 2560-3094 (Online)**

# **UNIVERSITY THOUGHT-PUBLICATION IN NATURAL SCIENCES**

## **Published by**

**University of Pristina-Faculty of Sciences**

**Kosovska Mitrovica-Republic of Serbia**

## **Aims and Scope**

The University Thought - Publication in Natural Sciences (Univ. thought, Publ. nat. sci.) is a scientific journal founded in 1994. by the University of Priština, and was published semi annually until 1998.

Today, the University Thought - Publication in Natural Sciences is an international, peer reviewed, Open Access journal, published semi annually in the online and print version by the University of Priština, temporarily settled in Kosovska Mitrovica, Serbia. The Journal publishes articles on all aspects of research in Biology, Chemistry, Geography, Information technologies, Mathematics and Physics in the form of original papers, short communications and reviews (invited) by authors from the country and abroad.

The University Thought - Publication in Natural Sciences serves as an interdisciplinary forum covering a wide range of topics for a truly international audience. Journal is endeavor of the University of Priština to acquaint the scientific world with its achievements and wish to affirm the intellectual potential and natural resources of own region. Our aim is to put forward attitude of principle that science is universal and we invite all scientists to cooperate wherever their scope of research may be. We are convinced that shall contribute to do victory of science over barriers of all kinds erected throughout the Balkans.

## **Directors**

Rade B. Grbić and Nebojša V. Živić

## **Editor in Chief**

Nebojša V. Živić

## **Deputy Editor in Chief**

Vidoslav S. Dekić

## **Associate Editors**

Ljubiša Kočinac; Ranko Simonović; Stefan Panić; Branko Drljača; Aleksandar Valjarević

## **Editorial Board**

Gordan Karaman, Montenegro; Gerhard Tarmann, Austria; Predrag Jakšić, Serbia; Slavica Petović, Montenegro; Momir Paunović, Serbia; Bojan Mitić, Serbia; Stevo Najman, Serbia; Zorica Svirčev, Serbia; Ranko Simonović, Serbia; Miloš Đuran, Serbia; Radosav Palić, Serbia; Snežana Mitić, Serbia; Slobodan Marković, Serbia; Milan Dimitrijević, Serbia; Sylvie Sahal-Brechot, France; Milivoj Gavrilov, Serbia; Jelena Golijanin, Bosnia and Herzegovina; Dragoljub Sekulović, Serbia; Dragica Živković, Serbia; Stefan Panić, Serbia; Petros Bithas, Greece; Zoran Hadzi-Velkov, R. Macedonia; Ivo Kostić, Montenegro; Petar Spalević, Serbia; Marko Petković, Serbia; Milan Simić, Australia; Darius Andriukaitis, Lithuania; Marko Beko, Portugal; Milcho Tsvetkov, Bulgaria; Gradimir Milovanovic, Serbia; Ljubiša Kočinac, Serbia; Ekrem Savas, Turkey; Zoran Ognjanović, Serbia; Donco Dimovski, R. Macedonia; Nikita Šekutkovski, R. Macedonia; Leonid Chubarov, Russian Federation; Žarko Pavićević, Montenegro; Miloš Arsenović, Serbia; Svetislav Savović, Serbia; Slavoljub Mijović, Montenegro; Saša Kočinac, Serbia

## **Technical Secretary**

Danijel B. Došić

## **Editorial Office**

Ive Lola Ribara 29; 38220, Kosovska Mitrovica, Serbia, e-mail: editor.utnsjournal@pr.ac.rs, office.utnsjournal@pr.ac.rs, office.utnsjournal@gmail.com; fax: +381 28 425 397

## **Available Online**

This journal is available online. Please visit <http://www.utnsjournal.pr.ac.rs> or <http://www.utnsjournal.com> to search and download published articles.

# UNIVERSITY THOUGHT-PUBLICATION IN NATURAL SCIENCES

Vol. 8, N° 1, 2018.

## CONTENTS

### BIOLOGY

Miroslav Nikolić

HUMIRON® IS AN EFFECTIVE BIODEGRADABLE SOURCE OF CHELATED IRON FOR PLANTS: AN IRON-59 UPTAKE STUDY ..... 1

Tatjana R. Jakšić, Predrag S. Vasić, Nenad Đ. Labus, Olivera M. Papović, Miloš R. Stanojević, Nikola N. Đukić  
THE SPRINGTAILS (INSECTA: COLLEMBOLA) FAUNA AT DIFFERENT MICROHABITATS OF BEČIĆI BEACH, MONTENEGRO ..... 5

Danijela Prodanović, Zoran Krivošej, Miloš Stanojević, Slavica Ćirić

SUPPLEMENT TO THE PHYTOGEOGRAPHICAL STUDIES OF THE RARE AND INTERNATIONALLY SIGNIFICANT SPECIES IN THE FLORA OF SERBIA, KOSOVO AND METOHIJA NORTH..... 10

### CHEMISTRY

Dragana Sejmanović, Ružica Micić, Ranko Simonović

KINETIC-CATALYTIC DETERMINATION OF ULTRAMICRO AMOUNTS OF Co(II) USING 4-HYDROXYCOUMARINE-PERMANGANATE REDOX REACTION ..... 17

Dragoslav Ilić

STATISTICAL ANALYSIS OF THE PRODUCTION OF BLUESTONE FROM GRANULATES (ELEMENTARY COPPER) BY OXIDATION WITH HYDROGEN PEROXIDE MIXED WITH STOCK SOLUTION OF BLUESTONE AND SULFURIC ACID ..... 22

### GEOGRAPHY, GEOSCIENCE AND ASTRONOMY

Jovo Medojević

CULTURAL-GEOGRAPHIC DETERMINANTS OF JERUSALEM ..... 30

Saša Milosavljević

CONTEMPORARY MIGRATORY MOVEMENTS IN THE MUNICIPALITY OF TRSTENIK ..... 34

### MATHEMATICS, COMPUTER SCIENCE AND MECHANICS

Vladica Stojanović, Tijana Kevkić

HOMOTOPY PERTURBATIONS METHOD: THEORETICAL ASPECTS & APPLICATIONS ..... 40

Marija S. Najdanović, Ljubica S. Velimirović

INFINITESIMAL BENDING OF CURVES ON THE RULED SURFACES ..... 46

### PHYSICS

Ljiljana Gulan

TEMPORAL AND SPATIAL VARIATIONS OF AMBIENT DOSE EQUIVALENT RATE IN URBAN AND RURAL SITES ..... 52

Dragana D. Milosavljević

INFLUENCE OF METEOROLOGICAL PARAMETERS ON THE OPERATION OF A GRID - CONNECTED PV SOLAR PLANT ..... 56

# HUMIRON® IS AN EFFECTIVE BIODEGRADABLE SOURCE OF CHELATED IRON FOR PLANTS: AN IRON-59 UPTAKE STUDY

MIROSLAV NIKOLIĆ<sup>1\*</sup>

<sup>1</sup>Institute for Multidisciplinary Research, University of Belgrade, Belgrade, Serbia

## ABSTRACT

Here we tested plants' ability to use iron (Fe) from the water-soluble commercial product Humiron® (a complex of Fe with highly purified and solubilized humic acids extracted from leonardite) as a source of chelated Fe for both strategy 1 (e.g. cucumber) and strategy 2 (e.g. barley) plant species grown under low Fe conditions. Iron from radioactive <sup>59</sup>Fe-labelled Humiron® can easily be acquired by strategy 1 plant species via reduction of Fe<sup>III</sup> by the inducible plasma membrane-bound reductase, similarly to the reduction of synthetic Fe<sup>III</sup>-chelates. Strategy 2 plant species can also efficiently utilize Fe from Humiron® via ligand exchange between humates and phytosiderophores (PS). Moreover, the efficacy of Humiron® is comparable to Fe complexed with water-extractable humic substances obtained from peat. Being easily biodegradable this product can be used as an effective Fe source for organic crop production.

**Keywords:** Barley, Chlorosis, Cucumber, Humate Complex, Iron Root-acquisition Strategies, Transport.

## INTRODUCTION

Even though the fourth most abundant mineral element in the Earth's crust, iron (Fe) in soils occurs mostly in the insoluble Fe<sup>III</sup> forms which are unavailable to plants. The concentrations of available Fe from the Fe chelated compounds (e.g. Fe humates) in most well-aerated soils are often lower than required for an adequate plant growth, especially at neutral and alkaline soil pH (Römheld & Nikolic, 2006). According to Römheld & Marschner (1994), higher plants respond to a lack of Fe by developing two different strategies. Dicots and nongraminaceous monocots employ the strategy 1 response on low soluble Fe in the rhizosphere by: 1) release more protons, thereby decrease rhizosphere pH and increase Fe solubility (*AHA1* genes coding for a plasma membrane H<sup>+</sup>-ATPase), and 2) induction of plasma membrane-bound Fe<sup>III</sup>-chelate reductase (encoded by *FRO* genes), which is followed by the uptake of Fe<sup>2+</sup> via an inducible IRT1 transporter. Strategy 2 plants, which include all grasses (Poaceae), release low-molecular-weight compounds, so-called phytosiderophores (PS) that chelate Fe<sup>3+</sup> ions, and take up the Fe<sup>III</sup>-PS complex via the root YS1 transporters (for review see Nikolic & Pavlovic, 2018).

The use of various commercial synthetic Fe-chelates, i.e. Fe complexed with ethylenediaminetetraacetate (EDTA) or ethylenediamine-di-o-hydroxyphenylacetate (EDDHA), as soil amendment is a frequent measure for remedy of Fe deficiency chlorosis in agricultural practice (Römheld & Nikolic, 2006). However, their costs and the environmental risk of leaching and groundwater pollution by heavy metals may limit the interest for these products, particularly in sustainable agriculture. On the other hand limited number of organic acidic

anions (e.g. citrate and malate) are able to form stable complexes with Fe<sup>III</sup>, which are however highly degradable by soil microbes and/or also photo labile (Cesco et al., 2002; Römheld & Nikolic, 2006). Some naturally occurring Fe-chelates in soils, such as Fe chelated to the microbial siderophores (e.g. Fe<sup>III</sup>-dihydroxamate; Hördt et al., 2000) as well as humic substances, could be an alternative to synthetic Fe-chelates. It has been demonstrated that the roots of both strategy 1 and strategy 2 plants can utilize Fe bound to the water-extractable humic substances (WEHS; e.g. Pinton et al., 1999; Cesco et al., 2002).

In this work we tested plants' ability to use Fe from the water-soluble commercial product Humiron® as a source of chelated Fe for both the strategy 1 and the strategy 2 plant species. Thus, the major objective was to study the possible mechanisms involved in utilization of Fe from the radioactive <sup>59</sup>Fe-labelled Fe-humate product in Humiron®, by cucumber (strategy 1) and barley (strategy 2) plants subjected to nutrient solution model experiments.

## MATERIALS AND METHODS

Humiron® (kindly provided by HUMINTECH GmbH, Düsseldorf, Germany) is a complex of Fe with highly purified and solubilized humic acids extracted from leonardite (an oxidized form of lignite, a byproduct of coal mining).

The experiments were carried out according to the methodology previously described by Cesco et al. (2002). After germination in quartz sand moistened with saturated CaSO<sub>4</sub>, cucumber (*Cucumis sativus* L., cv. Chinese long) and barley (*Hordeum vulgare* L., cv. Europa) seedling were transferred to the complete nutrient solutions as reported by Cesco et al. (2002), either without (–Fe) or with (+Fe) 50 µM Fe-EDTA. The nutrient solutions were renewed completely every 3 d and continuously aerated. Plants were grown for 7 d under controlled

\* Corresponding author: mnikolic@imsi.bg.ac.rs

environmental conditions in a growth chamber with light/dark regime of 16/8 h, temperature regime of 24/20°C, photon flux density of approximately 300  $\mu\text{mol}^{-2} \text{s}^{-1}$  at plant height and relative humidity of about 70%.

Determination of  $\text{Fe}^{\text{III}}$  reduction capacity by intact cucumber roots was carried out in an assay solution containing 0.5 mM  $\text{CaSO}_4$ , 1  $\mu\text{M}$  Fe (supplied as either Fe-EDTA or Humiron®), 200  $\mu\text{M}$  bathophenanthrolinedisulfonate (BPDS), and 10 mM Mes/NaOH (pH 6.0) or 10 mM Hepes/NaOH (pH 7.8) for 30 min in darkness. Reduction rates were determined as a formed red  $\text{Fe}^{\text{II}}$ (BPDS)<sub>3</sub> complex by measuring absorbance at 535 nm against blanks (without roots) and using an extinction coefficient of 22.14  $\text{mM}^{-1} \text{cm}^{-1}$  for calculation (Nikolic et al., 2007).

In  $^{59}\text{Fe}$  uptake experiments, Fe-chelates were labelled by mixing  $^{59}\text{FeCl}_3$  with either Humiron® or Fe-EDDHA (specific radioactivity 0.2  $\mu\text{Ci } \mu\text{mol}^{-1}$  Fe) following the procedure previously described by Nikolic et al. (2000). The final concentration of Fe in the uptake solutions was 1  $\mu\text{M}$ . For cucumber plants the  $^{59}\text{Fe}$ -labelled uptake solution was buffered at pH 6.0 with 10 mM Mes/NaOH or at pH 7.8 with 10 mM Hepes/NaOH, and the uptake period was 6 h. For barley plants, the uptake lasted 4 h and was performed in the morning (period of high PS release; 2 h after onset of light) or in the evening (period of low PS release; 12 h after onset of light). Additionally, 2'-deoxymugineic acid (DMA) collected from the exudates of Fe-deficient barley roots and purified following the method of Awad et al. (1988) was added in the uptake solution at final concentration of 20  $\mu\text{M}$  during evening experiment.

After the uptake periods, the plants were transferred to a freshly prepared  $^{59}\text{Fe}$ -free nutrient solution for 10 min and then harvested. The extraplasmatic  $^{59}\text{Fe}$  pool was removed by reductive incubation of roots with 1.5 mM bipyridyl and 7.5 mM sodium dithionite (Bienfait et al., 1985; Cesco et al., 2002). Roots and shoots were oven-dried at 80°C, weighed, ashed at 550°C, and suspended in 1% (w/v) HCl for  $^{59}\text{Fe}$  determination by a liquid scintillation counting.

## RESULTS AND DISCUSSION

Preculture of cucumber plants in Fe-free nutrient solution for 7 days induced  $\text{Fe}^{\text{III}}$  reductase activity in the roots for both Fe chelates (i.e. Fe-EDTA and Humiron®), which was 4-5 times higher compared to the plants grown in nutrient solution adequately supplied with Fe (Fig. 1). The root reduction capacity for Humiron® was about 20% lower than that measured for Fe-EDTA as a substrate. It has been shown that  $\text{Fe}^{\text{III}}$  complexed with WEHS can easily be reduced at the plasma membrane of both root and leaf cells (Cesco et al., 2000, 2002; Nikolic et al., 2003). Exposure of -Fe roots to high pH of the root medium decreased the  $\text{Fe}^{\text{III}}$  reduction capacity for both Fe chelates by 3-4 times as compared to the roots at low pH. The measured

reduction rates were comparable to +Fe roots at pH 6.0. These findings undoubtedly confirm that Humiron® is a suitable  $\text{Fe}^{\text{III}}$  chelate substrate for  $\text{Fe}^{\text{III}}$  reduction via a plasma membrane-associated low-Fe-inducible  $\text{Fe}^{\text{III}}$  reductase.

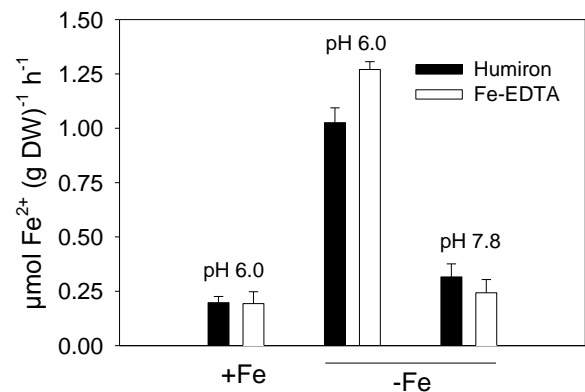


**Figure 1.**  $\text{Fe}^{\text{III}}$ -chelate reduction capacity of cucumber roots for Humiron® ( $\text{Fe}^{\text{III}}$ -humate complex) and  $\text{Fe}^{\text{III}}$ -EDTA (control) as affected by rhizosphere pH and Fe nutritional status.

Both high root pH (7.8) and addition of BPDS (strong  $\text{Fe}^{2+}$  scavenger) inhibited Fe uptake and root-to-shoot translocation of Fe from  $^{59}\text{Fe}$ -labelled Humiron® in -Fe cucumber plants (Fig. 2), indicating that the preceding  $\text{Fe}^{\text{III}}$  reduction of Humiron® (see Fig. 1) was a necessary step for the uptake of  $\text{Fe}^{2+}$  by Fe deprived roots. On the other hand, significantly less  $^{59}\text{Fe}$  was taken up by roots and thereby translocated to shoots of +Fe plants. Uptake and translocation of  $^{59}\text{Fe}$  from Humiron® did not differ in principle from that of Fe-EDDHA complex (Fig. 2). Utilization of  $^{59}\text{Fe}$  from  $^{59}\text{Fe}$ -labelled Humiron® was strongly enhanced by a low pH of the root external solution, the conditions conducive for enhanced reduction of  $\text{Fe}^{\text{III}}$ -chelates and thereby root uptake of this micronutrient (Römheld and Marschner, 1994). However, the uptake and especially translocation rates were significantly higher for  $^{59}\text{Fe}$ -EDDHA, while the extraplasmatic Fe was found to be about 3-4 times higher in the roots exposed to  $^{59}\text{Fe}$ -humate, indicating higher precipitation of Fe from Humiron® in the root apoplast (Fig. 3). This is in accordance with data of Cesco et al. (2002), which showed a large pool of extraplasmatic Fe formed in cucumber roots after supplying Fe-WEHS complex. Their study also demonstrated that cucumber plants were able to mobilize extraplasmatic  $^{59}\text{Fe}$  precipitated after roots being incubated in Fe-WEHS supplied nutrient solution. Remobilization of extraplasmatic Fe was particularly evident at acidic condition (Bienfait et al., 1985; Zhang et al., 1991; Strasser et al., 1999). Hence, this extraplasmatic Fe pool can act as a good buffer for available Fe in the rhizosphere which, depending of the capacity of strategy 1 plant species to acidify rhizosphere, allows the mobilization and translocation to the shoot of considerable amounts of apoplastic Fe.

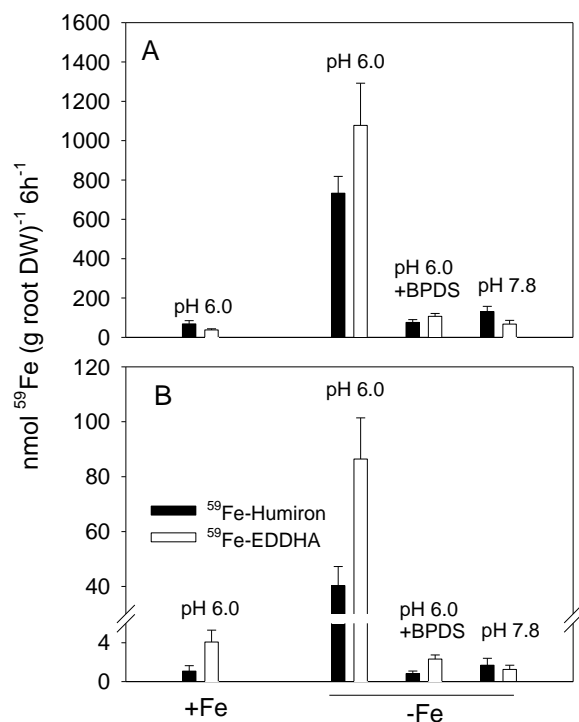


**Figure 2.** Root uptake (A) and root-to-shoot translocation (B) of  $^{59}\text{Fe}$  in Fe-sufficient (+Fe) and Fe-deficient (-Fe) cucumber plants (strategy 1) after 6-h-exposure to  $^{59}\text{Fe}$ -labelled Humiron® and  $^{59}\text{Fe}$ -EDDHA (control). Translocation rate was calculated as a sum of root and shoot Fe content divided by the root DW.

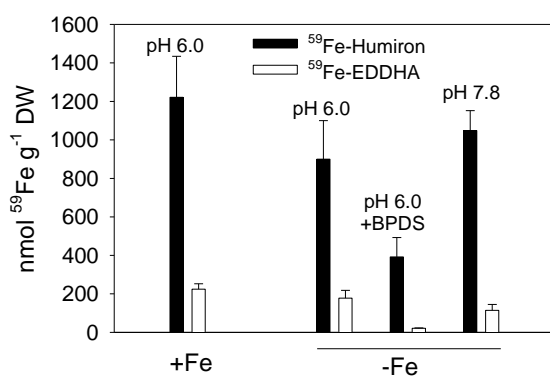


**Figure 3.** The concentration of extraplasmatic Fe of Fe-sufficient (+Fe) and Fe-deficient (-Fe) cucumber roots after 6-h-exposure to  $^{59}\text{Fe}$ -labelled Humiron® and  $^{59}\text{Fe}$ -EDDHA (control).

It is well known that the release of PS shows a diurnal rhythm with a morning maximum and an evening minimum. During the morning experiment barley plants precultured in -Fe nutrient solution took up about 4 times more Fe from  $^{59}\text{Fe}$ -labelled Humiron® as compared either with +Fe plants (morning experiment) or with -Fe plants (evening experiment) (Fig. 4A). About 40% of the total Fe taken up by the roots from Humiron® was translocated to the shoots during 4 hours (Fig. 4B). Addition of deoxymugineic acid (DMA) in the uptake solution at final

concentration of 20  $\mu\text{M}$  during the evening experiment, increased both uptake and translocation rates of  $^{59}\text{Fe}$  in -Fe plants approaching the levels recorded in the morning experiment (Fig. 4). Addition of DMA also significantly increased  $^{59}\text{Fe}$  uptake and translocation by +Fe plants. Root extraplasmatic Fe in barley (not shown) was found to be about 2 times higher in the conditions with a lack of PS release (evening experiment) than in the uptake solution with high PS concentration (morning experiment or addition of 20  $\mu\text{M}$  DMA in the evening).

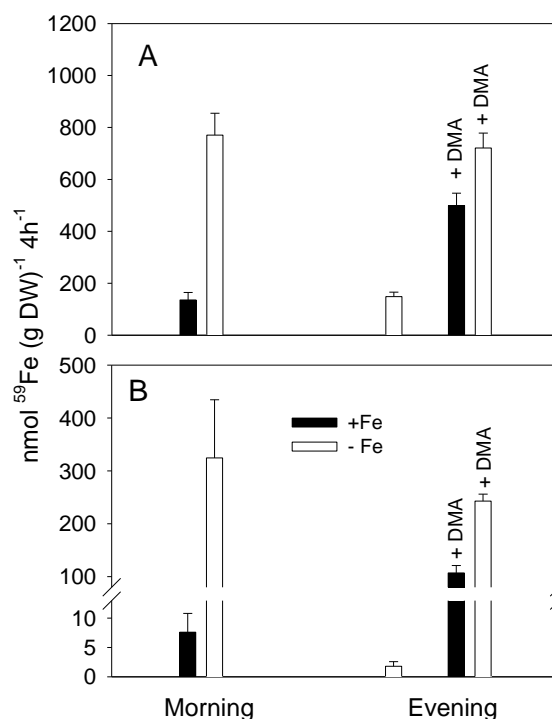


**Figure 4.** Root uptake (A) and root-to-shoot translocation (B) of  $^{59}\text{Fe}$  in Fe-sufficient (+Fe) and Fe-deficient (-Fe) barley plants (strategy 2) after 4-h-exposure to  $^{59}\text{Fe}$ -labelled Humiron®. To prevent latent Fe deficiency plants were sprayed with 0.3% (w/v) Fe-citrate twice daily. DMA was added to the uptake solution at the final concentration of 20  $\mu\text{M}$ . Morning, period of high root PS release; evening, period of low root PS release. Translocation rate was calculated as a sum of root and shoot Fe content divided by the root DW.

## CONCLUSION

Iron from Humiron® can easily be acquired by strategy 1 plant species (e.g. cucumber) via the reduction of  $\text{Fe}^{\text{III}}$ -humates by the inducible plasma membrane-bound reductase, similarly to Fe acquisition from synthetic  $\text{Fe}^{\text{III}}$  chelates such as Fe-EDTA or Fe-EDDHA. Strategy 2 plant species (e.g. barley) can also efficiently utilize Fe from Humiron® via ligand exchange between humates and PS released under Fe deficiency. Thus, utilization of Fe from Humiron® is comparable to the utilization

of Fe bound to water-extractable humic substances (extracted from peat) as has previously been reported by Cesco et al. (2002). There is a high potential for application of natural-based Fe-chelates such as Humiron® in organic crop production, as these chelates are more biodegradable than the synthetic ones, and therefore environmentally benign.

## REFERENCES

- Awad, F., Römheld, V., & Marschner, H. 1988. Mobilization of ferric iron from a calcareous soil by plant-borne chelators (Phytosiderophores). *Journal of Plant Nutrition*, 11(6-11), pp. 701-713. doi:10.1080/01904168809363835
- Bienfait, H.F., van den Briel, W., & Mesland-Mul, N.T. 1985. Free Space Iron Pools in Roots: Generation and Mobilization. *Plant Physiology*, 78(3), pp. 596-600. doi:10.1104/pp.78.3.596
- Cesco, S., Römheld, V., Varanini, Z., & Pinton, R. 2000. Solubilization of iron by water-extractable humic substances. *Journal of Plant Nutrition and Soil Science*, 163(3), pp. 285-290. doi:10.1002/1522-2624(200006)163:3<285::aid-jpln285>3.0.co;2-z
- Cesco, S., Nikolic, M., Römheld, V., Varanini, Z., & Pinton, R. 2002. Uptake of <sup>59</sup>Fe from soluble <sup>59</sup>Fe-humate complexes by cucumber and barley plants. *Plant and Soil*, 241(1), pp. 121-128. doi:10.1023/a:1016061003397
- Hördt, W., Römheld, V., & Winkelmann, G. 2000. Fusarinines and dimerum acid, mono- and dihydroxamate siderophores from *Penicillium chrysogenum*, improve iron utilization by strategy I and strategy II plants. *BioMetals*, 13, 37-46.
- Marschner, H., & Römheld, V. 1994. Strategies of plants for acquisition of iron. *Plant and Soil*, 165(2), pp. 261-274. doi:10.1007/bf00008069
- Nikolic, M., Cesco, S., Römheld, V., Varanini, Z., & Pinton, R. 2003. Uptake of Iron (<sup>59</sup>Fe) complexed to water-extractable humic substances by sunflower leaves. *Journal of Plant Nutrition*, 26(10-11), pp. 2243-2252. doi:10.1081/pln-120024278
- Nikolic, M., Cesco, S., Römheld, V., Varanini, Z., & Pinton, R. 2007. Short-term interactions between nitrate and iron nutrition in cucumber. *Functional Plant Biology*, 34(5), pp. 402-408. doi:10.1071/fp07022
- Nikolic, M., & Pavlovic, J. 2018. Plant responses to iron deficiency and toxicity and iron use efficiency in plants. In A.M. Hossain et al. Eds., *Plant Micronutrient Use Efficiency: Molecular and Genomic Perspectives in Crop Plants*, pp. 55-69. San Diego: Academic Press.
- Pinton, R., Cesco, S., Santi, S., Agnoloni, F., & Varanini, Z. 1999. Water extractable humic substances enhance iron deficiency responses to Fe-deficient cucumber plants. *Plant and Soil*, 210(2), pp. 145-157. doi:10.1023/a:1004329513498
- Römheld, V., & Nikolic, M. 2006. Iron. In A. Barker & D. Pilbeam Eds., *Handbook of Plant Nutrition*. Boca Raton: CRC Press., pp. 329-350. doi:10.1201/9781420014877.ch11
- Strasser, O., Köhl, K., & Römheld, V. 1999. Overestimation of apoplastic Fe in roots of soil grown plants. *Plant and Soil*, 210(2), pp. 179-189. doi:10.1023/a:1004650506592
- Zhang, F.S., Romheld, V., & Marschner, H. 1991. Role of the root apoplasm for iron acquisition by wheat plants. *Plant Physiology*, 97(4), pp. 1302-1305. doi:10.1104/pp.97.4.1302

# THE SPRINGTAILS (INSECTA: COLLEMBOLA) FAUNA AT DIFFERENT MICROHABITATS OF BEČIĆI BEACH, MONTENEGRO

TATJANA R. JAKŠIĆ<sup>1\*</sup>, PREDRAG S. VASIĆ<sup>1</sup>, NENAD Đ. LABUS<sup>1</sup>, OLIVERA M. PAPOVIĆ<sup>1</sup>, MILOŠ R. STANOJEVIĆ<sup>1</sup>, NIKOLA N. ĐUKIĆ<sup>1</sup>

<sup>1</sup>Faculty of Sciences and Mathematics, University of Pristina, Kosovska Mitrovica, Serbia

## ABSTRACT

Collembola fauna has been investigated at different microhabitats near the beach in Bečići, Montenegro. Samples were collected from four locations: Hotel "Tara", "Sveti Toma" Church (St. Thomas), Hotel "Naftagas" and "Zelena Stena" (Green Rock). Each of the location presented different microhabitat: under the palm tree, cypresses tree, larch tree and white pine tree. Samples were taken in May and September 2015 and results presented as qualitative findings.

Total number of 30 Collembola species was identified, classified into six families and 17 genera. Representatives of the family Hypogastruridae and Isotomidae were recorded at all of the studied sites, while representatives of the families: Naenuridae, Onychiuridae, Entomobryidae and Sminthuridae were present on some of locations.

The biggest number of species and the highest Collembola population density was found at the Green Stone site, 24 species in total, microhabitat- white pine, and the smallest number of species, 6 on site "St. Thomas" Church, microhabitat- cypresses trees.

**Keywords:** Collembola, microhabitats, Bečići Beach, Montenegro.

## INTRODUCTION

Springtails (Insecta: Collembola) communities have been shown to vary in abundance and species composition according to changes in vegetation and soil conditions (Hågvar, 1982; Ponge, 1993; Chagnon et al., 2000). Soil acidity, mainly through associated changes in food and habitat, but also through chemical composition or osmolarity of the soil solution may favor or disfavor some species (Hågvar & Abrahamsen, 1984; Vilkamaa & Huhta, 1986; Salmon & Ponge, 2002), and pH 5 has been noted as a landmark between two distinct types of communities (Ponge, 1993). The opposition between grassland and woodland can also be traced by the species composition of springtails population (Gisin, 1943; Rusek, 1989; Ponge, 1993). As a whole, Collembola are highly tolerant to a wide range of environmental conditions, including agricultural and industrial pollution, but species differ in their sensitivity to environmental stress (Lebrun, 1976; Prasse, 1985; Sterzyńska, 1990).

The springtails biodiversity in Montenegro is poorly investigated. Till now the Collembola fauna was studied in the surrounding area of fishing village Bigova, on the south coast of Trašte Bay. A total number of 16 Collembola species was noted classified in 5 families and 11 genera (Bogojević, 1978).

Collembolan fauna of Yugoslavia (Serbia and Montenegro) is a rich and diverse; total number of 233 species is known in Serbia. They are classified in 43 genera and 5 families. 89 species were recorded. In Montenegro classified in 10 genera and

7 families. 28 species and subspecies are endemic for Serbia (12,02%) and 11 for Montenegro (12,36%). Most of the endemic and relict forms live in caves, but some of them inhabits forests and cultivated steppe. Two centers of endemic Collembola differentiations are recognized in Yugoslavia: northern and eastern part (eastern Serbia) and the second one in the south and west (Montenegro, western and south-western Serbia) (Ćurčić & Lučić, 1997). According to Ćurčić et al., (2008), 8 springtails cave species have been recorded in Montenegro.

The aim of this study is to identify and evaluate collembolan fauna in selected microhabitat that are situated near the Bečići Beach and mostly under influence of human activities.

## MATERIAL AND METHODS

The collembolan specimens considered herein were collected in the region of Bečići Beach (Figure 1), Montenegro from four different microhabitats.

Samples were taken from four locations: Hotel "Tara", Church "Sveti Toma" (St. Thomas), Hotel "Naftagas" and "Zelena Stena" (Green Rock) and from four different microhabitats. On the first site, sampling was done under the palm tree (*Phoenix canariensis* Chabaud). This site is under the firm influence of human activities. These include regular grass cutting, watering and probably occasional fertilization. On the second site samples were taken under the cypresses tree (*Cupressus sempervirens* L.). This sampling spot is facing south and exposed to the direct sun influence. On the third site, samples were taken from two microhabitats: under the larch tree (*Larix decidua* Mill.) and white pine (*Pinus sylvestris* L.) and on

\* Corresponding author: tatjana.jaksic@pr.ac.rs

the fourth site under the white pine tree pine (*Pinus sylvestris* L.). Samples were taken in May, during the rainy season and September 2015, after the drought season for each location, and results were presented as qualitative findings.



**Figure 1.** Bečići Beach with studied sites: 1. Hotel "Tara", 2. "St. Thomas" Church, 3. Hotel "Naftagas", 4. Green Stone.

Total number of 8 samples was collected. The soil samples, all together with leaf-litter was dimension 10X10X 10cm. Soil animals were separated using modified Berlese-Tullgren funnel. Collembola specimens were separated and preserved in 75% ethyl-alcohol with few drops of glycerin. The slides were mounted in DPX. It was studied using KRÜSS MML 1204 (400X magnification) and TENSION EUMC 1600 (1000X magnification) microscopes. Identification was done using following dichotomous keys: Gisin (1960), Stach (1956), Stach (1960), Stach (1963) and Bellinger et al., (2015) Checklist of the Collembola of the world. Available from <http://www.collembola.org>.

Specimens at the present are deposited in the collection of the Faculty of Sciences and Mathematics, University of Priština with settlement in Kosovska Mitrovica.

## RESULTS AND DISCUSSION

Total number of 30 species of Collembola were identified, classified into six families and 17 genera at all of four investigated sites. (Table 1).

### Site 1- „Tara“ Hotel

Site is situated nearby, Tara“ Hotel in Boreti, coordinates N: 42.282628, E: 18.863026. The microhabitat investigated here was the area surrounding the palm tree *Phoenix canariensis*. This site is under the firm influence of human activities with shallow and hard soil with little litter. These include regular grass cutting, watering and probably occasional fertilization. Beside several species of mites and spiders, we have identified 11 Collembola species: *Neanura muscorum* MacGillivray, 1893, *Bilobella mahunkai* Danyi, 2010, *Anurida maritima* Guérin-Méneville, 1836, *Hypogastrura viatica* Tullberg, 1872, *H. distincta* Axelson, 1902, *Onychiurus sp.*, *Isotomurus alticolus* Handschin, 1919, *Isotomurus*

*italicus* Carapelli, A., Frati, F., Fanciulli, P.P. et Dallai, R., 1995, *I. stuxbergi* Tullberg, 1877, *Isotoma riparia* Nicolet, 1842, and *Entomobrya multifasciata* Tullberg, 1821. The abundance of the collembolan community was very low. A total of 38 collembolan individuals were counted in both samples with the dominance of *Isotomurus* genera.

Mites and spiders were abundant in the sample, and few insects' larvae were present.

### Site 2- "St. Thomas" Church

Site 2 was chosen as specific place with cypresses trees community, coordinates: N: 42.281302, E: 18.870366. There is no significant human activities in the sense of grass cutting, watering, fertilization, etc.. The sampling spot is facing south and thus exposed to the direct sun influence and very close to the beach itself. The halophyte-psammophyte vegetation was present and typical foredune zone. Total number of 6 springtails species was identified: *Hypogastrura viatica* Tullberg, 1872, *H. distincta* Axelson, 1902, *H. purpurescens* Lubbock, 1870, *Onychiurus sp.*, *Isotomurus alticolus* Handschin, 1919 and *Sminthurus hispanicus* Nayrolles, 1995. Collembolan community was abundant, with the highest diversity, richness and equitability of species from *Hypogastrura* family that is in compliance with Fernandes et al., (2009) for foredune zone.

There were very few mites and spiders present in the sample. One representative of Scorpiones order and one of Pseudoscorpiones order were present. *Polyxenus lagurus* L., 1758 (Diplopoda) has also been identified in this sample.

### Site 3- "Naftagas" Hotel

Site 3 is located nearby "Naftagas" Hotel in Bečići, coordinates: N: 42.282234, E: 18.874273. Two different microhabitats were investigated at this site: under the larch tree and white pine tree. The larch tree microhabitat was similar to the site 1 and 7 collembolan species were common for these two sites (Table 1). The soil was hard with little litter. 9 collembolan species have been identified at this spot: *Hypogastrura viatica* Tullberg, 1872, *H. purpurescens* Lubbock, 1870,, *Isotomurus alticolus* Handschin, 1919, *I. fucicolus* Axelson, 1906, *I. italicus* Carapelli, A., Frati, F., Fanciulli, P.P. et Dallai, R., 1995, *I. stuxbergi* Tullberg, 1877, *Folsomia quadrioculata* Tullberg, 1871, *Entomobrya multifasciata* Tullberg, 1821 and *Cyphoderus bidenticulatus* Börner, 1903 with the dominance of species from *Isotomurus* genera. From the same site, but second microhabitat-under the white pine tree, similar to the "Green Stone" site, but not so close to the beach, 12 collembolan species have been identified: *Neanura muscorum* MacGillivray, 1893, *Pseudachorutes parvulus* Börner, 1901, *Hypogastrura viatica* Tullberg, 1872,, *H. distincta* Axelson, 1902,, *H. purpurescens* Lubbock, 1870 , *Onychiurus sp.*, *Isotomurus alticolus* Handschin, 1919, *I. fucicolus* Axelson, 1906, *I. italicus* Carapelli, A., Frati, F., Fanciulli, P.P. et Dallai, R., 1995, *I. stuxbergi* Tullberg, 1877, *Entomobrya muscorum* Nicolet, 1842 and *E. nicoleti* Lubbock, 1870. 10 species were common with site 4 with the same

microhabitat. Total number of (Table 1) the species identified was 15 for both microhabitats, out of which six were common.

**Table 1.** Collembola species on studied sites at Bečići beach

Sites		“Tara” Hotel Palm tree	“St. Thomas” Cypresses tree	“Naftagas” Hotel White pine tree	“Naftagas” Hotel Larch tree	Green Rock White pine tree
Collembola	Species					
Neanuridae Börner, 1901	<i>Neanura muscorum</i> MacGillivray, 1893	+		+		+
	<i>Bilobella mahunkai</i> Danyi, 2010	+				
	<i>Anurida maritima</i> Guérin- Méneville, 1836	+				+
	<i>Anurida granaria</i> , Tullberg, 1869					+
	<i>Pseudachorutes palmiensis</i> Börner, 1903					+
	<i>Pseudachorutes parvulus</i> Börner, 1901			+		
	<i>Xenylla grisea</i> Axelson, 1900					+
	<i>Xenylla maritima</i> Tullberg, 1896					+
	<i>Ceratophysella bengtssoni</i> Ågren, 1904					+
Hypogastruridae Börner, 1901	<i>Ceratophysella succinea</i> Gisin, 1949					+
	<i>Hypogastrura viatica</i> Tullberg, 1872	+	+	+	+	+
	<i>Hypogastrura distincta</i> Axelson, 1902	+	+	+		+
	<i>Hypogastrura purpureescens</i> Lubbock, 1870		+	+	+	+
	<i>Onychiurus sp.</i>	+	+	+		
Isotomidae Schäffer, 1896	<i>Isotomurus alticolus</i> Handschin, 1919	+	+	+	+	+
	<i>Isotomurus fucicolus</i> Axelson, 1906			+	+	+
	<i>Isotomurus italicus</i> Carapelli, A., Frati, F., Fanciulli, P.P. et Dallai, R., 1995	+		+	+	+
	<i>Isotomurus stuxbergi</i> Tullberg, 1877	+		+	+	+
	<i>Isotoma riparia</i> Nicolet, 1842	+				+
	<i>Isotoma viridis</i> Bourlet, 1839					+
	<i>Folsomia quadrioculata</i> Tullberg, 1871				+	
Entomobryidae Schäffer, 1896	<i>Orchesella flavescens</i> Bourlet, 1839					+
	<i>Entomobrya muscorum</i> Nicolet, 1842			+		+
	<i>Entomobrya albanica</i> Stach, 1922					+
	<i>Entomobrya multifasciata</i> Tullberg, 1821	+			+	
	<i>Entomobrya nicoleti</i> Lubbock, 1870			+		+
	<i>Lepydocyrtus lusitanicus</i> da Gama, 1964					+
	<i>Cyphoderus bidenticulatus</i> Börner, 1903				+	
Sminthuriade Lubbock, 1862	<i>Sminthurus hispanicus</i> Nayrolles, 1995		+			+
	<i>Arropalithes caecus</i> Tullberg, 1871					+

Under the white pine tree, two specimen of *Polyxenus lagurus* L., 1758 (Diplopoda) were registered, and abundant communities of ants, mites and insects' larvae.

#### Site 4- Green Stone

This site is situated close to popular place on Bečići Beach, so called „Green Stone“, coordinates: N: 42.280915, E: 18.878272. The microhabitat chosen for this site was under the white pine tree with humusly soil covered with litter in deep shadow. In the time of sampling, the site was fenced in order to protect construction works that haven't started at the time of sampling. Following springtails have been indentified at this site: *Neanura muscorum* MacGillivray, 1893, *Anurida maritima* Guérin-Méneville, 1836, *A. granaria* Tullberg, 1869 *Pseudachorutes palmiensis* Börner, 1903, *Xenylla grisea* Axelson, 1900 *Xenylla maritima* Tullberg, 1896, *Ceratophysella bengtssoni* Ågren, 1904, *C. succinea* Gisin, 1949, *Hypogastrura viatica* Tullberg, 1872, *H. distincta* Axelson, 1902, *H. purpurescens* Lubbock, 1870, *Isotomurus alticolus* Handschin, 1919, *I. fucicolus* Axelson, 1906, *I. italicus* Carapelli, A., Frati, F., Fanciulli, P.P. et Dallai, R., 1995, *I. stuxbergi* Tullberg, 1877, *Isotoma riparia* Nicolet, 1842, *Isotoma viridis* Bourlet, 1839, *Orchesella flavescens* Bourlet, 1839, *Entomobrya muscorum* Nicolet, 1842, *E. albanica* Stach, 1922, *E. nicoleti* Lubbock, 1870, *Lepidocyrtus lusitanicus* da Gama, 1964, *Sminthurus hispanicus* Nayrolles, 1995 and *Arropalithes caecus* Tullberg, 1871, 24 species in total. Species from *Hypogastrura* genera were numerous, but there were also many individuals from *Isotomurus* genera at the site, with no domination of certain groups.

There were poor communities of other expected biological groups, as recorded on the previously sites; mites were present, but with small abundance.

## CONCLUSION

The springtails (Insecta: Collembola) fauna has been investigated during May and September 2015 in at specific microhabitats near by Bečići Beach, Montenegro. Total number of 30 species out from 17 genera and 6 families have been recorded at four investigated sites.

The „Green Stone“ site had the reachest springtail diversity, with 24 species recorded. The poorest community was recorded at “St. Thomas” Church site, 6 species in total.. At the same time, population density was high, predominated by representatives of the Hypogastruridae family. 11 species were recorded at „Tara“ Hotel site. The soil at the sampling site was shallow and hard, with occasional watering of the palm trees during the drought. Diverse community was recorded at the „Naftagas“ Hotel site with 15 recorded species, out of which six were common at both investigated microhabitats.

Hypogastruridae family had the biggest share in the Collembola community at the all of studied sites.. At the “Green Stone” site, although the richest with the number of the species, no group was dominant, but the community was unified.

Representatives of the family Hypogastruridae and Isotomidae were recorded at all of the studied sites, while representatives of the families: Naenuridae, Onychiuridae, Entomobryidae and Sminthuridae were present on some of locations.

## REFERENCES

- Bellinger, P.F., Christiansen, K. A., Janssens, F. Checklist of the Collembola of the world. Available from: <http://www.collembola.org>
- Bogojević, J. 1978. Prilog poznavanju faune Collembola Crnogorskog primorja. Glasnik Prirodnjačkog muzeja. Beograd, Vol. 33, pp.157-161.
- Chagnon, M., Hébert, C., Paré, D. 2000. Community structure of Collembola in sugar maple forest: relation to humus type and seasonal trends. Pedobiologia, 44, pp. 148-174.
- Ćurčić, B.P.M. & Lučić, L.R. 1997. On the Biodiversity of Springtails (Collembola, Insecta) in Yugoslavia (Serbia and Montenegro). Arch. Biol. Sci. Belgrade, 49, pp. 13-14.
- Ćurčić, B.P.M., Decu, V., Juberthie, C. 2008. Cave-dwelling Invertebrates in Montenegro. Advances in arachnology and Development Biology. Monographs, 12, pp. 35-55. Vienna-Belgrade-Sofia.
- Fernandes, L.H., Nessimian, J.L., Mendonça, M.C. 2009. Structure of Poduromorpha (Collembola) communities in “resting” environments in Brazil. Pesquisa Agropecuária Brasileira, Brasília, 44 (8), pp. 1033-1039.
- Gisin, H. 1943. Öcologic und Lebengemeinschaften der Collembolen im schweizerischen Exkursionsgebiet Basels. Revue Suisse de Zoologie, 50, pp. 131-224.
- Gisin, H. 1960. Collembolenfauna Europas. Museum D'Historie Naturelle. Geneve, pp. 312.
- Hågvar, S. 1982. Collembola in Norwegian coniferous forest soil. I. Relation to plant communities and soil fertility. Pedobiologia, 24, pp. 255-296.
- Hågvar, S. & Abrahamsen, G. 1984. Collembola in Norwegian coniferous forest soil. III. Relation to soil chemistry. Pedobiologia, 27, pp. 331-339.
- Lebrun, P. 1976. Effects écologiques de la pollution atmosphérique sur les populations et communautés de microarthropodes corticoles (Acariens, Collembolés et Ptérygotes). Bull. Soc. Ecol. 7, pp. 417-430.
- Ponge, J.F. 1993. Biocenoses of Collembola in atlantic temperate grass-woodland ecosystems. Pedobiologia, 37(4), pp. 223-244.
- Prasse, I., 1985. Indications of structural changes in the communities of microarthropods of the soil in an agro-ecosystem after applying herbicides. Agriculture, Ecosystems and Environment 13, pp. 205-215.
- Rusek, J., 1989. Collembola and Protura in a meadow-forest ecotone. In: Dallai, R. (Ed.), Third Seminar on Apterygota. University of Siena, Siena, pp. 413-418.
- Salmon, S., Ponge, J.F., Van straalen, N.M., 2002. Ionic identity of pore water influences Ph preference in Collembola. Soil Biology and Biochemistry 34, pp. 1663-1667.
- Stach, J. 1956. The Apterygoten fauna of Poland in relation to the World fauna of this group of insects. Sminthuridae. Krakow.

- Stach, J. 1960. The Apterygoten fauna of Poland in relation to the World fauna of this group of insects. Tribe: Orchesellini. Krakow.
- Stach, J. 1963. The Apterygoten fauna of Poland in relation to the World fauna of this group of insects. Tribe: Entomobryini. Krakow.
- Sterzyńska, M. 1990. Communities of Collembola in natural and transformed soils of the linden-oak-hornbeam sites of the Mazovian Lowland. *Fragmenta Faunistica*, 34, pp. 165-262.
- Vilkamaa, P. & Huntha, V. 1986. Effects of fertilization and Ph on communities in pine forest soil. *Ann. Zool. Fenn.* 23, pp. 167-174.

# SUPPLEMENT TO THE PHYTOGEOGRAPHICAL STUDIES OF THE RARE AND INTERNATIONALLY SIGNIFICANT SPECIES IN THE FLORA OF SERBIA, KOSOVO AND METOHİJA NORTH

DANIJELA PRODANOVIĆ<sup>1\*</sup>, ZORAN KRIVOŠEJ<sup>2</sup>, MILOŠ STANOJEVIĆ<sup>2</sup>, SLAVICA ĆIRIĆ<sup>1</sup>

<sup>1</sup>Faculty of Agriculture, University of Priština, Lešak, Serbia

<sup>2</sup>Faculty of Natural Science and Mathematics, University of Priština, Kosovska Mitrovica, Serbia

## ABSTRACT

This paper reports the chorological data on 3 internationally significant floristic species in Serbia, in the Ibar river valley, Kosovo and Metohija North. Those are: *Gladiolus palustris* Gaudin, *Himantoglossum caprinum* (M. Bieb) Spreng. and *Narcissus poeticus* subsp. *radiiflorus* (Salisb.) Baker. It also reports new research findings on a rare species of vascular flora of Serbia - *Phlomis tuberosa* (L.) Moench. The distribution of the mentioned species is shown in UTM 10 km X 10 km squares, based on the field researches, herbarium collections inspections and literature data. As the studied species belong to the group of internationally important and rare species, the familiarity with the status of their populations and degree of their vulnerability would present a good basis for monitoring their protection both in Serbia and Europe.

**Keywords:** Flora of Serbia, Internationally significant species, Rare species, Ibar river valley, Phytogeographical study.

## INTRODUCTION

The Republic of Serbia covers only 1.9% of the whole of the European territory. This area is inhabited by 3662 taxa of vascular plants, classified as species and subspecies (Stevanović et al., 1995) and they present approximately 18% of vascular European flora (Mijović et al., 2012). Serbia is a country of rich ecosystem and species diversity. The diversity of ecosystems in Serbia is primarily evident in the diversity and specific character of its vegetation (IUCN, 2017). Endemic plant species give a special contribution to the floristic abundance of the Republic of Serbia because 547 Balkan endemic taxa were reported on its territory (Tomović, 2007). Out of total number of floral species in the Republic of Serbia, 1128 vascular species are protected by national legislation and 161 species belong to the group of internationally significant floral species (Stojanović et al., 2015).

In terms of biodiversity conservation, refugial areas (high mountainous regions, salt marshes, canyons and gorges) have a special significance. Thus the Ibar river gorge, Kosovo and Metohija North, with the serpentine mountains encircling it, presents an important region of the floristic diversity, endemism in our country, rare species and the species that are subjected to different categories of protection in international legislations (IUCN, The Berne Convention, CITES etc.).

The largest serpentine areas in Europe are in the Balkan peninsula. In Serbia there are several serpentine zones located primarily in central, western and south-western Serbia and in Kosovo and Metohija (Jakovljević et al., 2011). On the territory

of Kosovo and Metohija the largest complexes are found in the valley of the Ibar river, and the same are continued in a discontinuous chain through Koznica and Goleš, to the southwest.

All types of floristic field studies have been continuously conducted in these areas in the middle course of the Ibar, Kosovo and Metohija's Far North since 2002. Hitherto researches on the serpentine in the Kosovo part of the Ibar gorge have reported around 950 taxa and they represent more than 25% of total flora of Serbia. The result of these researches have revealed totally new and hitherto unknown chorological data on some internationally significant and endemic plant species, as well as on the species rarely present in the flora of Serbia.

## EXPERIMENTAL

### Materials and methods

On the basis of the material collected during the field work (from 2008-2017), on the serpentine of the Ibar river valley in Kosovo's part, we present study for four mentioned vascular plants.

Identification of the collected plant material is made according to Flora of Serbia (Josifović 1974, 1975, 1976; Sarić 1986) and Flora Europae (Tutin et al., 1972, 1980); the nomenclature was adjusted to The Plant List (2013).

Besides the field survey, checking of herbarium material and relevant literature sources were used to present an overall distribution for studied taxa in Serbia. The given taxa are mapped on 10 x 10 sq km at UTM grid system (UTM Zone 34T) (Lampinen, 2001).

\* Corresponding author: danijela.prodanovic@pr.ac.rs

The threats that potentially jeopardize the survival of the species have been recognized and the measures to protect them have been recommended.

## RESULTS AND DISCUSSION

Fam.: IRIDACEAE

*Gladiolus palustris* Gaud.

General distribution: middle and southern Europe. North of the Alps, it ranges from eastern France and the Alsace, Germany, Czech Republic, Slovakia, Poland eastwards with fragmented patches in Belarus, Ukraine and Russia. South of the Alps, it extends from the Appenines in Italy to eastern Austria and Hungary where it extends to western Bulgaria and Albania in the Balkans (Bilz, 2011).

Distribution in Serbia: Grdelička klisura, Kosanica, Luka below Stol mountain, Studena mt., Pešterska Highlands, Podvrška, Veliki Deli Jovan, Ušće; Kosovo and Metohija-Brezovica, Jezerska planina, Koritnik, Koznik, Kodža Balkan, Popovica, Radipolje, Tumba (Stojanović et al., 2015); Ibar river valley, from Brnjak to Kosovska Mitrovica (Tomić-Stanković, 1967).

New chorological data in Serbia (Figure 1): village Bube (Ibarski Kolašin), meadow near the road: 42° 59' 39,8" N, 20° 48' 07,9" E (925 m a.s.l) UTM 34 TDN74 (leg./det. Krivošej, Z. & Prodanović, D., 19-June-2008); village Bube, meadow near the school: 42° 58' 67,9" N, 20° 37' 33,2" E (972 m a.s.l) UTM 34 TDN74 (leg./det. Krivošej, Z. & Prodanović, D., 01-June-2008); village Dren, near Mokra Gora Mountain: 42° 51' 88,0" N, 20° 38' 55,7" E (1004 m a.s.l) UTM 34 TDN65 (leg./det. Krivošej, Z. & Prodanović, D., 30-July-2008)

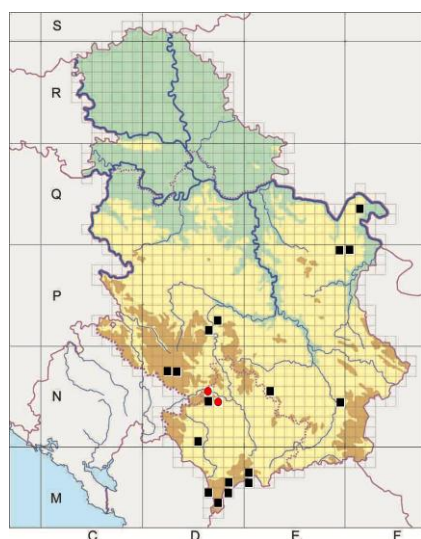


**Figure 1.** Distribution of the species *Gladiolus palustris* Gaud. in Serbia. New records marked with red circle.

Species *Gladiolus palustris* is a European endemic. It prefers periodically wet meadows but is tolerant to dryness. If

the habitat is not periodically wet the populations decrease due to competition from other plants (Käsermann & Moser, 1999).

Even though the literature data (Tomić-Stanković, 1967) on the presence of species in Ibarski Kolašin, from Brnjak to Kosovska Mitrovica, existed, it was not included in the 1976 edition of The Flora of Serbia (Josifović). This may have been caused by the extinction of the natural habitats due to the construction of the artificial Gazivode lake (1973-1977), which completely jeopardized the survival of species. The 2010 field checkout did not find species in the Brnjak village area nor in the lower course of the river towards Kosovska Mitrovica.

This internationally important floral species was identified on the wet meadows in the vicinity of the village of Bube, Ibarski Kolašin. It grows, along with a rather rare fern species *Ophioglossum vulgatum* L., on the wet meadow above the school (Table 1).

**Table 1.** Phytocenologic recording for species *Gladiolus palustris* Gaud.

Locality	Ibarski Kolašin-village Bube
GPS	42° 58' 67,9" N 20° 37' 33,2" E
Size of the sampled area (P)	400 m <sup>2</sup>
Date	01.06.2008.
Altitude (m)	925
Exposition	SW
Slope	40°
Geological substratum	siliceous soil
<i>Gladiolus palustris</i> Gaud.	3.3
<i>Ophioglossum vulgatum</i> L.	3.3
<i>Filipendula vulgaris</i> Moench.	3.3
<i>Trifolium incarnatum</i> L.	2.2
<i>Genista sagittalis</i> L.	2.2
<i>Lathyrus pratensis</i> L.	2.2
<i>Vicia cracca</i> L.	2.2
<i>Cynosurus cristatus</i> L.	2.2
<i>Festuca</i> sp.	1.2
<i>Anthoxanthum odoratum</i> L.	1.2
<i>Briza media</i> L.	1.2
<i>Oenanthe silaifolia</i> M.	1.1
Bieb.	
<i>Moenchia mantica</i> (L.)	1.1
Bartl.	
<i>Galium verum</i> L.	1.1
<i>Dianthus deltoides</i> L.	1.1
<i>Plantago media</i> L.	1.1
<i>Anacamptis morio</i> (L.)	1.1
R.M.Bateman, Pridgeon & M.W.Chase	
<i>Trifolium patens</i> Schreb.	1.1
<i>Trifolium montanum</i> L.	1.1
<i>Danthonia calycina</i> Roem & Schult.	1.1
<i>Hypochaeris maculata</i> L.	1.1
<i>Rumex acetosa</i> L.	1.1
<i>Alopecurus pratensis</i> L.	1.1
<i>Dianthus carthusianorum</i> L.	1.1
<i>Neotinea ustulata</i> (L.)	+
R.M.Bateman, Pridgeon & M.W. Chase	
<i>Trifolium pratense</i> L.	+

In another locality, a meadow which lies under a mixed oak tree wood keeps water and humidity in its lower part for the greater part of the year creating favourable conditions for the growth of marsh gladiolus. The mentioned localities boast a considerable number of individuals. There are several hundred individuals in each locality. The species was discovered in the vicinity of the village of Dren, at the foot of Mokra Gora mountain at later phenological stage, when the capsules were formed, so it was slightly difficult to estimate its number (approximately a hundred individuals).

Since these areas are sparsely populated, they are not constantly threatened by man, although the cattle are periodically taken out to pastures. Cutting grass may also present a threat to the gladiolus population. Another real manace would be its overexploitation due to its decorative feature. Nevertheless, it is still not considered an acute anthropogenic activity. A considerable decrease in number of species and the species extinction are reported in the European continent. The species is protected in Serbia by The Habitats Directive, Bern Convention, by the Law on Nature Protection and the Law on Trade in Endangered and Protected Species of Wild Flora and Fauna.

Fam.: ORCHIDACEAE

*Himantoglossum caprinum* (M. Bieb.) Spreng.

General distribution: southeastern Europe and Middle East.

Distribution in Serbia: Vojvodina-Fruška gora; Serbia: Đavolja varoš, Đerdap, Đetinja, Jadovnik, Jelašnička George, Svrliški Timok George, Jerma George, Mileševka George, Ozren, Mokra gora, Pešter highland, Sićevačka George, Suva mt., Zaovine, Zlatibor, Zlotska George; Kosovo and Metohija-Grmija, near by Priština, canyon of Miruša, Prokletije, Šarplanina (mt.) (Stojanović et al., 2015).

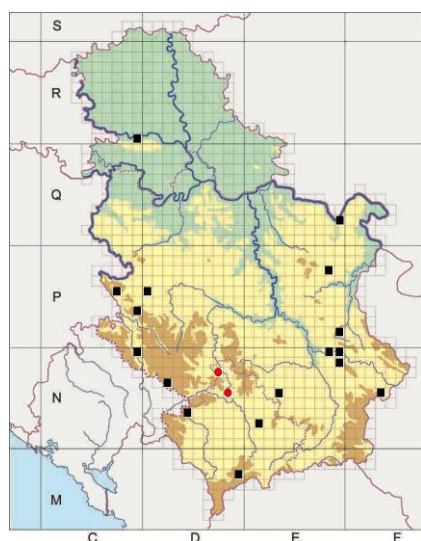


**Figure 2.** Distribution of the species *Himantoglossum caprinum* (M.Bieb.) Spreng. in Serbia. New records marked with red circle.

New chorological data in Serbia (Figure 2): villages Žitkovac-Valač (near Kosovska Mitrovica town): 42° 56' 77,9" N,

20° 49' 50,6" E (579 m a.s.l) UTM 34 TDN85 (leg./det. Krivošej, Z.& Prodanović, D., 14-June-2010); 42° 36' 33,8" N, 21° 12' 97,5" E (544 m a.s.l) UTM 34 TDN85 (leg./det. Krivošej, Z.& Prodanović, D., 14-June-2010; village Vračevo (Ibar river valley) 43° 10' 93,3" N, 20° 40' 47,4" E (473 m a.s.l) UTM 34 TDN77 (leg./det. Krivošej, Z.& Prodanović, D., 08-July-2011).

*Himantoglossum caprinum* grows in poor grassland, woodland edges, forest-steppes, and open woodland such as oak groves (Rankou, 2011). It prefers dry and calcareous soils.

This perennial orchid in newly-discovered localities in Valač (Table 2) and Vračevo village areas, grows as solitary individuals in very small groups, but is easily remarkable due to its imposing size and beauty.

Although it is cited in the Flora of Serbia (Josifović, 1976) and recent literature (Rankou, 2011; Stojanovic et al., 2015) that it grows in habitats with limestone background, the existence of this species on the serpentines of the Ibar gorge proves that other types of soil (composed predominantly of silica) can also host it.

**Table 2.** Phytocenologic recording for species *Himantoglossum caprinum* (M. Bieb.) Spreng.

Locality	Village Žitkovac-Valač
GPS	42° 56' 77,9" N, 20° 49' 50,6" E
Size of the sampled area (P)	20 m <sup>2</sup>
Date	14.06.2010.
Altitude (m)	579
Exposition	W
Slope	10°
Geological substratum	siliceous rocky ground
<i>Quercus cerris</i> L.	+
<i>Quercus frainetto</i> Ten.	+
<i>Himantoglossum caprinum</i> (M.Bieb.) Spreng	r
<i>Lotus corniculatus</i> L.	1.1
<i>Petrorhagia saxifraga</i> (L) Link.	1.1
<i>Lathyrus niger</i> (L.) Bernh.	1.1
<i>Achillea millefolium</i> L.	+
<i>Digitalis lanata</i> Ehrh.	+
<i>Trifolium alpestre</i> L.	+
<i>Astragalus glycyphyllos</i> L.	+
<i>Helleborus odoratus</i> Waldst. & Kit. ex Willd.	r
<i>Prunus spinosa</i> L.	r

Species *Himantoglossum carpinum* has unresolved taxonomic status and then existence of this taxon in the territory of Serbia is questioned. According to Molnár et al., (2012) the name *H. caprinum* has been consistently and correctly applied to Crimean lizard orchid, which does not actually occur to central European territories. The name *H. caprinum*, which was misused for this species, was replaced with *H. jankae* Somlyay, Kreutz & Óvári. A new name, *Himantoglossum jankae*, is given to the widely recognised lizard orchid species that is distributed primarily in Slovakia, Hungary, Romania, Croatia, Serbia, Montenegro, Macedonia, Albania, Bulgaria, Greece, northern Turkey. Molnár et al., (2012) for the territory of Serbia cite subsp. *caprinum* near Vršac; by their opinion it's *H. jankae*. The

recent data in the check list (WCSP, 2017) present as accepted taxonomic name for this species *Himantoglossum caprinum* subsp. *jankae* (Somlyay, Kreutz & Óvári) R.M. Bateman, Molnar & Sramkó, Peerj 5 (e2893):69 (2016). We think that a taxonomic revision of the data taken from the literature should include verification of herbarium material in future work (It is necessary to clarify the taxonomic status of the subspecies by checking the herbarium material to determine exactly where the species referred to as *caprinum* is growing in Serbia). Also, our phytogeographical supplement should be taken into account.

The species is strictly protected under the name of *Himantoglossum hircinum* (L.) Spreng. by the Law on Trade in Endangered and Protected Species of Wild Flora and Fauna as well by International Conventions-Bern Convention and CITES.

Removal from the habitat by woody invasive plants, afforestation, soil erosion and accumulation present a threat to the species (Stojanović et al., 2015). In two newly- discovered localities in the Ibar valley, Kosovo and Metohija North, pastures on the edges of the forests and plant gathering due to its decorative features were identified as potential dangers.

Fam. AMARYLLIDACEAE

*Narcissus poeticus* subsp. *radiiflorus* (Salisb.) Baker (syn. *Narcissus angustifolius* G.Don).

The *Narcissus* genus comprises 20-40 species (The Flora of Serbia) or over 140 species (The Plant List, 2013), mostly distributed in the Mediterranean and in Middle and East Asia. Only one species grows indigenously in the Flora of Serbia.

General distribution: southern and east-central Europe (Alps, Carpatians), extends to the Ukraine, former Yugoslav republics, northern Greece (Chadburn, 2014).

Distribution in Serbia: Divčibare, Đetinja, Maljen, Ozren, Preševo (Miratovac), Stolovi (Svračak), Studena mountain (Kraljevo), Tara, Uvac, Zlatibor, Kopaonik (probably extinct, by Stojanović et al., 2105). Our observations shows that the species is growing on the slopes of the Kopaonik, near the Jošanička banja ; Kosovo and Metohija: Drenica, Glogovac (Dobroševac), Podujevo, Priština, Šar-planina/mountain, Uroševac.

New chorological data in Serbia (Figure 3): village Rudine (Rogozna mountain): 43° 01' 260" N, 20° 45' 153" E (910 m a.s.l) UTM 34 TDN76 (leg./det. Krivošej, Z.& Prodanović, D., 12-May-2012); 43° 01' 387" N, 20° 45' 307" E (895 m a.s.l) UTM 34 TDN76 (leg./det. Krivošej, Z.& Prodanović, D., 12-May-2012).

During the 2012 field researches on Rogozna Mt., Kosovo and Metohija North, this perennial plant or geophyte was identified in two relatively close localities. In both localities, the species inhabits wet meadows with mountainous streams running through it. From the beginning of summer season they are filled with water and then they become dry in the hottest part of the year. In both localities their number is exceptionally large and is estimated from several hundred to a thousand individuals, so the localities become real narcissus fields at the blooming season in May.

Floristic composition can be best observed from the following phytocenologic recording (Table 3).

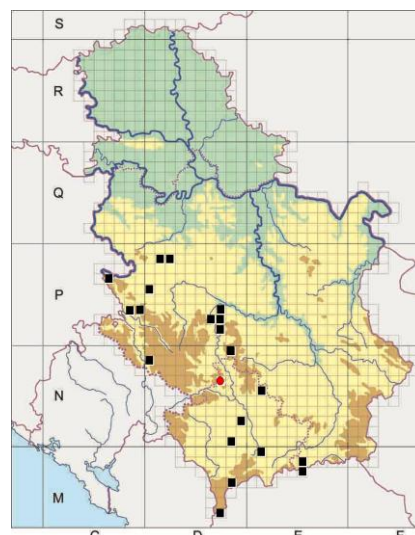


**Figure 3.** Distribution of the species *Narcissus poeticus* subsp. *radiiflorus* (Salisb.) Baker in Serbia. New record marked with red circle.

**Table 3.** Phytocenologic recording for species *Narcissus poeticus* subsp. *radiiflorus* (Salisb.) Baker

Locality	Rogozna Mountain-Rudine village
GPS	43° 01' 260" N, 20° 45' 153" E
Size of the sampled area (P)	400 m <sup>2</sup>
Date	12.05.2012.
Altitude(m)	910
Exposition	N
Slope	40°
Geological substratum	siliceous ground
<i>Narcissus poeticus</i> subsp. <i>radiiflorus</i> (Salisb.) Baker	4.4
<i>Thalictrum minus</i> L.	2.2
<i>Filipendula vulgaris</i> Moench	2.2
<i>Ranunculus acris</i> L.	2.2
<i>Pedicularis palustris</i> L.	1.2
<i>Eleocharis palustris</i> (L.) Roem. & Schult.	1.2
<i>Oenanthe silaifolia</i> M.Bieb	1.1
<i>Galium verum</i> L	1.1
<i>Rumex acetosa</i> L.	1.1
<i>Lathyrus pratensis</i> L.	1.1
<i>Ajuga genevensis</i> L	1.1
<i>Veronica austriaca</i> L	+
<i>Mercurialis ovata</i> Sternb.& Hoppe	+
<i>Plantago argentea</i> Chaix	+
<i>Anacamptis morio</i> (L.) R.M. Bateman, Pridgeon & M.W. Chase M.W	+
<i>Polygala comosa</i> Schkuhr	+
<i>Potentilla erecta</i> (L.) Raeusch.	+
<i>Carex filiformis</i> L.	+
<i>Sanguisorba officinalis</i> L	+
<i>Quercus petraea</i> (Matt.) Liebl	r

Since the newly - discovered localities are far away from the settlements and thoroughfares, it is assumed that there is no real danger for the narcissus population caused by anthropogenic activity. First of all, it refers to the spontaneous plant gathering due to its decorative features, which is a common and frequent case in other localities in Serbia. Likewise, cattle grazing should not present a real danger at the moment as the cattle (sheep and cows were noticed during the field researches) avoid eating narcissus because of its toxic ingredients in all parts of the plant.

Fam. LAMIACEAE

*Phlomoides tuberosa* (L.) Moench.

General distribution: from Siberia to Caucasus, northern Iraqi and Asia, through middle and southern part of Russia, along Danube river to Hungary.

Distribution in Serbia: Lešje (Ćuprija), Pirkovac, Niševci (Knjaževac), Blace; Kosovo: okolina Srbice.

New chorological data in Serbia (Figure 4): village Ibarska Slatina (Ibar river valley): 43° 02' 85.4" N, 20° 49' 0.30" E (451 m a.s.l) UTM 34 TDN87 (leg./det. Krivošej, Z., Prodanović, D.& Stanojević, M. 15-June-2017).

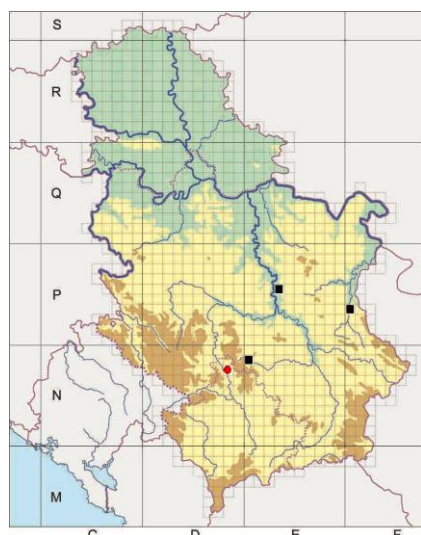


**Figure 4.** Distribution of the species *Phlomoides tuberosa* (L.) Moench. in Serbia. New record marked with red circle.

The genus *Phlomoides* Moench with about 150–170 species belongs to *Lamiaceae*, subfamily *Lamioideae*, tribe *Phlomideae* (Salmaki & Yonarchi, 2014). The distribution area of the genus extends from central Europe to the Russian Far East. The major centers of diversity of *Phlomoides* are Central Asia, the Iranian highlands, including Afghanistan, Iran, W Pakistan, SW Turkmenistan, and China, but includes a few species extending to Mediterranean Europe (Salmaki et al., 2012).

The Flora of Serbia describes only one species as *Phlomoides* genus (described as *Phlomis* in old classification), *Ph. tuberosa*. In June 2017, we conducted field researches on the serpentine of the Ibar valley, in close proximity to Kosovska Mitrovica- Kraljevo highway, on the right bank of the Ibar, in

Ibarska Slatina area. (Figure 5). We came across a new locality in Kosovo and Metohija with this rather rare steppe relict species (Stevanović, 1999) in the flora of Serbia. It is the second presently known locality in Kosovo and Metohija territory. Although the Flora of Serbia (1974) mentions the presence of the species in eastern Serbia, recent researches do not corroborate this data (Bogosavljević et al., 2007).



**Figure 5.** *Phlomoides tuberosa* (L.) Moench. in Ibarska Slatina locality (photo. D. Prodanović).

The floristic structure in the Ibarska Slatina locality can be seen from next phytocenological record (Table 4).

**Table 4.** Phytocenologic recording for species *Phlomoides tuberosa* (L.) Moench.

Locality	Village Ibarska Slatina
GPS	43° 02' 85.4" N, 20° 49' 0.30" E
Size of the sampled area (P)	30 m <sup>2</sup>
Date	15.07.2017.
Altitude (m)	451
Exposition	NE
Slope	30°
Geological substratum	siliceous ground
<i>Xeranthemum annuum</i> L	3.3
<i>Poa pratensis</i> L.	2.2
<i>Phlomoides tuberosa</i> (L.) Moench	1.1
<i>Achillea millefolium</i> L.	1.1
<i>Vicia cracca</i> L.	1.1
<i>Galium verum</i> L.	1.1
<i>Onobrychis cyri</i> Grossh	1.1
<i>Melilotus officinalis</i> (L.) Pall.	1.1
<i>Anthericum liliago</i> L	1.1
<i>Salvia pratensis</i> L.	1.1
<i>Euphorbia esula</i> L.	1.1
<i>Tragopogon dubius</i> Scop.	1.1
<i>Triticum durum</i> Desf.	1.1
<i>Plantago media</i> L.	1.1
<i>Plantago lanceolata</i> L.	1.1
<i>Eryngium campestre</i> L.	1.1
<i>Securigea varia</i> (L.) Lassen	1.1
<i>Cichorium intybus</i> L	1.1
<i>Galium aparine</i> L.	1.1
<i>Arrhenatherum elatius</i> (L.) P. Beauv. ex J. Presl & C. Presl.	1.1
<i>Ulmus carpinifolia</i> Gled	+
<i>Pyrus amygdaliformis</i> Vill	+

The *Phlomoides tuberosa* is a perennial plant with a well developed cylindrical rhizome and small roots with partly thickened tubers. The grass cutting continuously performed on the meadow where the species was reported should not cause the reduction of its number or the species extinction. Since it is identified in few localities, adequate measures should be certainly undertaken to prevent the decrease in number of the species or the extinction of the present habitats. The species in Serbia is protected by the Law on Nature Protection (Official gazette of RS", no. 5/2010 and 47/2011), which means that the trade and use are monitored according to special regulatory standards.

## CONCLUSION

New chorological data from Kosovo and Metohija North on the European endemic species *Gladiolus palustris* Gaud. May largely contribute to the evaluation of the degree of endangerment of the species population and the possible application of protection measures in order to prevent destruction and change of the habitats of this species. The new two localities of species *Himantoglossum caprinum* (M. Bieb.) Spreng. on the territory of Kosovo and Metohija could explain the area of this type in the flora of Serbia, which will enable proper protection of this species. The localities on Rogozna Mt. represent new and so far unknown localities for the *Narcissus poeticus* subsp. *radiiflorus* (Salisb.) Baker species and may serve as a good data on the chorology of this species in the Flora of Serbia and offer a good basis for proposing preventive and protective measures and actions. Since there were only few records of *Phlomodites tuberosa* in Serbia, new finding in the Ibar valley present second locality for Kosovo territory and important contribution to the chorology of this very rare plant in Serbian flora.

The familiarity with the distribution of the mentioned species, the conditions of their habitats and potentially threatening factors would present a good foundation for the protection of these plants, which may secure their survival in Serbia.

## REFERENCES

- Bilz, M. 2011. *Gladiolus palustris*. The IUCN Red List of Threatened Species, pp. 162188-162188. doi:10.2305/IUCN.UK.2011-1.RLTS.T162188A5555329.en
- Bogosavljević, S., Zlatković, B., & Randelović, V. 2007. Flora klisure Svrliškog Timoka. In: 9th Symposium of Flora of Southeastern Serbia and Neighbouring Regions. Niš (Serbia) September 01-03. Proceeding, pp. 41-54.
- Chadburn, H. 2014. *Narcissus poeticus*. The IUCN Red List of Threatened Species, p. 193504. doi:10.2305/IUCN.UK.20141.RLTS.T193504A2239955.en
- CITES Secretariat. 2011. Convention on International Trade in Endangered Species of Wild Fauna and Flora. Retrieved from <http://www.cites.org/>.
- IUCN. 2017. The IUCN Red List of Threatened Species. Version 2017-2. Retrieved from <http://www.iucnredlist.org>
- Jakovljević, K., Lakušić, D., Vukojević, S., Tomović, G., Šinžar-Sekulić, J., & Stevanović, V. 2011. Richness and diversity of Pontic flora on serpentine of Serbia. Central European Journal of Biology, 6(2), pp. 260-274. doi:10.2478/s11535-010-0110-5
- Josifović, M. (Ed.). 1974. Flora SR Srbije VI. In. Beograd: Srpska Akademija Nauka i Umetnosti - Odeljenje prirodno-matematičkih nauka.
- Josifović, M. (Ed.). 1975. Flora SR Srbije VII. Beograd: Srpska Akademija Nauka i Umetnosti - Odeljenje prirodno-matematičkih nauka.
- Josifović, M. (Ed.). 1976. Flora SR Srbije VIII. Beograd: Srpska Akademija Nauka i Umetnosti - Odeljenje prirodno-matematičkih nauka.
- Käsermann, C., & Moser, D.M. 1999. Fiches pratiques pour la conservation-Plantes à fleurs et fougères (situation octobre 1999). Berne: Edité par l'Office fédéral de l'environnement, des forêts et du paysage (OFEFP).
- Lampinen, R. 2001. Universal Transverse Mercator (UTM) and Military grid Reference System (MGRS). Retrieved from <http://www.luomus.fi/english/botany/afe/map/utm.htm>.
- Mijović, A., Sekulić, N., Lazarević, P., Stojanović, V., & Mišić, D. 2012. Biodiverzitet Srbije - stanje i perspektive. Beograd: Zavod za zaštitu prirode Srbije.
- Molnár, V.A., Kreutz, K., Óvári, M., Sennikov, A., Bateman, R., Takács, A., Somlyay, L., & Sramkó, G. 2012. *Himantoglossum jankae* (Orchidaceae: Orchideae), a new name for a long-misnamed lizard orchid. Phytotaxa 73, pp. 8-12. DOI: <http://dx.doi.org/10.11646/phytotaxa.73.1.2>
- Službeni glasnik RS 2010. Pravilnik o proglašenju i zaštiti strogo zaštićenih i zaštićenih divljih vrsta biljaka, životinja i gljiva. Službeni glasnik RS, br. 05/2010 i 47/2011.
- Rankou, H. 2011. *Himantoglossum caprinum*. The IUCN Red List of Threatened Species, p. 162090.
- Salmaki, Y., Zarre, S., & Heubl, G. 2012. The genus *Phlomoides* Moench (Lamiaceae; Lamioideae; Phlomideae) in Iran: An updated synopsis. Iran J. Bot., 18(2), pp. 207-220.
- Salmaki, Y., & Jonarchi, M.R. 2014. *Phlomoides binaludensis* (Phlomioideae, Lamioideae, Lamiaceae), a new species from northeastern Iran. Phytotaxa, 172(3), pp. 265-270. doi:10.11646/phytotaxa.172.3.7
- Sarić, M.R. (Ed.). 1986. Flora SR Srbije X. Beograd: Srpska Akademija Nauka i Umetnosti - Odeljenje prirodno-matematičkih nauka.
- Stevanović, V., Vasić, V. (Eds.). 1995. Biodiverzitet Jugoslavije sa pregledom vrsta od međunarodnog značaja. Beograd: Biološki fakultet / Ecolibri.
- Stevanović, V. (Ed.). 1999. Iščezli i krajnje ugroženi taksoni. In Crvena knjiga flore Srbije. 1. Beograd: Ministarstvo za životnu sredinu Republike Srbije / Biološki fakultet / Zavod za zaštitu prirode Republike Srbije.
- Stojanović, V., Rilak, S., Jelić, I., Perić, R., Saboljević, M., & Lazarević, P. 2015. Biljke od međunarodnog značaja u flori Srbije. Beograd: Zavod za zaštitu prirode Srbije.
- The Plant List, Version 1. 1 2013. Retrieved from <http://www.theplantlist.org/>.

- Tomić-Stanković, K. 1967. Prilog poznavanju flore Ibarskog Kolašina. Zbornik Filozofskog fakulteta u Prištini, 4, pp. 69-83. B.
- Tomović, G. 2007. Fitogeografska pripadnost, distribucija i centri diverziteta balkanske endemične flore u Srbiji. Univerzitet u Beogradu - Biološki fakultet. Doktorska disertacija.
- Tutin, T.G., Heywood, V.H., Burges, N.A., Moore, D.M., Valentine, D.H., Walters, S.M., Webb, D.A. (Eds.).1972. Flora Europaea 3. Cambridge: University Press.
- Tutin, T.G., Heywood, V.H., Burges, N.A., Moore, D.M., Valentine, D.H., Walters, S.M., Webb, D.A. (Eds.).1980. Flora Europaea 5. Cambridge: University Press.
- WCSP (2017). World Checklist of Selected Plant Families, Facilitated by the Royal Botanic Gardens, Kew. Retrieved from <http://wmsp.science.kew.org>.

# KINETIC-CATALYTIC DETERMINATION OF ULTRAMICRO AMOUNTS OF Co(II) USING 4-HYDROXYCOUMARINE-PERMANGANATE REDOX REACTION

DRAGANA SEJMANOVIĆ<sup>1\*</sup>, RUŽICA MICIĆ<sup>1</sup>, RANKO SIMONOVIĆ<sup>1</sup>

<sup>1</sup>Faculty of Natural Sciences and Mathematics, University of Priština, Kosovska Mitrovica, Serbia

## ABSTRACT

**Determination of Co(II) based on its catalytic effect on the reaction between 4-hydroxycoumarine and potassium permanganate, in the presence of acetate buffer was described. The method development includes optimization of the reagent concentration and temperature. Absorbance of potassium permanganate was measured at 525 nm. The calibration curve was linear in the range of 0.5 - 4 ng/cm<sup>3</sup> of Co(II). The relative standard deviation was in the interval 6.25-2.60 % of the concentration range of 0.6-3 ng/cm<sup>3</sup> Co(II), respectively. The interference effects of foreign ions were determined for the assessment of the selectivity of the method. The proposed method was found to have excellent sensitivity, relatively good selectivity and simplicity.**

**Keywords:** cobalt(II), kinetic method, 4-hydroxycoumarine.

## INTRODUCTION

Cobalt is an essential element in trace amounts for humans and animal as an integral part of the vitamin B<sub>12</sub> complex; also necessary for the synthesis of a number of hormones, neurotransmitters and other compounds (Medina-Escriche et al., 1987). However, in higher concentrations cobalt is toxic to humans, animals and plants. The essentiality of cobalt has also been demonstrated in the environment elsewhere: as a micronutrient for some blue-green algae, required for nitrogen-fixation in legumes, in growth enhancement of some terrestrial plants at low concentration (Kiran et al., 2012). Cobalt is used as a pigment in glass, ceramics and paints; as a catalyst for the petroleum industry and in batteries. Cobalt is also found in low concentration in marine waters.

Although a number of methods are available for the determination of cobalt ions such as flame atomic absorption spectroscopy (FAAS), graphite furnace atomic absorption spectroscopy (GFAAS) (Jiang et al., 2008), inductively-coupled plasma optical emission spectroscopy (ICP-OES) (Mikula et al., 2007; Suleiman et al., 2007), inductively-coupled plasma coupled with mass spectrometry (ICP-MS) (Juvonen et al., 2002). These modern sophisticated sensitive methods are relatively expensive and require time for sample preparation, also can be applied after preliminary treatments such as preconcentration and extraction. Catalytic-kinetic methods have some advantages, including high sensitivity, short analysis time and minimum, low cost and easy available instruments (Mitić et al., 2009; Li, 1998; Safavi et al., 2002). Hence, due to these reasons simple colorimetric methods are still popular. Kinetic methods determined Co(II) as the catalyst of various reactions of oxidation with hydrogen peroxide or KIO<sub>4</sub> as the oxidant and

different organic, aromatic oxy-compound, as the reductant. Different sensitive analytical methods including extractive spectrophotometry (Kamble et al., 2011), non-extractive derivative spectrophotometry, cloud-point extraction (Safavi et al., 2004), electro chemical detection (ECE) coupled with liquid chromatography (Suleiman et al., 2007) and kinetic spectrophotometric methods have been recognized as offering a valuable approach for the trace analysis (Bahram et al., 2012; Naseri et al., 2011; Wang et al., 2003; Ghasemi et al., 1998) of cobalt.

The aim of this study was to develop a simple trace kinetic-spectrophotometric method for the determination of cobalt(II) ions. An indicator reaction (oxidation 4-hydroxycoumarine by KMnO<sub>4</sub>) has not previously been used for the kinetic determination of trace amounts of Co(II). The method is based on the catalytic effect of Co(II) on the oxidation 4-hydroxycoumarine by KMnO<sub>4</sub> in acetate buffer solution at pH=3.8, at 25±0.1°C. Diminution of the colour intensity of the oxidant (KMnO<sub>4</sub>) was followed spectrophotometrically as the change of absorbance(A) in time (t).

## EXPERIMENTAL

### *Reagents and Solutions*

Analytical grade reagents, deionized water and polyethylene vessels were used throughout the study. A solution of KMnO<sub>4</sub> was prepared from an ampoule produced by „Merck" by dissolving in a volumetric flask. Before the experiment, the concentration of the solution was checked spectrophotometrically (at 525 nm). The solution of KMnO<sub>4</sub> was saved in a dark reagent flask.

A 1.25×10<sup>-3</sup> mol/dm<sup>3</sup> solution of 4-hydroxycoumarine (in the text we have marked as 4-OHcoum.) was prepared by dissolving the appropriate amount of the solid compound. To improve its solubility, an equivalent amount of NaOH was

\* Corresponding author: dragana.sejmanovic@pr.ac.rs

added. A stock solution of Co(II) (1000 ppm) was prepared by dissolving 1g of metal of cobalt analytical grade in 50 cm<sup>3</sup> of HCl (1:1) and diluted to 1 dm<sup>3</sup>.

The exact concentration was determined electrogravimetrically from a more concentrated solution. A acetate buffer solution was prepared from 0.2mol/dm<sup>3</sup> CH<sub>3</sub>COOH and 1 mol/dm<sup>3</sup> NaOH solutions.

#### Apparatus

A MA9524 SPECOL 221 (Carl Zeiss-Iskra) spectrophotometer equipped with thermostat system was used for spectrophotometric measurements. A cell of path-length 10mm, were used. The pH was measured by means of a radiometer (PHM 29b pH-meter) equipped with a GK 2311 C combined electrode. All solutions were kept in a thermostatic water-bath („Sutjeska“, type 10) at 25±1°C before beginning the reaction.

#### Procedure

The method continual variations were performed, so the concentrations of the examined reactant was varied in given interval, while others were kept constant.

The selected volumes of the reactants were put into a 10 cm<sup>3</sup> standard flask in the following order: 4-hydroxycoumarine, acetate buffer, standard solution of Co(II) and water to make up exactly to the predetermined volume. The flask was kept in a thermostat for 10 min., and then the solution was made up to the mark with KMnO<sub>4</sub> and water. The content of the flask was mixed well. The cell of the photometer was rinsed well and filled with the prepared solution. Time changes of the absorbance, dA/dt, were measured every 30s over a period of 5-6 min. during the reaction. The dA/dt was proportional to the reaction rate (dc/dt) expressed as:

$$dA/dt = \varepsilon \times l \times dc/dt = \tan \alpha$$

where  $\varepsilon$  is molar absorptivity,  $l$  the cell path-length,  $c$  the concentration of the KMnO<sub>4</sub>,  $\tan \alpha$  the slope of the linear part of the A against t.

The initial concentrations of the reagent solutions after the dilution to 10 cm<sup>3</sup> were: 5×10<sup>-5</sup>-2.5×10<sup>-4</sup> mol/dm<sup>3</sup> of 4-hydroxycoumarine, 4×10<sup>-5</sup>-3.2×10<sup>-4</sup> mol/dm<sup>3</sup> KMnO<sub>4</sub>, 0.5-4 ng/cm<sup>3</sup> Co(II). An unknown concentration of cobalt(II) was calculated from the equation (1).

## RESULTS AND DISCUSSION

The exact mechanism of reaction and the nature of reaction products were not the main interest of our investigation, but only important analytical meaning. As the reaction progresses, the initial red color of the solution fades and the colorless reaction product forms. All spectrophotometric measurements were performed at the wavelength of the absorption maximum of KMnO<sub>4</sub> in acetate buffer (525nm).

#### Effect of the experimental conditions

For finding the optimum experimental conditions, the effect of pH, potassium permanganate concentration, concentration of 4-hydroxycoumarine and concentration of acetate buffer, on the reaction rate were studied by differential variant of the tangent method. The differential variant of the tangent method was used for processing the kinetic data, because there is a linear relation between the absorbance and time during the first 2-5 min. after mixing.

Keeping concentrations of the other reactants constant we studied the effect of pH on the rates of catalytic and non-catalytic reactions in the range of 3.2-5.0.

The results are presented in Fig. 1. Figure 1 shows that there is complicated relationship between the pH and the catalytic and non-catalytic reaction rate in the studied pH range. The best results were obtained for the value pH of 3.80, and this value was selected as the optimum pH value for the system studied. At lower pH values, drastically increases the rate of reactions, and error in the determination of  $\tan \alpha$  becomes larger.

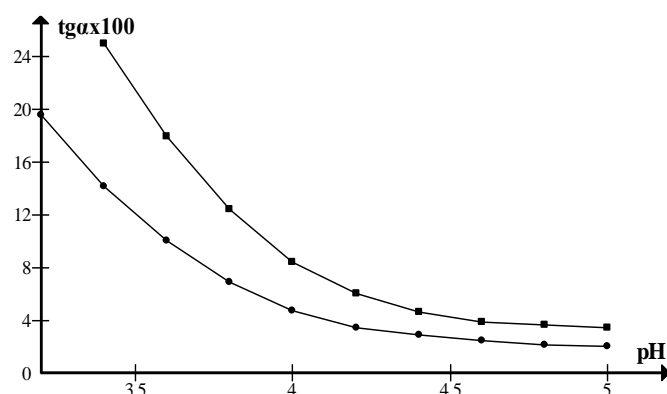


**Figure 1.** Effect of pH on determination of Co(II). Experimental conditions: 2×10<sup>-4</sup> mol/dm<sup>3</sup> of KMnO<sub>4</sub>, 1.5×10<sup>-4</sup> mol/dm<sup>3</sup> of 4-OHcoum., 5ng/cm<sup>3</sup> of Co(II). (■)-catalytic reaction, (●)-non-catalytic reaction.

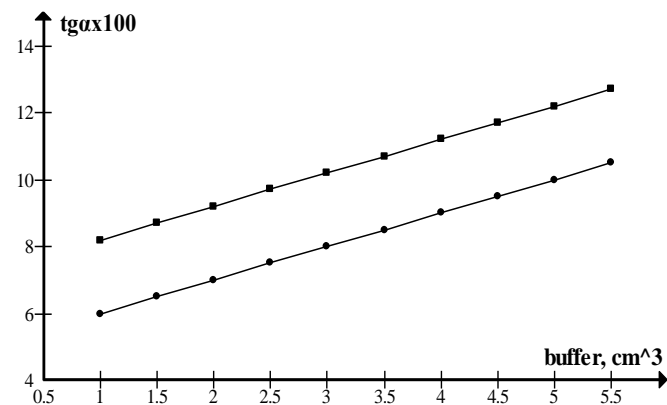


**Figure 2.** Effect of volume of acetate buffer on determination of Co(II). Experimental conditions: 2×10<sup>-4</sup> mol/dm<sup>3</sup> of KMnO<sub>4</sub>, 1.5×10<sup>-4</sup> mol/dm<sup>3</sup> of 4-OHcoum., 5ng/cm<sup>3</sup> of Co(II). (■)-catalytic reaction, (●)-non-catalytic reaction.

The dependence of the volume of acetate buffer on the reaction rate was studied in the range of 1.0 to 5.5 cm<sup>3</sup>. The results are presented in Figure 2. In this interval both reactions show the first order dependence of the volume of acetate buffer. The concentration of acetate buffer:  $6.5 \times 10^{-2}$  mol/dm<sup>3</sup> CH<sub>3</sub>COOH,  $7.3 \times 10^{-3}$  mol/dm<sup>3</sup> acetate ion chose as optimum concentration which respond the volume of 2.5 cm<sup>3</sup> of acetate buffer. At higher concentration the rates of the catalytic and non-catalytic reaction accelerate.

The effect of 4-hydroxycoumarine concentration on the reaction rate was investigated in the concentration range of  $5 \times 10^{-5}$  to  $2.5 \times 10^{-4}$  mol/dm<sup>3</sup> (Figure 3).

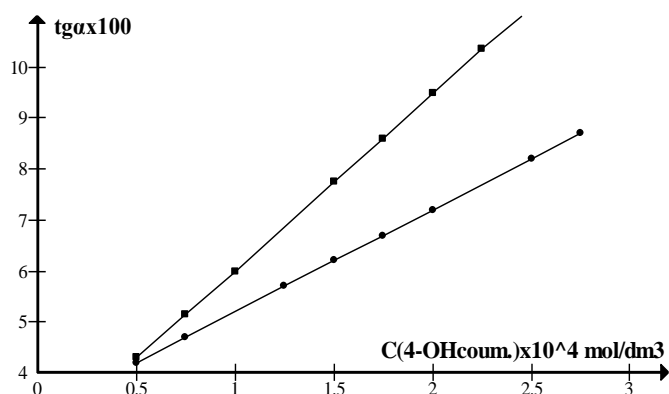


**Figure 3.** Effect of 4-OHcoum. concentration on determination of Co(II). Experimental conditions:  $2 \times 10^{-4}$  mol/dm<sup>3</sup> of KMnO<sub>4</sub>, 5 ng/cm<sup>3</sup> of Co(II), pH=3.8. (▪)-catalytic reaction, (•)-non-catalytic reaction.

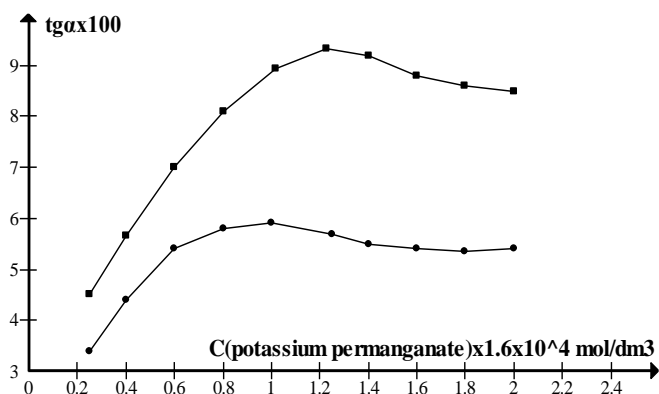


**Figure 4.** Effect of KMnO<sub>4</sub> concentration on determination of Co(II). Experimental conditions:  $1.5 \times 10^{-4}$  mol/dm<sup>3</sup> of 4-OHcoum., 5 ng/cm<sup>3</sup> of Co(II), pH=3.8. (▪)-catalytic reaction, (•)-non-catalytic reaction.

The catalytic and non-catalytic reactions were of the first order with respect to the concentration of 4-hydroxycoumarine. For further work a concentration of 4-hydroxycoumarine of  $1.5 \times 10^{-4}$  mol/dm<sup>3</sup> was selected as the optimum concentration. At higher concentration of 4-hydroxycoumarine absorbance significantly increased when the error of spectrophotometric measurement becomes higher (area of Beer's law validity).

The effect of oxidant concentration on the reaction rate was also investigated. The results are illustrated in Fig. 4. The relationship between the concentration of KMnO<sub>4</sub> and the reaction rate was complex. The reaction order depending on KMnO<sub>4</sub> concentration within the studied concentration of KMnO<sub>4</sub>. For further work a concentration of  $2 \times 10^{-4}$  mol/dm<sup>3</sup> of KMnO<sub>4</sub> was chosen. At higher concentration of  $2 \times 10^{-4}$  mol/dm<sup>3</sup> leads to the formation of insoluble reducing the product of KMnO<sub>4</sub> adding the problem of contamination the cell of the photometer.

#### Calibration graph

For the optimal conditions described above (pH=3.8; C<sub>4-OHcoum</sub>= $1.5 \times 10^{-4}$  mol/dm<sup>3</sup>; C<sub>KMnO<sub>4</sub></sub>= $2 \times 10^{-4}$  mol/dm<sup>3</sup>) a calibration graph was constructed at two different temperatures at  $25 \pm 0.1^\circ\text{C}$  and  $30 \pm 0.1^\circ\text{C}$ . A Co(II) concentration under optimum conditions was varied from 0.5 ng/cm<sup>3</sup> to 4 ng/cm<sup>3</sup>.

Figure 5 shows the corresponding calibration graph, which were used for determination of Co(II) concentration in the interval mentioned. The slopes of the calibration lines (1) and (2) were very similar, however the temperature of  $25 \pm 0.1^\circ\text{C}$  is recommended as appropriated.

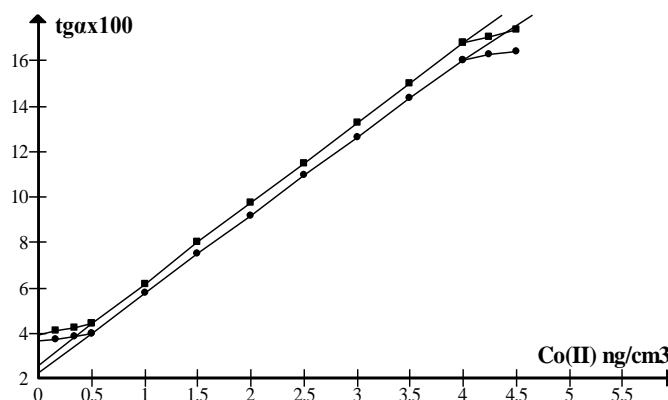


**Figure 5.** Effect of Co(II) concentration on the reaction rate. Experimental conditions:  $2 \times 10^{-4}$  mol/dm<sup>3</sup> of KMnO<sub>4</sub>,  $1.5 \times 10^{-4}$  mol/dm<sup>3</sup> of 4-OHcoum., pH=3.8. (•)-temperature  $25 \pm 0.1^\circ\text{C}$ , (▪)-temperature  $30 \pm 0.1^\circ\text{C}$

The unknown concentration of Co(II) was determined using the following equations which were obtained by the least-squares method:

$$C_{\text{Co(II)}} = (\text{tg}\alpha - 0.026) / 0.0346 \text{ (ng/cm}^3\text{)} \quad (1)$$

The following kinetic equations were deduced on the basis of the graphic correlations obtained for the investigated catalytic and non-catalytic reactions (at constant pH).

For the catalytic reaction:

$$-dc/dt = k_1 \times C_{\text{KMnO}_4}^m \times C_{4\text{-OHcoum}} \times C_{\text{Co(II)}} \quad (2)$$

where m is a variable, k<sub>1</sub> is a catalytic reaction rate constant.

For the non-catalytic reaction:

$$-dc/dt = k_0 \times C_{\text{KMnO}_4}^p \times C_{4\text{-OHcoum}} \quad (3)$$

where  $p$  is a variable,  $k_0$  is non-catalytic reaction rate constant.

Limit of detection (LOD) of the method was calculated as  $(3\sigma/S)$  is  $0.0867 \text{ ng/cm}^3$  and limit of quantification  $(10\sigma/S)$  is  $0.289 \text{ ng/cm}^3$ , with coefficient of determination ( $R^2$ ) of  $0.9998$ .

#### Accuracy and precision

Four sets of working solutions with different concentrations of Co(II) were analyzed under the optimum conditions using a differential variant of the tangent method.

The results for estimated precision and accuracy are summarized in Table 1. The relative standard deviation ranged from  $2.60\%$  to  $6.25\%$  for Co(II) concentration range  $3 - 0.6 \text{ ng/cm}^3$ .

**Table 1.** Accuracy and precision of Co(II) determination

Taken( $\mu$ ) ( $\text{ng/cm}^3$ )	Found( $\bar{x}$ ) ( $\text{ng/cm}^3$ )	n	RSD (%)	$(\bar{x}-\mu)/\mu * 100$
0.60	$0.64 \pm 0.04$	5	6.25	6.60
1.00	$1.02 \pm 0.05$	5	4.90	1.50
2.00	$2.02 \pm 0.05$	5	2.48	1.00
3.00	$3.07 \pm 0.08$	5	2.60	2.33

$\bar{x}$  - mean value  $\pm$  standard deviation;  $\mu$  - true value; RSD - relative standard deviation;  $(\bar{x} - \mu)/\mu * 100$  - accuracy

#### Interference study

To study the selectivity of the method we undertook a systematic study of the effect of foreign ions on the catalytic reaction rate, under the optimal conditions mentioned above, at a constant concentration of Co(II) ( $4 \text{ ng/cm}^3$ ). Each ion was added in eight known concentration ratios ( $10^5:1$ ,  $10^4:1$ ,  $10^3:1$ ,  $10^2:1$ ,  $10:1$ ,  $1:1$ ,  $10^{-1}:1$  and  $10^{-2}:1$ ) against the constant Co(II) concentration of  $4 \text{ ng/cm}^3$ .

The presence of  $\text{K}^+$  and  $\text{Cl}^-$ , in the ratio  $10^5:1$ ,  $\text{NH}_4^+$  and  $\text{SO}_4^{2-}$ , in the ratio  $10^4:1$ ,  $\text{Mg}^{2+}$ ,  $\text{Cu}^{2+}$ ,  $\text{Mn}^{2+}$ ,  $\text{I}^-$ , in the ratio  $10^3:1$ ,  $\text{Ca}^{2+}$ ,  $\text{Ba}^{2+}$ ,  $\text{Sr}^{2+}$ ,  $\text{Pb}^{2+}$ ,  $\text{Cd}^{2+}$ ,  $\text{Sn}^{2+}$ , in the ratio  $10^2:1$  has practically no influence on the reaction rate. The presence of  $\text{Fe}^{3+}$ , in the ratio  $10^2:1$ ,  $\text{Zn}^{2+}$ , in the ratio  $10^{-1}:1$  and  $\text{Ni}^{2+}$ , in the ratio  $10:1$  further catalyzes the determination of cobalt.  $\text{SCN}^-$ ,  $\text{PO}_4^{3-}$ ,  $\text{C}_2\text{O}_4^{2-}$ , in the ratio  $10:1$  have a slight inhibiting effect. The results reveal that proposed method for Co(II) determination have a very good selectivity.

#### CONCLUSION

Development of the fast, simple, inexpensive and applicable kinetic-spectrophotometric method for the determination of Co(II) traces were reported in this paper. The method has very low detection limit, which falls within the range of more sensitive methods for Co(II) determination. Therefore, this method could be appropriate for the fast monitoring of traces

amounts of Co(II) in different samples, with available and cheap chemicals and instrumentation.

#### REFERENCES

- Bahram, M., & Khezri, S. 2012. Multivariate optimization of cloud point extraction for the simultaneous spectrophotometric determination of cobalt and nickel in water samples. *Anal. Methods*, 4(2), pp. 384-393. doi:10.1039/c2ay05527a
- Ghasemi, J., Niazi, A., & Safavi, A. 2001. Simultaneous catalytic determination of cobalt, nickel and copper using resazurine sulfide reaction and partial square s calibration method. *Analytical Letters*, 34(8), pp. 1389-1399. doi:10.1081/al-100104162
- Jiang, H., Qin, Y., & Hu, B. 2008. Dispersive liquid phase microextraction (DLPME) combined with graphite furnace atomic absorption spectrometry (GFAAS) for determination of trace Co and Ni in environmental water and rice samples. *Talanta*, 74(5), pp. 1160-1165. doi:10.1016/j.talanta.2007.08.022
- Juvonen, R., Lakomaa, T., & Soikkeli, L. 2002. Determination of gold and the platinum group elements in geological samples by ICP-MS after nickel sulphide fire assay: difficulties encountered with different types of geological samples. *Talanta*, 58(3), pp. 595-603. doi:10.1016/s0039-9140(02)00330-2
- Kamble, G.S., Ghare, A.A., Kolekar, S.S., Han, S.H., & Anuse, M.A. 2011. Development of an reliable analytical method for synergistic extractive spectrophotometric determination of cobalt(II) from alloys and nano composite samples by using chromogenic chelating ligand. *Spectrochimica Acta Part A: Molecular and Biomolecular Spectroscopy*, 84(1), pp. 117-124. doi:10.1016/j.saa.2011.09.015
- Kiran, B.V., Dubey, S., & Rao, B.S. 2012. Kinetic-Spectrophotometric Determination of Co(II) in Vegetable Samples by Using indigo-carmin. *International Journal of Pharmaceutical Research*, 4(3), pp. 64-68.
- Li, Y. 1998. Catalytic kinetic spectrophotometric determination of trace cobalt(II). *Huaxue Fence*, 34, pp. 408-409.
- Medina-Escriche, J., Hernández-Llorens, M.L., Llobat-Estelles, M., & Sevillano-Cabeza, A. 1987. Determination of vitamin B12 as cobalt by use of a catalytic spectrophotometric method. *The Analyst*, 112(3), pp. 309-311. doi:10.1039/an9871200309
- Mikuła, B., & Puzio, B. 2007. Determination of trace metals by ICP-OES in plant materials after preconcentration of 1,10-phenanthroline complexes on activated carbon. *Talanta*, 71(1), pp. 136-140. doi:10.1016/j.talanta.2006.03.041
- Mitić, S.S., Micić, R.J., & Budimir, M.V. 2009. Highly Sensitive Determination of Traces of Co(II) in Pharmaceutical and Urine Samples Using Kinetic-Spectrophotometric Method. *Analytical Letters*, 42(7), pp. 935-947. doi:10.1080/00032710902809017
- Naseri, A., Bahram, M., & Mabhooti, M. 2011. A second-order standard addition method based on the data treatment by calculation of variation matrix of kinetic systems analyzed by MCR-ALS. *Journal of the Brazilian Chemical*

- Society, 22(11), pp. 2206-2215. doi:10.1590/s0103-50532011001100026
- Safavi, A., Abdollahi, H., Hormozi, N.M.R., & Kamali, R. 2004. Cloud point extraction, preconcentration and simultaneous spectrophotometric determination of nickel and cobalt in water samples. *Spectrochimica Acta Part A: Molecular and Biomolecular Spectroscopy*, 60(12), pp. 2897-2901. doi:10.1016/j.saa.2004.02.001
- Safavi, A., Abdollahi, H., & Nezhad, M.R.H. 2002. Indirect kinetic spectrophotometric determination of Co (II) based on the reaction with iron (III) in the presence of 1,10-phenantroline. *Spectroscopy Letters*, 35(5), pp. 681-688. doi:10.1081/sl-120014939
- Suleiman, J.S., Hu, B., Xulli, P., Huang, C., & Jinag, Z. 2007. Nanometer sized zirconium dioxide microcolumn separation/preconcentration of trace metals and their determination by ICP-OES in environmental samples and biological samples. *Microc. Acta*, 159(3-4), pp. 379-385.
- Wang, X. 2003. Catalytic spectrophotometric determination of trace cobalt based on oxidation of alizarin green by H<sub>2</sub>O<sub>2</sub>. *Yejin Fenxi*, 23, pp. 17-18.

# STATISTICAL ANALYSIS OF THE PRODUCTION OF BLUESTONE FROM GRANULATES (ELEMENTARY COPPER) BY OXIDATION WITH HYDROGEN PEROXIDE MIXED WITH STOCK SOLUTION OF BLUESTONE AND SULFURIC ACID

DRAGOSLAV ILIĆ<sup>1\*</sup>

<sup>1</sup>High Medical School of Professional Studies, Čuprija

## ABSTRACT

The technological process for the production of bluestone consists of three phases: the melting of waste copper in stationary flame furnaces, the granulate dissolution with sulfuric acid in the presence of the stock solvent of copper sulphate and hydrogen peroxide, and the crystallization of copper sulphate from a saturated blue stone solution in natural baths for crystallization. This paper describes the production of bluestone using hydrogen peroxide as an oxidation agent in a mixture of sulfuric acid and a stock solution of copper sulphate as well as the statistical description and graphic representation of the dissipation of copper Cu in (%), lead Pb in (%) and nickel Ni in (%) in the production of copper sulphate. On the basis of the statistical analysis, the value of copper Cu in (%) ranged from 70.3 to 99.78%, with an arithmetic mean of 91.88800%, which shows that the value of copper only in point 4 was below 80%.

**Keywords:** Bluestone, Copper, Copper sulphate, Oxidation.

## INTRODUCTION

The most important copper salt is copper sulphate of the chemical formula  $\text{CuSO}_4 \times 5\text{H}_2\text{O}$ .

The crystalline form of bluestone is blue, which comes from the presence of 5 molecules of water. The crystalline water is easily lost by heating. At 100°C blue crystals lose 4 molecules of water, and at 230°C the last water molecule is lost and a white anhydrous salt is formed, which is very hydrophobic and absorbs water from the atmosphere, and again turns into blue crystalhydrate (Aufl 11 Band, 1960).

Blue stone is used mostly as an additive for the synthesis of premixes for fodder, it is also used as an ore flotation reagent, as well as raw material for the production of other copper salts used as plant protection agents such as: base copper carbonate, copper oxychloride, bacroxysulphate.

Research of physical-chemical properties of copper and copper nanoparticles is given in papers (Chen et al., 2014, Gavriluta et al., 2017, Hu et al., 2017, Kaluđerović-Radoičić et al., 2015, Meng et al., 2016, Vlcek & Pohanka, 2018, Zuev et al., 2016).

## THEORETICAL PART

For the production of bluestone, copper of different quality and origin is used, sulfuric acid, solvents and oxidation agents.

The technological process itself can be classified into three phases:

**First phase:** Melting of waste copper in stationary flame furnaces. This phase also includes purifying the copper from a impurities such as iron, tin, lead, nickel, cadmium, selenium zinc and aluminum. Purification yields a pure copper granulate.

**Second phase:** The dissolution of the granulate with sulfuric acid in the presence of the stock solution of copper sulfate, and an oxidizing agent with heating.

**Third phase:** Crystallization of bluestone from a saturated solution of bluestone in natural way in baths for crystallization.

The following tasks are foreseen in this paper:

- The dissolution of granulates or elementary copper in diluted acid in the presence of oxygen as an oxidizing agent takes place very slowly, the oxidation lasts for 20 days at a temperature of 80°C. In this paper, we took a stronger oxidizing agent hydrogen peroxide of the concentration of 20% of the technical quality. The quantity of hydrogen peroxide added is 30% of the total weight of spraying solution. We controlled how long the reaction is accelerating and how much is shorter the dissolution time of the granules in the presence of peroxide.
- Analyze copper granulates on the content of copper, iron, lead, cadmium, tin, zinc and aluminum.
- Performing an analysis of copper slag resulting from the process of refining the copper on the same metals.
- Conducting the analyses of the finished product on the contents of the same elements.

\* Corresponding author: dragoslavilicks@gmail.com

## EXPERIMENTAL PART

The experimental part of this paper was done at the factory CI Župa from Kruševac.

Approximately 7 tons of granulates previously measured on a technical scale are inserted in a 7.5 m<sup>3</sup> tower. The dilution of the granulates is done with a diluted sulfuric acid of 200g/l concentration. The sulfuric acid used is of a technical quality. About 20% of the stock blue stone solution (which remained from the previous production) is added to the solution, the concentration of copper sulphate in the matrix is 20% . The matrix density is  $\rho=1.20 \text{ g/cm}^3$ .

Also, about 20% of hydrogen peroxide was added, of the technical quality and of the concentration about 35%

After batching and preparation of the spraying solution, the granulate is heated with water vapor through the ejector at a temperature of 80°C. After reaching the temperature, the spraying of the granulates is started. The dosing of the solution is continuous and is carried out by free fall through the Segner

wheel that rotates due to the reaction force of the solution, thus allowing the uniform spraying of the entire surface of the copper granulate evenly. The solution passes through a mass of heated copper granulate, dissolves the copper and at the bottom of the tower as shown in the Figure 1 the solution of the cuprous sulphate is distinguished. At the same time, the tower is constantly replenished with new quantities of copper granulate, so the process is continuous. At the beginning of the dissolution of the granulates, the concentration of the blue stone is small, so the solution is recirculated until the density of the solution is 1.36-1.30 g/cm<sup>3</sup>, and the free sulfuric acid content in the solution is not 20 g/cm<sup>3</sup>. If the density of the solution is lower or the content of the free sulfuric acid is higher, it is a sign that the dosage of the solution is enhanced and it is necessary to reduce the dosing rate of the solution, which allows longer contact of the reactants and increase of the copper sulphate solution.

A tower for the production of a blue stone solution is shown in Fig. 1.

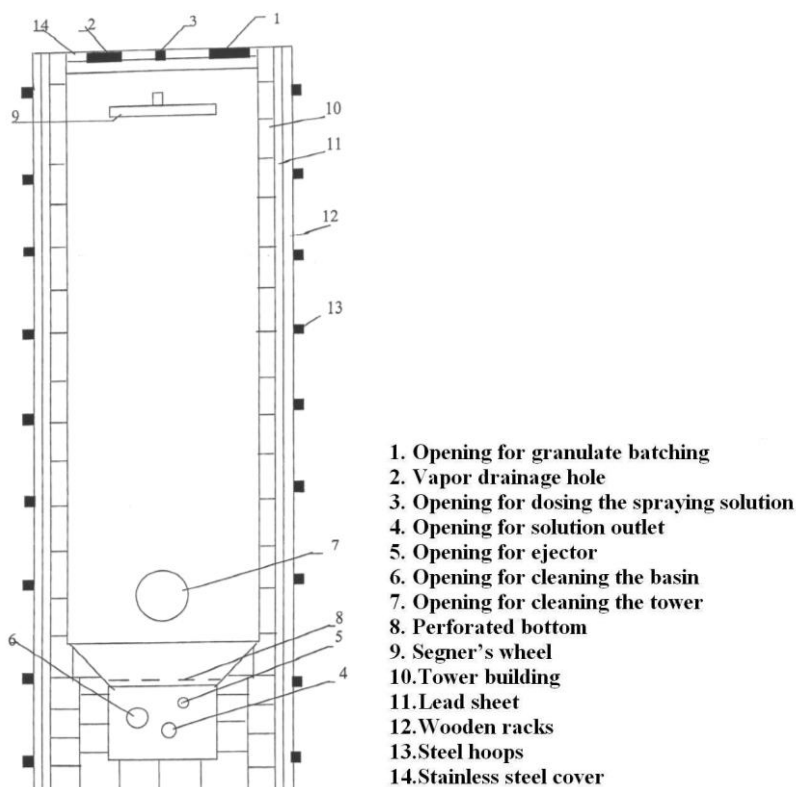
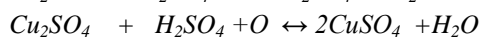
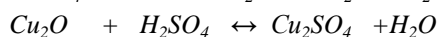
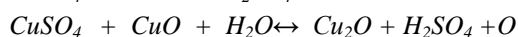
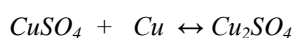


**Figure 1.** The tower for the production of a blue stone solution.

The role of copper sulphate from the stock that is mixed with the sulfuric acid solution and the hydrogen peroxide is to convert the cuprous sulphate into cupric sulphate:



The reaction is exothermic and the temperature of the reaction is increased by the presence of hydrogen peroxide, which causes a lower energy consumption and increases the rate of dissolution of the granulates, thus reducing the technological process of producing blue stone (Kirk-Othner, 1965).

The rate of dissolution of copper granules, that is, the rate of copper sulphate production depends on several factors:

The size of the surface of the copper granulate and the spraying solution. The maximum contact surface is achieved if the granules are hallow with as thin walls as possible.

From the presence of  $\text{H}_3\text{O}^+$  ions in solution. By examining the conductivity of the sulfuric acid solution and the dissolved copper sulphate solutions, it was found that the maximum presence of  $\text{H}_3\text{O}^+$  ions is between 130-160 g/l of sulfuric acid (Jovanović & Jovanović, 1970).

From the rate of diffusion of hydrogen ions from sulfuric acid. The diffusion velocity at the stationary solutions is for each agent one constant. It can be increased by initiating a solvent or solute or by initiating both reaction subjects. All of this relates to the condition of the complete contact of the reactants. When dissolving the copper granulate, the solution for dissolution moves through the Segner wheel and further movement from the top to the bottom of the tower by free fall, i.e. by gravity, passing over the granules of copper with which the tower is filled and which is immobile. In this way, the maximum speed is reached, beyond which the higher speed does not produce a greater effect.

From the coating of copper granules with sludge, which is separated during the dissolution of granules derived from sulfuric acid and copper granulates. This phenomenon reduces the rate of dissolution of copper granules because the created sludge isolates the granules from the solvents. The partial removal of sludge during operation of the tower is done by closing the valve a solution of copper sulphate solution, where the level of the solution in the tower is lifted and the granules are sunk, and the

water vapor flowing through the tower rinses the settled sludge (Dibina, 1962, Vssermann, 1962).

## RESULTS AND DISCUSION

The density of the solution from the towers which flows into the collecting basins which are heated with steam is 1.36-1.40 g/cm<sup>3</sup>. The content of copper sulphate is 680-700 g/l containing 5-10 g/l of free sulfuric acid. This solution, as mentioned earlier, goes into the sedimentation tanks built of reinforced concrete, clad with steel sheets and resistant to sulphates. Sedimentation tanks are heated by the respective heaters through which water vapor is flowing to maintain a temperature of 80 degrees. Upon standing of the solution in the reservoirs, the solution is purified by settling the impurities. From the solution, a higher density of 1.46 g / cm<sup>3</sup> is achieved by heating the solution, which enables the rapid crystallization of the blue stone. The precipitation of the solution is about 24 hours. This solution is transported by free fall into baths for crystallization of blue stone. This is natural crystallization and the time depending on the temperature is 10 to 15 days.

Table 1 shows the results of the analysis of the used granulate for the production of blue stone, and Table 2 a statistical description of the data from Table 1 is shown.

**Table 1.** Results of the analysis of the used granulate for the production of blue stone

No.	Cu (%)	Fe (%)	Pb (%)	Ni (%)	Cd (pmm)	Sn (%)	Zn (pmm)	Al (pmm)
1	87.81	0.033	0.4985	0.0795	3.8	/	95	39
2	97.82	0.005	0.1711	0.0232	/	/	67	20
3	90.70	0.004	0.7336	0.1753	2.2	/	33	44
4	70.30	0.003	0.5729	0.1051	/	0.0485	42	66
5	83.49	0.005	1.1899	0.0600	/	0.0775	75	22
6	97.94	0.002	0.2975	0.0179	2.3	0.0070	50	70
7	99.65	0.002	0.712	0.1215	1.6	0.0144	41	/
8	89.91	0.003	0.1788	0.0598	3.9	0.0137	41	40
9	94.72	0.004	0.8537	0.0510	6.1	0.0245	60	20
10	99.09	0.004	0.4140	0.0250	6.6	0.0234	77	44
11	99.78	0.004	0.8845	0.0313	/	0.0290	70	37
12	92.05	0.005	0.3570	0.0196	4.2	0.0125	48	21
13	91.93	0.003	0.5883	0.0547	/	0.0201	60	/
14	84.55	0.002	0.2602	0.0123	12.5	0.0146	33	/
15	98.5	0.003	1.1388	0.1040	/	0.0161	54	40
16	95.03	0.004	1.2403	0.0242	/	0.0196	67	/
17	96.69	0.006	0.4158	0.0191	22.2	0.0121	111	40
18	82.71	0.009	0.8493	0.0484	8.4	0.0315	103	42
19	93.36	0.002	2.0035	0.0339	/	0.017	78	/
20	91.73	0.002	0.958	0.2485	/	0.0178	39	/

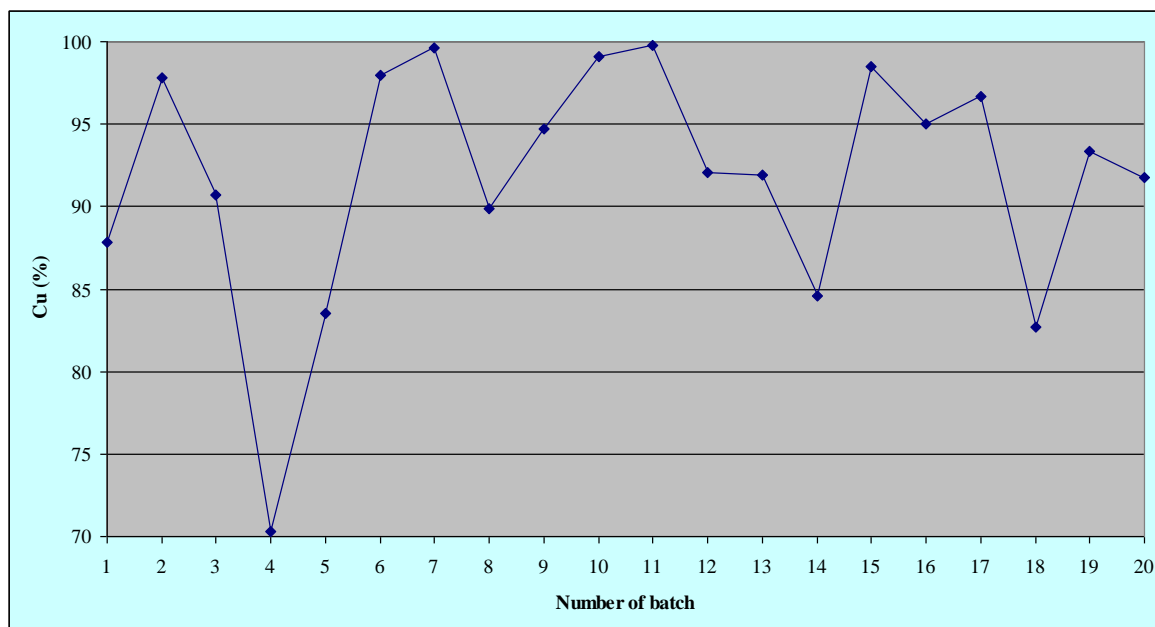
**Table 2.** Statistical description of the results of the analysis of the used granulate for the production of blue stone

Measures	Sign	Cu (%)	Fe (%)	Pb (%)	Ni (%)	Cd (pmm)	Sn (%)	Zn (pmm)	Al (pmm)
Sample size	N	20	20	20	20	20	20	20	20
Minimum	Min	70.3	0.002	0.1711	0.0123	0	0	33	0
Maximum	Max	99.78	0.033	2.0035	0.2485	22.2	0.0775	111	70
Range	Rx	29.48	0.031	1.8324	0.2362	22.2	0.0775	78	70
Total	Sum	1210.05	0.051	10.1422	0.7318	63.9	0.2519	841	284
Mean	Aver	91.88800	0.00525	0.71589	0.06572	3.69000	0.01997	62.20000	28.68421
Geometric mean	GM	91.58443	0.00388	0.59033	0.04697			58.42917	
Harmonic mean	HM	91.25448	0.00334	0.47585	0.03521			54.93846	
Median	Me	92.705	0.004	0.65015	0.0497	1.9	0.01655	60	37
Std. deviation	SD	7.36174	0.00675	0.44854	0.06038	5.56340	0.01774	22.75638	21.95210
Variance	Var	54.19528	0.00005	0.20119	0.00365	30.95147	0.00031	517.85263	481.89474
Coef. of variation	CV	8.01165	128.57607	62.65546	91.88070	150.76978	88.86427	36.58581	76.53026
Skewness	Sk	-1.41867	4.02983	1.22132	1.84806	2.27596	1.97364	0.66778	0.10557
Kurtosis	Ku	2.55663	17.12341	2.15899	3.57508	5.93995	5.32764	-0.27350	-0.74556

The table 1 shows clearly that the heavy metal granulate contains the highest concentration of lead. Other impurities are not represented in large concentrations, which means that refining or separation of impurities by melting or refining is performed well.

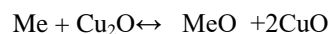
Copper content was determined electrogravimetrically and all other metals on AAS (PERKIN-ELMER1100).

Primes in the melted copper are separated as an sludge that is removed from the surface of melted copper. Copper values in Cu granulate (%) ranged from 70.3 to 99.78% (Fig. 2). The value of the arithmetic mean of copper Cu in (%) was 91.88800%, the geometric mean was 91.58443%, the harmonic mean was 91.25448%, the median was 92.705%, and the standard deviation was 7.36174.

**Figure 2.** Graphic representation of the copper content Cu in (%) in 20 successive copper granulate batches

In order to better remove the heavy metals, as the melting agent the quartz sand is added, and in addition, the air is blown into the furnace to oxidize the metal. The oxidation is also done by the oxygen crossing from the cuprous oxide to the present metals.

Metal impurities react as follows:



This reaction takes place until a balance is established.

Lead is easily oxidized to PbO. Lead oxide partially evaporates and the remaining greater part falls to the bottom of the furnace and represents the biggest problem of removal from the granules, since it is specifically heavier than copper,  $\rho_{\text{Pb}}$  is  $9.2 \text{ g/cm}^3$ , and  $\rho_{\text{Cu}} = 8.3 \text{ g/cm}^3$ , for this reason it is very difficult to remove the lead from melted copper, which is manifested by increased lead content in the finished product. To completely remove lead from molten copper, we need a second melting agent. The removal of the increased content of lead is performed

by adding quartz sand to the lead in the furnace before the beginning of the refining to pull the lead and leave the lead as a slag. The results are good so that the finished product contains satisfactory values.

The values of lead Pb in (%) ranged from 0.1711 to 2.0035% (Figure 3). The value of the arithmetic mean of lead Pb in (%) was 0.71589%, the geometric mean was 0.59033%, the harmonic mean was 0.47585%, the median was 0.65015%, and the standard deviation was 0.44854.

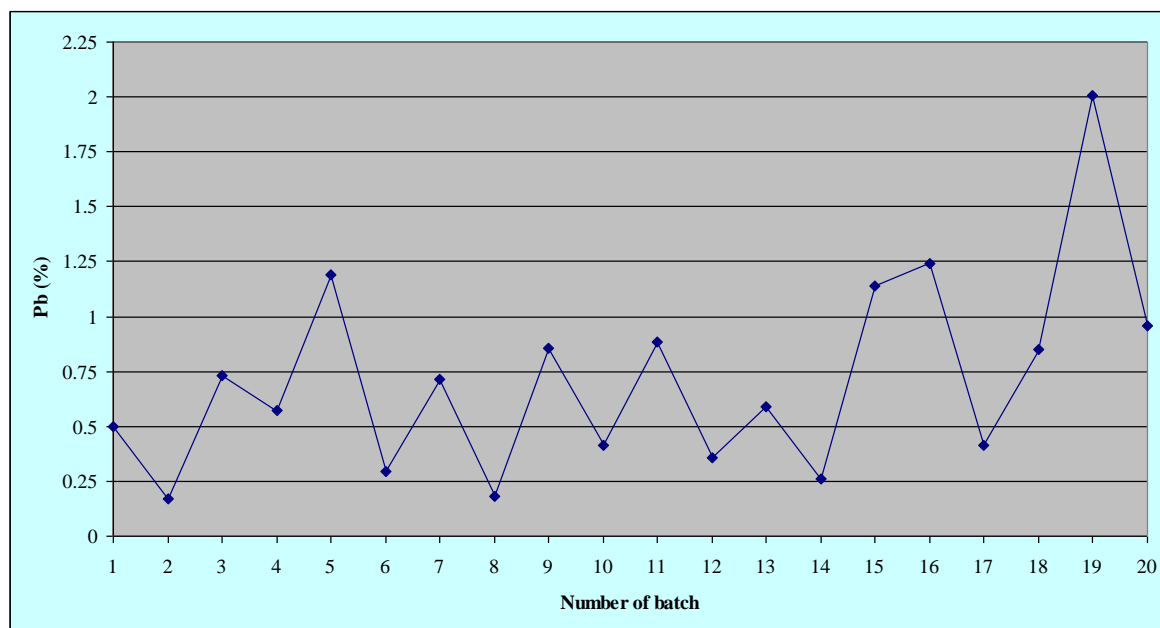


**Figure 3.** Graphic representation of the lead content Pb in (%) in 20 successive copper granulate batches.

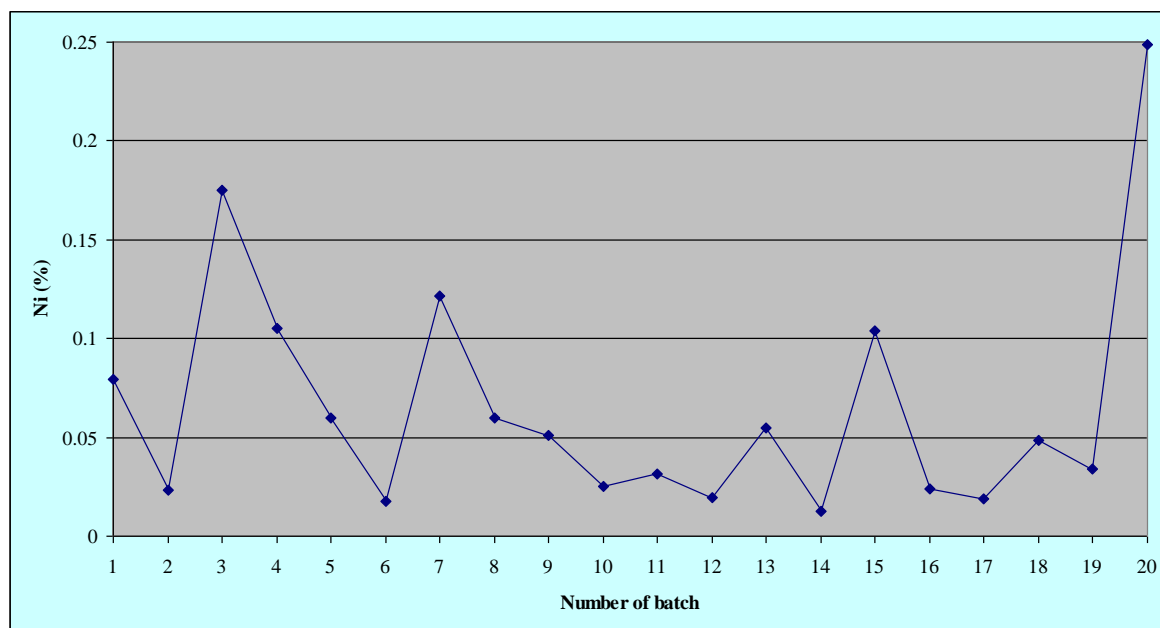


**Figure 4.** Graphic representation of the Nickel content Ni in (%) in 20 successive copper granulate batches.

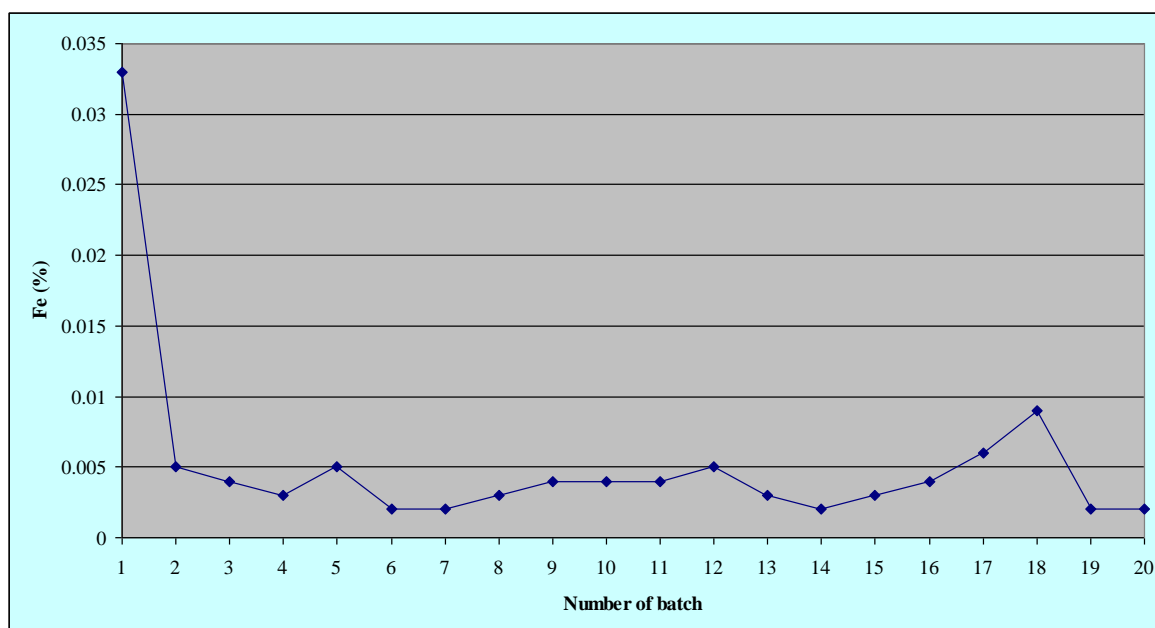


**Figure 5.** Graphic representation of the Ferrum content Fe in (%) in 20 successive copper granulate batches.

The nickel values Ni in (%) ranged from 0.0123 to 0.2485% (Figure 4). The value of the arithmetic mean of nickel Ni (%) was 0.06572%, the geometric mean was 0.04697%, the harmonic mean was 0.03521%, the median was 0.0497% and the standard deviation was 0.06038.

Iron ferrum values Fe in (%) ranged from 0.002 to 0.033% (Figure 5). The value of the arithmetic mean of Ferrum, Fe in (%) was 0.00525%, the geometric mean was 0.00388%, the harmonic mean was 0.00334%, the median was 0.004%, and the standard deviation was 0.00675.

Copper slag occurs as a by-product in the production of blue stone. It is formed by forming a slag in the furnace from the melting agent and a mixture of oxides of metal and copper. It is removed from the furnace, but thereat incorporated copper is also extracted.

Table 3 gives the content of copper and other impurities in the slag.

**Table 3.** The content of copper and other impurities in the slag

No.	Cu (%)	Fe (%)	Pb (%)	Ni (%)	Cd (ppm)	Sn (%)	Zn (%)	Al (%)
1	17.51	15.34	0.793	0.09	6.1	1.133	2.173	0.86
2	7.83	28.08	0.074	0.12	/	/	0.95	0.84
3	16.39	6.287	1.153	0.11	/	1.01	1.33	1.46
4	5.655	4.05	0.04	0.01	/	0.055	0.186	0.23
5	18.06	18.81	0.22	0.07	4.6	0.186	0.245	1.77
6	46.0	17.92	4.55	0.29	25.0	3.01	11.11	0.15
7	30.44	3.26	1.84	0.13	5.5	0.88	3.29	0.19

As it can be seen, there is a rather great copper content in the slag. The goal is to obtain a slag with less copper content.

After finishing the process of dissolving the granules, settling the blue stone solution in the deposition tanks and achieving the density of the solution of 1.46 g/cm<sup>3</sup>, the solution is transferred to natural crystallizers. The crystallisers are about 9 m<sup>3</sup> in volume and are made of acid-resistant steel material 4574. The crystallization takes 10-15 days depending on weather conditions. Crystals obtained by natural crystallization are large, monolithic and are distributed along the walls and bottom of the

bath. After the completion of the crystallization process, the syphoning of the stock solution above the crystals is carried out and put into special reservoirs.

After that the crystals are removed from the bath and centrifuged. Centrifuge is vertical by type. It consists of an outer drum that collects the stock solution, the conical shutter for emptying, the braking mechanism. The centrifuge operation is discontinuous (batched).

The centrifugation time depends on the amount of moisture and free sulfuric acid we want to have in the finished product,

usually the centrifugation time is about 30 min. Together with centrifuging, the washing of crystals with communal water is done.

After the completion of the centrifugation process, natural drying of the crystals of blue stone is done. Given the increasing commercial demands that the moisture content of the crystal is kept as small as possible (0.05-0.07%), we dry the crystal for so

long and in the final product we have obtained moisture in this range.

After the completion of the drying process, we made an analysis of the blue stone (finished product) to the following parameters from several samples.

Table 4 gives some results of the analysis of the finished product from the warehouse.

**Table 4.** Results of the analysis of the finished product from the warehouse

No.	CuSO <sub>4</sub> 5H <sub>2</sub> O (%)	Fe (ppm)	Pb (ppm)	Ni (ppm)	Cd (ppm)	Al (ppm)	Zn (ppm)	Sn (ppm)	As (ppm)	slobodna H <sub>2</sub> SO <sub>4</sub> K	Vlaga (%)
1	98.74	297	40.0	25.0	0.8	7.9	62.4	15.8	/	0.05	0.5
2	99.11	299	85.0	35.2	1.4	19.9	51.8	27.9	/	0.06	0.6
3	98.11	297	90.0	25.9	1.4	7.8	62.4	15.8	/	/	0.65
4	99.60	200	68.0	35.4	0.7	9.9	/	/	/	0.07	0.63
5	99.07	337	74.9	56.0	1.0	/	69	19.7	0.23	0.06	0.64
6	99.12	297	78.6	70.5	0.8	/	/	/	/	0.065	0.7
7	99.05	269	85.0	73.4	0.7	/	/	/	0.22	0.03	0.55
8	99.12	180	91.0	89.0	0.8	/	/	/	0.20	/	0.5
9	99.23	170	66.0	90.0	0.8	/	/	/	0.21	/	0.4

Quality control of the finished product was done at each 5 t of finished product.

The analysis of the content of blue stone (copper) was performed by electrogravimetry and titration with thiosulphate (iodometric).

The heavy metal analysis was performed on the atomic absorption spectrophotometer (perkin -elmer)

Mercury is analyzed on AAS using hydride technique.

Free sulfuric acid analysis was performed by titration with sodium hydroxide.

The moisture content was carried out by drying at a temperature of 105 °C (gravimetrically).

## CONCLUSION

In this paper, we have demonstrated that using hydrogen peroxide at a concentration of 20% as the oxidation agent mixed with a sulfuric acid solution of 200 g/l of the stock blue stone solution (25% of blue stone) results in a very rapid dissolution of the granulates than when the oxidation is carried out only with oxygen. This results in a significantly shorter duration of the reaction -instead of 20 days the reaction per tower was been completed within 10 days.

The shorter time of dissolving granulates has a huge significance in the energy-fluids saving, water vapor, and therefore the time of production of blue stone is significantly reduced.

The solution obtained by dissolving the granulate is of substantially better quality than the solution obtained without the presence of peroxide. Using peroxide we do not have an

insoluble residue when dissolving the granulates, which results in a significantly shorter time of settling, i.e. clarification of the solutions in the precipitators, the foreign ions do not penetrate using peroxide solution to contaminate the solution.

The amount of sludge at the bottom of the basin is considerably smaller, which is very important because the deposit is an ecological problem that the plant has to solve.

It is most important that the quality of the finished product of blue stone is satisfactory.

The table shows that all parameters meet the requirements that are stickt and that such a blue stone can be used as an additive for the preparation of premixes for fodder.

In the final product, we have slightly increased lead content compared to other metals, but the results are within reasonable limits, which resulted from the suggestion that, before each refining at the very bottom of the flame furnace, a small amount of the silicon dioxide solvent is added, which leads the lead as a heavier metal than copper at the surface of melted copper.

## REFERENCE

- Chen, H., Zheng, X., Chen, Y., Li, M., Liu, K., & Li, X. 2014. Influence of Copper Nanoparticles on the Physical-Chemical Properties of Activated Sludge. PLoS One, 9(3), p. 92871. doi:10.1371/journal.pone.0092871
- Dibina, P.V. 1962. Tehnologija mineralnih solej. Goshimizdat, pp. 448-471.
- Gavriluta, A., Fix, T., Nonat, A., Slaoui, A., Guillemoles, J., & Charbonnière, L.J. 2017. Tuning the chemical properties of europium complexes as downshifting agents for copper indium gallium selenide solar cells. Journal of Materials

- Chemistry A, 5(27), pp. 14031-14040. doi:10.1039/c7ta02892j
- Hu, S., Wu, Y., Yi, N., Zhang, S., Zhang, Y., & Xin, X. 2017. Chemical properties of dissolved organic matter derived from sugarcane rind and the impacts on copper adsorption onto red soil. *Environmental Science and Pollution Research*, 24(27), pp. 21750-21760. doi:10.1007/s11356-017-9834-3
- Jovanović, L.J.S., & Jovanović, S.M. 1970. Osnovi kvalitativne hemijske analize. Beograd: Naučna knjiga.
- Kaluđerović-Radoičić, T., Radović, I., Ivanović, M., Rajić, N., & Grbavčić, Ž. 2015. Proračun i optimizacija procesa proizvodnje bakar(II)-sulfat-monohidrata iz bakar(II)-sulfat-pentahidrata u sušnicama sa fluidizovanim slojem. *Hemijska industrija*, Vol. 69, Issue 3, pp. 275-286.
- Kirk-Othner, 1965. *Encyclopedia of Chemical Technology*. Sec.ed. vol. 6, pp. 276-278.
- Meng, D., Chen, H., & Xue, G. 2016. Interaction effects of typical PPCPs and copper nanoparticles on physical-chemical properties. *Huagong Xuebao/CIESC Journal*, Vol. 67, Issue 10, pp. 4455-4460.
- Ulmanns enciklopedie der technishen Chemie 1960. Aufl 11 Band. 3. pp. 246-250.
- Vlček, V., & Pohanka, M. 2018. Adsorption of Copper in Soil and its Dependence on Physical and Chemical Properties. *Acta Universitatis Agriculturae et Silviculturae Mendelianae Brunensis*, 66(1), pp. 219-224. doi:10.11118/actaun201866010219
- Vssermanm, I.M. 1962. Proizvodstvo mineraljnih soli. Gshimizdat, pp. 132-189.
- Zuev, K.V., Perevalov, V.P., Vinokurov, E.G., Zhigunov, F.N., & Koldaeva, T.Y. 2016. Physical-Chemical Properties of Modified Copper-Phthalocyanine and Its Aqueous Dispersions. *Macroheterocycles*, 9(3), pp. 250-256. doi:10.6060/mhc160212z

# CULTURAL-GEOGRAPHIC DETERMINANTS OF JERUSALEM

JOVO MEDOJEVIĆ<sup>1\*</sup>

<sup>1</sup>Faculty of Natural Science and Mathematics, University of Priština, Kosovska Mitrovica, Serbia

## ABSTRACT

**Culture and cultural phenomena are always in the focus of studying cultural geography. The study of Jerusalem from the aspect of supranational spread of culture is a special challenge. The cultural-geographical determinants of Jerusalem represent the features seen through the factors of time and space in which Jerusalem became and survived. The study of the morphology of cultural-geographical determinants in Jerusalem represents scientifically study of the relationship between man and his environment, the man's belief and application of perception of cultural-geographic determinants.**

**Keywords:** Cultural-geography, Jerusalem, pilgrimage.

## INTRODUCTION

The empirical determination of cultural-geographical determinants of Jerusalem was seen as a very complex cultural system of all three great monotheistic religions: Judaism, Christianity and Islam. By connecting all these three aspects, you can see what place Jerusalem has had in all the epochs of civilization since creation until the present day. The cultural and geographical determinants of Jerusalem construct an original and unique cultural pattern in the function of understanding of Jerusalem as a universal aspect of culture.

## MATERIAL AND METHODS

Methodological research is based on explicitly-qualitative methods applied in the field of cultural geography. Socio-geographical methodology was used to understand the space of Jerusalem and its incorporation in geographical science. Also, the reflection method of historical research of representative examples of cultural and historical monuments of Jerusalem has a goal to indicate transcendental reflection of the God's existence according to the belief of Jews, Christians and Muslims. Methodology of sacral geography has for goal to point out the relation of culture and space, and to consider these relationships through the prism of religious traditions that always have a certain geographical component.

## THE COMPLEX OF THE CULTURAL SYSTEM OF JERUSALEM

There are hundreds of names for God and Jerusalem. One of these names is Salim (Shalem), which was first read from a tile found in Syria five thousand years ago. And in the Holy Bible, Jerusalem has been mentioned as Salim, which signifies perfection. Jerusalem is located in the central part of the Judean hills surrounded by a desert that begins right behind the Mount

of Olives. In its long history, Jerusalem hasn't resemble a look of a western cities or the Mediterranean (Nastić, 1997).

The Jerusalem landscape is unique, it refers to soul and eyes as well. This outer world of Jerusalem obsess everyone with a multitude of phenomena, color, stone, architecture, churches, synagogues, mosques. On the site of today's old city of Jerusalem, it was a smaller panel, with a wide and flat Rock about 2 meters high, which served as an altar to the pagan god Baal. This Rock was chosen by God to become an altar. On that Rock, Cain killed Abel. On that same Rock, Abram offered to God his son, Isaac, as the sacrifice. On that Rock God has appeared to Abram. This place was the center of the Jerusalem Temple Mount, at this place there was the Rock - the Sanctuary of the Saints, which is now under the golden dome of the Omar mosque. The Temple Mount has become a sacred place for the Jews, Christians and Muslims. On the west side of the Temple Mount there is surviving remnant of the Solomon's Temple, known as Western Wall which is the largest Jewish sanctuary. In Jerusalem, the Jews began to live according to divine laws of Moses or Mosaic Law.

The population of Jerusalem has been mixed since ancient times, so the city often changed name with the change of master: Jewish, Greek, Latin, and Arabic. Biblical name j.r.s.l.m. it is most similar to today's Hebrew pronunciation "Yerushalayim" (Ginsberg, 1956). The interpretation of the linguist is that this name represents the connection between the earthly and the heavenly. At the place where God had appeared to Abram, Solomon has built a temple for seven years and at the time that was the most perfect building that human eye has ever seen. The Jewish temple did not look like today's synagogues and churches in which faithful people gather to pray together. The Jerusalem Temple was God's house on earth, where only priests could enter. Solomon slaughtered 22,000 oxen and 120,000 sheep as a peace gift to God for the sanctification of his Temple (Nastić, 1997).

\* Corresponding author: jovo.medojevic@pr.ac.rs

## REFLECTIONS OF HISTORICAL-GEOGRAPHIC DETERMINANTS

By the end of the 4th century BC Jerusalem became part of the Hellenistic world. Greek culture has become acceptable for many Jews who wanted to be like Greeks. They learned and spoke Greek, they took Greek names. In 37th year BC Rome "Herod the Great" was named as King of Jews. The Arabs worshiped Jerusalem. For them it was the Holy City which God blessed among their cities, Mecca and Medina. The Arabs called Jerusalem "Beit el Makdis" (Holy House). After the Muslim conquest of Jerusalem on the Temple Mount, they prepared pilgrimage site for 3000 pilgrims. At this place in 705 year, El Valid built the El Aqsa mosque (Bahat, 1980). Suleiman the Magnificent surrounded Jerusalem with the walls in 1542. These walls have been preserved till today and make a clear border between the sacred and the profane world. After Suleyman's death, the Pasha administrators began to fight among themselves, and the sole interest of Carigrad was tax revenue. Jerusalem was ruined, and there were less and less pilgrims in Jerusalem (Grindea, 1980). The four centuries of Ottoman rule in Jerusalem (from 1517 to 1917) was overwhelmed by severe torture and Turkish zulum. Somehow a Greek church was held, it was privileged by the Turks. In 1815 Jerusalem Holy Places were subject to political debate between the European nations. Disagreements over the Holy Places were one of the causes of the Crimean War (1854-1856). Order privileges are given to France in terms of Holy Places in Jerusalem and Bethlehem, as well as in regard to protectors of Latin Christians. Russia has protected the Greek Church. At that time, there were about 68,000 inhabitants in Jerusalem. The city was spread outside the walls of the Old Town towards the western and southern hills. Suez Canal, opened in 1869, regained strategic importance for the entire region. At the same time, the route between Jaffa and Jerusalem (in the length of about 80 kilometers) was repaired, and in 1892 the railroad passed through the Holy Land. Pilgrims arrived to pilgrimage. Russian emperors organized free pilgrimages to Jerusalem. Thus, the Russian mass pilgrimage began in 1847. About 20,000 Russians gathered for Easter in Jerusalem. They were placed for free in the large Russian complex in Jerusalem. It is assumed that in the 19th century Jerusalem was visited by about a million pilgrims from Europe. In England, for over forty years (1840-1880), over 1,500 travelogues were written about Jerusalem (Peters, 1985). Jerusalem was liberated from the Turkish occupation by the British at December 9th, 1917. British General Edmund Allenby, occupied Jerusalem without a bullet, he dismounted his horse at the Gate of Jaffa and walked on foot to Jerusalem. Eyewitnesses claimed that they had never seen before the British general so meekly as when he was entering in the Holy City of Jerusalem. After the First World War, the British ruled Palestine on the basis of the mandate system of the League of Nations. Britain was in control of Palestine for thirty years. The first British

military governor in Jerusalem, Sir Ronald Storrs, in 1917, passed a law that the only building material that can be used in Jerusalem is a stone of amber colour. This law is still respected by the Jews and the Arabs. Jews, but not Muslims, until the 1967 were forbidden to enter in the Church of the Holy Sepulchre (Holy Grave) (Bostock, 1982). After the Second World War, in 1947. by the United Nations Resolution, Palestine was divided into Arab and Jewish states. The Arabs have never accepted this Resolution. On May 15th, 1948, the Israeli declaration of independence was declared. The Jordans tried to conquer Jerusalem, but after two weeks of fighting for each house, this attempt failed. Israeli military forces have established a corridor. The Jews kept control of the New City, and the Jordans stayed in the Old City of Jerusalem. It remains to be remembered that Jerusalem from 1948 to 1967 was divided by barbed wire. The Israeli-Jordanian truce, from 1949, guaranteed the free access of Jews to the Western Wall. However, the Jordans never complied with this arrangement. They forbid access to all sacred places to Jews, Muslims and Christians. Only Christians had access to the Holy Places for Christmas and Easter (Nastić, 1997). In the Six-day Israeli-Jordanian War, which began on June 5th, 1967, the Israeli army carried out a counter attack and took over the city and the entire West Bank to the Jordan River. In 1950, the Israeli Parliament proclaimed Jerusalem for the capital city, however, most countries do not accept this status, and state embassies are in Tel Aviv-Jaffa. Today, Jerusalem has about 700,000 inhabitants. The victors and the defeated, they all live together, but still divided sharing a huge level of animosity.

## REPRESENTATIVE CASES OF PILGRIMAGE

When Christian pilgrims go to a pilgrimage and they go to a worship visit to: Church of Mother of God, Holy Temple of the Mother of God in Nazareth and the cave of the Temple in Bethlehem where Jesus Christ was born, Golgotha and Holy Grave of Jesus Christ; place of the Ascension of Christ on the Mount of Olives, Saint Sion, Saint Mary's grave in Gethsemane and the tomb of Lazarus in Al-Elzariya and Mount Tabor; the Lake of Tiberias, and the sacred river of Jordan where Jesus Christ was baptized, and they visit other sacred places where you can worship Jesus Christ, the pilgrims become vouchsafe to be called Hajji (Wilkinson, 1977). The oldest testimony of the Serbs pilgrimage was left by Saint Sava, who was first to visit and worship the Holy Grave in 1229, and the second time in 1234. St. Sava went on pilgrimage to the Holy Land by boat from the Budva port, and his pilgrimage lasted for a year. St. Sava was highly respected in the Holy Land (Mirković et al., 1995). This feeling is especially evident in the Holy Sacred Monastery in the Judean Desert. In this Monastery St. Sava received the icon of the Mother of God and the sacred shepherd's crook. Serbian monks stayed in this monastery for 150 years. After his second pilgrimage, St. Sava passed away in Velika Trnova in 1236 (Milanović et al., 1995). Orthodoxy and Roman Catholicism

agree on the name, which is, Holy Land - and in Holy Land there is Jerusalem, a witness where Judaism, Christianity and Islam meet each others through ages. In the area of Holy Land, are located the remains of many civilizations: Jewish, Babylonian, Egyptian, Greek, Hellenistic, Roman, Byzantine, Islamic. On the eve of the Orthodox Easter in the holy city of Jerusalem, about 50,000 pilgrims, Orthodox Christians: Greeks, Russians, Serbs, Romanians, Syrians, Palestinians, Egyptians come to the holy city of Jerusalem. The Church of the Holy Sepulcher represents the most sacred Christian place because it is located at the place where Jesus Christ was crucified, where he died, where he was buried, and where he resurrected on the third day according to the Bible. The temple represents a complex in which there are about 40 altars: Greek, Roman Catholic, Armenian, Coptic. Below the vault of the Church of the Holy Sepulcher are: Greek Orthodox Monastery of Virgin Mary, Greek Orthodox shrine of St. James, Greek Orthodox shrine of St. John, Chapel of the Forty Martyrs, Greek Orthodox Monastery dedicated to Abram, Armenian Chapel of St. John the Evangelist, Ethiopian Chapel of St. Michael, Greek Orthodox Holy Mary of Egypt. On the right side on the entrance in the Temple there is a stairway that leads to Golgotha (the hill of the skull) where Christ was crucified on Good Friday (Hoade, 1971). In the architectural sight the Golgotha shrine is 11.45 x 9.25 meters on 4.5 meters above the basilica, which are divided in to two ships. The rock in which the Cross for Jesus Christ crucifixion was stuck makes up one third of this space and it is totally covered - today glazed (plexiglass). Golgotha was named after King and High Priest Salim Melchizedek found the skull of the forefather Adam in the city of Afule in Israel, and buried it here at the foothill of the Golgotha Rock. The blood of crucified Christ, shed on rock and on the skull of forefather Adam, and on that place today is a shrine dedicated to Adam. On the frescoes in churches and monasteries, at the footsteps of crucified Christ there is usually illustrated the skull of forefather Adam. On the Golgotha there is a Roman Catholic chapel (Chapel of Crucifixion) (located at the place where Christ was nailed on the Cross), and the small Greek shrine ( on the place where Jesus Christ died). On the Golgotha there is a Roman Catholic chapel of the Virgin Mary. At the very entrance at the Church of the Holy Sepulcher, there is an anointing plate where Jesus Christ was anointed before he was laid down in the tomb. Today that's a stone of beautiful purple color. It belongs to Greeks, Latinas, Armenians and Copts. Above the anointing plate there are cressets and 8 lamps. In a front of anointing plate there is a place called the Center of the World (Nastić, 1997). A small circular stone slab, surrounded by an iron grid, represents the place where the Virgin Mary and Mary Magdalene attended the crucifixion of Jesus Christ. This holy place belongs to the Armenians. The entrance in the Aedicula - Holy Grave of Jesus Christ, it represents the lobby of the Angel. The Aedicula length is 8.30 meters; same width and height-5.90 meters. Aedicula is the smallest diocese in the world.

The lobby of the Angel is in the front of the Holy Grave of Christ, which enters through a low entrance 1,33 meters high in the stone vault. The Christians enter on this door by kneeling through. The Holy Grave of Jesus Christ is the Church with length of 2.07 m , and 1.93 m wide. On the right side there is Christ's Grave, a white marble platter of 2,02 m long and 0,93 meter wide. Greek monks who are called Tafos or guards of Christ's Grave are allowed to let three devotees per once to approach (Gilbert, 1985). From 335 AD till today in the Church of the Holy Sepulcher in Jerusalem, pilgrims are becoming witnesses of one of the greatest miracles on this world, the Holy Fire. According to belief Holy Fire testifies the presence of God that enlighten a human. The pilgrims are awake all night on Good Friday. They wait patiently in long lines on the streets of the old city of Jerusalem. The most persistent stay on their feet more than 20 hours. The bluish-whitish flame of the Holy Fire, in a mysterious way, descends into the Church of the Holy Sepulcher where Christ's Grave is located. After the prayer of the Orthodox Patriarch of Jerusalem there is a prescribed procedure based on the provisions of the Law passed by the Ottoman government in 1852. established by Porta for various Christian communities and the entire complex of the Church of the oly Sepulcher (Gilbert, 1985). On Holy Saturday morning, a special commission composed from the members of all Christian communities, Jewish authorities and the Muslim family of Kavas Seljuk Turks) who have been guarding the Holy Grave for 250 years. Kavas wear a fes and tally (TF) – Tafos guardian of the Holy Grave. On the Holy Saturday, around 1 pm., the Patriarch of Jerusalem comes with the other Church's dignitaries and walks around Aedicula three times by singing the Eastern troparion. All lights, candles and cressets are off in the entire Church. The Church of Christ's Grave was previously sealed with a seal of wax and honey. Before the Patriarch unseal the entrance to Christ's Grave; representatives of the Jewish authorities and the police thoroughly search the Patriarch to make sure that he doesn't hide a match or a lighter somewhere. The Patriarch, together with the Armenian dignitary priest, unseal the Church of Christ's Grave and approaches to Holy Grave of Christ. Patriarch of Jerusalem knees to pray, reading special prayers on behalf of all Orthodox prayers, he prays to Jesus Christ to send them a Holy Fire as the testimony of His resurrection (Milinković, 1998). While Patriarch is praying, in the whole Temple with the greatest devotion, 10,000 prayers are praying with him, all together in one Church. Everyone on his own language brings prayers to the Lord. Believers hold their bouquets of 33 candles and wait for the descent of Holy Fire. Holy Fire first descends on the candles of the Patriarch of Jerusalem, who, first of all, lights up the creeset located inside of glass to keep and protect the Holy Fire from the intentional or unintentional negligence. Then, the Patriarch leaves the church with candles lit up. His appearance induce the enthusiasm of the faithful. A lot of people start to cry out of excitement. The Arabs and Christians hit the table with

hands and yell “Christ is Risen!”, “Trule, He is Risen!”. The flame from the Holy Fire has been quickly transferred from candle to candle, so that all blessed people in church in a few minutes will light up their bouquets of candles with the flame from the Holy Fire. At first couple minutes, the Holy Fire burns with a flame that doesn't sear. This miracle of the Holy Fire occurs only when the Orthodox Patriarch enters the Church of the Holy Sepulcher. Some examples from the past testify that this Orthodox right was threatened. The best example of threat is when the Armenian monophyses paid with money, sultan Murat IV to entrust them to conjure instead of Orthodox Christian the Holy Fire in 1549. It was at the time of the true Patriarch of Jerusalem's Sophrony the Second. At that time the Armenian Patriarch entered in to the Church of Holy Grave and unsuccessfully conjure the descent of Holy Fire. During that time, Orthodox Patriarch Sophronia was outside the Church, next to the pillar, which at one point cracked lengthwise, and from the cracked pillar, the Holy Fire appeared, igniting the candle held by the Patriarch. This pillar can still be seen on the left side entrance of the Church of the Holy Sepulcher (Popović, 2011).

## CONCLUSION

The cultural and geographical determinants of Jerusalem unambiguously point to his supranational identity. Throughout history, Jerusalem has constructed an original and unique cultural pattern. From this universal cultural aspect, Jerusalem is close to all people, ethnic and religious communities. In this cultural universe, cultural-geographical determinants point to the significance of Jerusalem for Serbs and their cultural and spiritual identity. This identity is reflected in the transcendental reflection of God's existence in Jerusalem and the belief of Orthodox Serbs whose attachment to Jerusalem is attributed to Saint Sava who was highly respected in the Holy Land. The meeting of St. Sava with Jerusalem and the Holy Land represents not only his personal but also literary and cultural approach to ancient area that was not well known to Serbs, except through the teaching of the Bible. Jerusalem was and remains a place of worship for members of all three monotheistic religions, and the witness of this is the history that evokes respect. Cultural-

geographical determinants point to the religious, military, economic and legal history of this city. The cultural and historical monuments, obviously, with their beauty and symbolism, reinforce the importance of Jerusalem. These places are today the object of cult and legend. Jerusalem is the only city in the world whose history is written in all three sacred books: Bible, Talmud, Quran. The cultural-geographical determination reveals enormous spiritual value, tradition and monumentality of Jerusalem. Jerusalem has an integrative function in modern society. Pilgrimages to Jerusalem are journeys that occupy a central place in the lives of the Jews, Christians and Muslims. The cultural and geographical determinants of Jerusalem point to it's interculturalism in contemporary world society and contribute to the permeation of cultures and civilizations, the wider values of peace culture among nations and leads to the phenomenon of globalization of general understanding among different nations and religions.

## REFERENCES

- Bahat, D. 1980. Carta's istroical Atlas of Jerusalem. Jerusalem: Carta.
- Bostoc, H. 1982. The great Ride. Perth: Artlook Books.
- Gilbert, R. 1985. Jerusalem the rebirth of City. London: Chatto & Windus.
- Ginsberg, L. 1956. Legends of the Bible, Jewis Publication Societi of Amerika. New York.
- Grindea, M. 1980. The image of Jerusalem: A literary chronicle of 3, 000 years. London: Adam International Review.
- Hoade, E. 1971. Guide to the Holy Land. Jerusalem: Franciscan Printing Press.
- Milinković, I. 1998. Sveti Oganj u Jerusalimu. Niš: Manastir svetog Jovana Krstitelja.
- Mirković, K., & Kalezić, D. 1995. Sveti Sava. Nikšić: Unireks; Beograd: Narodno delo.
- Nastić, D. 1997. Jerusalim istorija i vodič. Beograd: Ljiljana Nastić i Dimitrije Nastić.
- Peters, F.E. 1985. The Holy city in the eyes of the chroniclers, visitors, pilgrims. Princeton: Princeton legacy Library.
- Popović, D. 2011. Koga imam na nebu. Bonart, Nova Pazova.
- Wilkinson, J. 1977. Jerusalem Pilgrims. Lincoln, United Kingdom: Aris & Phillips.

# CONTEMPORARY MIGRATORY MOVEMENTS IN THE MUNICIPALITY OF TRSTENIK

SAŠA MILOSAVLJEVIĆ<sup>1\*</sup>

<sup>1</sup>Faculty of Natural Sciences and Mathematics, University of Priština, Kosovska Mitrovica, Serbia

## ABSTRACT

Municipality of Trstenik located in spacious valley of Zapadna Morava, has always provided favorable conditions for the settlement of the population and the development of settlements. After the World War II, there was a need for recruiting a large number of people because of a huge development of metal industry in Trstenik, and that fact attract the immigrants from the area of Rasina, Aleksandrovačka Župa, Podibra, Lepenica, Levač and Temnić. The ratio between autochthonous and migrant population according to 1961 Census was 69%:31%, while the same ratio for the 2011 census was 59%:41%. Nearly a quarter (24%) of total number of immigrants immigrated in the inter-census period from 1981. to 1991, and almost all (94% of immigrants) immigrated from the same area of the republic. The process of emigration particularly intensified in the early nineties of the XX century when young and highly educated population emigrate, and the main reason for that was a poor economic situation.

**Keywords:** population, migrations, Trstenik, Serbia.

## INTRODUCTION

Modern migratory movements in the world today represent an important demographic determinant. The intensity of migration movements is an important indicator of socio-economic and demographic situation in a country. Analyzing data from the last 2011 Census, it's evident that we have increasing emigration from the central and southern parts of Serbia, and vast resettlement to Belgrade region. In the last twenty years due to the unfavorable socio-economic situation the municipality of Trstenik has a problem with the outflow of population outside of the municipality, and too there is a problem with certain migratory movements inside the Trstenik. The emigration is primarily characteristic for youth who after graduation does not return to the home municipality, they rather prefer to stay in great economic centers where they start their families and where they have a job. These migration trends inevitably affect the municipality in terms of development and function of the settlement.

## MATERIAL AND METHODS

The methodology in this paper is according to the subject, objectives and tasks of the research. Field studies are carried through direct and systematic observation, as well as conducting surveys and interviews. The historical method contains the use of literature, written documents and other archive material and presents us knowledge about the past of the municipality of Trstenik. Data were collected in public institutions and in the Statistical Office of the Republic of Serbia.

## IMMIGRATION AND EMIGRATION COMPONENT

The settlement of Trstenik area had started at 1791. and the adoption of the firman, which allowed Serbs free trade of cattle and gave them certain privileges. The population has migrated from the Toplica, Župa, Rasina, from Kosovo and Srem too.

Intensive settlement continues after victories in the first and second Serbian uprising, population from Montenegro (people from Kolašin mostly), Sjenica, Novi Pazar and from Pešter (mountain area) immigrated to this area (Popović, 1968). In the postwar period, there have been significant changes and shifts in population structure. At the beginning of the application of the first five-year plans and the establishment of industrial enterprises 'Prva petoletka', during this period from 1948 to 1961, Trstenik was great place for inhabitants due to increased demand for labor. Population from surrounding villages and a population from the surrounding areas Rasina, Aleksandrovačka Župa, Podibra, Lepenica, Levač and Temnić, then from Vojvodina, Kosovo and Metohija, Bosnia and Herzegovina, Croatia, Slovenia, Macedonia, Montenegro and a certain number of those who were born abroad start to migrate to Trstenik (Medojević et al., 2011).

According to 1961 Census we conclude that the indigenous population on the territory of the municipality of Trstenik seemed more than two thirds of population of the municipality (69.03%) or relatively 40,485 inhabitants. Immigrant population was significantly lower - 18,166, or 30.97% of the population of the municipality. The difference between autochthonous and migrant population was 22,319 inhabitants (Table 1). Further development of the metal industry and opportunities for employment and favorable conditions of life had caused that municipality of Trstenik became the immigration area.

\* Corresponding author: sasa.milosavljevic@pr.ac.rs

**Table 1.** Autohthonous and migrant population in the municipality of Trstenik (1961 Census)

Municipality	AUTOHTHONOUS		MIGRANT		TOTAL
	Number	%	Number	%	
Trstenik, Velika Drenova	40.485	69.03	18.166	30.97	58.651

Source of data: 1961 Census of Population, Households and Dwellings, Book 12, Migrations, Data by municipalities and cities, Statistical Office of the Republic of Serbia, Belgrade, 1966.

The results of 2011 Census confirmed the process of immigration in the municipality, and show that in the municipality of Trstenik it is still outnumber the indigenous population (25.415 or 59.11% of the population of the municipality) in relation to the migrant population (17.581 or 40.89% of the population of the municipality), except the thing

that disproportion between these two populations is much lower and it is only 7.834 inhabitants or 18.22% of the population of the municipality (Table 2). Inhabitants born on territory of municipality Trstenik are concentrated in the other (rural) areas, while on the other side, the urban environment was more attractive for immigrants.

**Table 2.** Autohthonous and migrant population in the municipality of Trstenik (2011 Census)

MUNICIPALITY	AUTOHTHONOUS		MIGRANT		TOTAL
	Number	%	Number	%	
Trstenik	25.415	59.11	17.581	40.89	42.996

Source of data: 2011 Census of Population, Households and Dwellings, Book 9, Migrations, Data by municipalities and cities, Statistical Office of the Republic of Serbia, Belgrade, 2013.

According to Census 1961 figures from Statistical Office of the Republic of Serbia show that until that time, the largest population on the territory of today's municipality had moved before 1940. - 6,863 or 38.05% immigrant population. After this period there is a period from 1946 to 1952. with 3,848

immigrants or 21.32% and after that there is a period from 1953 to 1957 with 3,176 immigrants or 17.60%, and period from 1958 to 1961 with 3,022 immigrants or 16.74% of the total immigrant population. During World War II there was a 1,136 inhabitants migrants or 6.29% (Table 3).

**Table 3.** The population in the municipality of Trstenik according to time of immigration (1961 Census)

YEAR	Municipalities of Trstenik and Velika Drenova	
	Number	%
before 1940	6.863	38.05
1941-1945	1.136	6.29
1946-1952	3.848	21.32
1953-1957	3.176	17.60
1958-1961	3.022	16.74
TOTAL	18.045	100

Source of data: 1961 Census of Population, Households and Dwellings, Book 12, Migrations, Data by municipalities and cities, Statistical Office of the Republic of Serbia, Belgrade, 1966.

Results from 2011 Census confirmed the same trend with certain derogations from the above mentioned reasons, cause until the 1963, Velika Drenova existed as an independent municipality and after abolishment of this municipality part of the settlement was added to municipality of Trstenik and other part of territory was added to municipality of Kruševac. Thus, according to 2011 Census of population, we have a situation that the smallest number of immigrants was in the period 2001-2005. precisely 999 immigrants or 5.69% and in the period from 1991 to 1995, 1,055 immigrants or 6%. The construction of the

industrial enterprises 'Prva petoletka' which during the period from 1950 to 1990 was one of the largest manufacturers of hydraulics and pneumatics in Europe. That contributed to the municipality of Trstenik to become immigration area, so in that period before 1980 year, 8,463 inhabitants were moved or 48.13% of the total immigrant population. After this period the following periods from 1981 to 1985. (1,673 immigrants- 9.52%), 1986-1990. (1,448 immigrants - 8.24%). A smaller number of immigrants was recorded during the period between 1996 and 2000 (1,211 - 6.88%) and during the period after 2006

(1,361-7.75%). For the 1,371 inhabitants or 7.79% of immigrants is not reliably established when they moved (Table 4).

**Table 4.** The population in the municipality of Trstenik according to time of immigration (2011 Census)

YEAR	Municipality of Trstenik	
	Number	%
1980. and earlier	8.463	48.13
1981-1985	1.673	9.52
1986-1990	1.448	8.24
1991-1995	1.055	6.00
1996-2000	1.211	6.88
2001-2005	999	5.69
2006. and later	1.361	7.75
Unknown year	1.371	7.79
TOTAL	17.581	100

Source of data: 2011 Census of Population, Households and Dwellings, Book 9, Migrations, Data by municipalities and cities, Statistical Office of the Republic of Serbia, Belgrade, 2013.

Based on the results according to 1961 Census, we can conclude that today's municipality of Trstenik largest population has been moved from different places but from same municipality - 9,671 inhabitants or 53.27% immigrant population. After that the population that moved from other municipalities of the same republic - 7,676 residents or 42.28%, while the much smaller number of immigrants moved from another Socialist Republic or the Autonomous Province – 792

inhabitants or 4.38% of immigrant population. The number of immigrants from other countries is negligible (Table 5). This trend of immigration has been continued after forty years, that remains that the most immigrants comes from the same or other municipalities, which leads us to the conclusion that the municipality of Trstenik is not attractive for immigrants from remote areas, but it attracts the immigrants from smaller distances.

**Table 5.** Migrants population in the municipality of Trstenik according to the areas (1961. Census)

AREA	Municipalities of Trstenik and Velika Drenova	
	Number	%
Different places same municipality	9.671	53.27
Different municipality same republic	7.676	42.28
Different republic and autonomous province	792	4.38
Different country	14	0.07
TOTAL	18.153	100

Source of data: 1961 Census of Population, Households and Dwellings, Book 12, Migrations, Data by municipalities and cities, Statistical Office of the Republic of Serbia, Belgrade, 1966.

According to the 2011 Census of population, the highest number of immigrants consists from the population from the territory of the same municipality 8.390 or 47.73%, after that the immigrants from other areas 5,518 or 31.39%, and immigrants from other municipalities 2,582 or 14.68%. The smallest proportion of immigrants are those from the former Yugoslav republics - 865, or 4.93%, and other countries, 219 or only 1.25% of the total number of immigrant population (Table 6). Area of municipality of Trstenik was quite attractive for immigration until the beginning of the last decade of the twentieth century. Reasons for that was an employment, opportunities for individuals in their professions, the opportunity

to acquire higher income as well as the ability to have suitable living conditions (Đurđev, 1998).

The disintegration of former Yugoslavia, beginning of the civil war in the former state, international sanctions, inflation, poverty and the difficult economic situation were reasons for the difficult living conditions in the municipality. The largest number of active population was employed at the firm complex 'Prva petoletka', but because of losing a large market of former Yugoslavia and large parts of the European market this firm was operating with major problems. This led to the first emigration of highly educated people with their families to Belgrade and abroad. After the democratic changes in the year 2000, the

situation has not significantly improved, so we can conclude that the emigration intensified in the last fifteen years. The

immigrants were mostly part of younger and middle age population.

**Table 6.** Migrants population in the municipality of Trstenik according to the areas (2011. Census)

AREA	Municipality of Trstenik	
	Number	%
Different settlement same municipality	8.390	47.73
Different municipality same republic	2.582	14.68
Different areas	5.518	31.39
Former republics of SFRJ	865	4.93
Other countries	219	1.25
Unknown	4	0.02
TOTAL	17.581	100

Source of data: 2011 Census of Population, Households and Dwellings, Book 9, Migrations, Data by municipalities and cities, Statistical Office of the Republic of Serbia, Belgrade, 2013.

As a result of crisis, the development of the municipality was almost stopped and parts of companies and enterprises have failed. Trstenik is a traditional community that every year sends a large number of students to college, mostly in Belgrade. Students who successfully completed their studies they start working for private companies in Belgrade or go to abroad where they remain to live, and start their families. And students who fail to successfully finalize the study, also remain in large university centers of Serbia because it's easier to find a job and secure existence.

Young people are not only moving out from the municipality center, but from all villages in the municipality. By the last decade of the twentieth century the population has migrated from villages to urban or suburban areas mainly because of work in the city. A lack of jobs in the city center caused the extension of the migration of population to other cities. Rural households that rely on agriculture have difficult task to generate income, especially since the state is constantly increasing taxes, prices of seeds, fuel prices and without guaranteed purchase prices of agricultural products. The lack of adequate social, cultural and sports life make things even worse in villages around Trstenik. Young people who do not want to stay with parents migrate to areas where it is easier to find a job, solve existential problems and easier to secure good life for themselves and their families. It is estimated that 84 inhabitants of the municipality of Trstenik went to abroad on temporary stay. 68 of them are on temporary work and 16 of them are members of their families. 41 resident was from urban area at work and five residents were members of their families. There is a similar number of residents in abroad from the villages of the municipality, out of 43 inhabitants, 32 of them were working and 11 of them are members of their families. Villages which present the greatest emigrational center to foreign countries are: Ridevštica, Jasikovica, Brezovica and Stublica. The municipality

of Trstenik has markedly developed agricultural production and therefore the need for agricultural workers is bigger. In large villages in the municipality, especially in the Velika Drenova and Stopanja, year after year the number of seasonal migrant workers from Bulgaria and Romania is increasing.

## COMMUTING-DAYTIME POPULATION

Part of the population of the municipality of Trstenik presenting the urban-rural and rural-urban commuting pattern. This part of the population belongs to the employees of the city's economy, youth who study in the municipal center and the urban population employed in rural areas, which together belong to the group of continuous commuters.

According to the 2011 census, the municipality of Trstenik have 4,088 active migrants or 9.5% of the total population of the municipality. In other (rural) settlements the largest number of active migrants are 3,360 compared to 728 who live in urban areas. The highest percentage of migrants (76.1%) work in different settlement in the same municipality, mainly in the municipal center. A small number of inhabitants, 292 of them, or 7.1%, have to go to work in other municipalities. It is interesting to compare active migrants from rural and urban areas. From rural areas 85.1% of residents commute to Trstenik (mainly for work in the firm 'Prva petoletka'), while only 5.5% migrates to other municipalities, to other areas migrates 684 inhabitants, or 16.7%. The situation is different in urban settlements where more than half of the population commute to other areas, 370 of them or 50.8% of commuters, after them there is a big number of commuters inside the municipality 251 migrants or 34.5%, while the minimum commuters travel to other municipalities (Vrnjačka Banja, Kruševac, Kraljevo) with 185 migrants or 5.5% (Table 7).

**Table 7.** Commuters of active population in the municipality of Trstenik (2011. Census)

Settlement	TOTAL ACTIVE	Same municipality		Different municipality		Different area		Different country	
		Number	%	Number	%	Number	%	Number	%
Trstenik (municipality)	4.088	3.111	76.1	292	7.1	684	16.7	1	0.1
City settlements	728	251	34.5	107	14.7	370	50.8	-	-
Other settlements	3.360	2.860	85.1	185	5.5	314	9.3	1	0.1

Source of data: 2011 Census of Population, Households and Dwellings, Book 11, Daily migrants, Data by municipalities and cities, Statistical Office of the Republic of Serbia, Belgrade, 2013.

The second group of continuous commuters consists of youth or students. Pupils and students have a share of 35.2% in total daily migration in the municipality of Trstenik. Most of these migrants originated from other (rural) settlements, 2,006 compared to 214 in urban areas. In other settlements in the municipality study 1,538 pupils and students, while in the other municipalities of the Republic of Serbia study 282 pupils and students from the municipality of Trstenik. In other areas of the republic study 399 pupils and students or 17.9% (Table 8). Because of Technical school and gymnasium in Trstenik the

largest number of students come from rural areas. The number of students from the municipality of Trstenik who are studying at the Technical College and private universities in Trstenik is much lower. The largest number of students from the municipality of Trstenik study in large university centers of Serbia. Occasional daily migrations are done from time to time. People who come to Trstenik for selling goods at markets shopping in the city, or people with some personal needs and private business are participating in occasional daily migrations.

**Table 8.** Commuters students in the municipality of Trstenik (2011. Census)

Settlement	TOTAL	Same municipality		Different municipality		Different area		Other country	
		Number	%	Number	%	Number	%	Number	%
Trstenik (municipality)	2.220	1.538	69.3	282	12.7	399	17.9	1	0.1
City settlements	214	20	9.34	55	25.7	139	64.9	-	-
Other settlements	2.006	1.518	75.7	227	11.3	260	12.9	1	0.1

Source of data: 2011 Census of Population, Households and Dwellings, Book 11, Daily migrants, Data by municipalities and cities, Statistical Office of the Republic of Serbia, Belgrade, 2013.

## CONCLUSION

Geographical position of Trstenik has always provided favorable conditions for the settlement of population. The main settlement of Trstenik area starts from 1791 when immigrants from Montenegro, Pešter, Toplica and Kosovo and Metohija came to Trstenik. After the World War II, more intensive development of agriculture and particularly the opening of industrial enterprises 'Prva petoletka' make that the municipality of Trstenik became an immigrant region. During this period, in each inter-census interval there wasn't less than 3,000 newly settled inhabitants in the municipality. This trend lasted until the early nineties of the twentieth century. The disintegration of the former state, war in the region, international sanctions and the difficult economic situation cause that municipality of Trstenik

becomes emigration area. From the municipality of Trstenik population emigrate to Belgrade and to other regional centers of the republic, mostly young, educated and fertile age population. This process entails a number of other processes where the most important are depopulation and demographic aging. State and local governments must use their stimulus measures to try to slow the process of emigration by creating favorable living and working environment for people who are living in rural and smaller urban areas.

## REFERENCES

- Durđev, B. 1998. Geografija stanovništva. Novi Sad: Prirodno-matematički fakultet.  
 Medojević, J., Pavlović, M., & Milosavljević, S. 2011. Demographic analysis of forced migrations in Kosovo and

- Metohia from 1999 to 2011, Global Modern Demographic problems: Migration and emigrational policy. Moscow: Russian Academy of Sciences - Russian State University for the Humanities. pp. 124-135.
- Popović, M. 1968. Trstenik i okolina. Trstenik: SO Trstenik.
- Republički zavod za statistiku. 2013. Popis stanovništva, domaćinstava i stanova u 2011. godini. In Migracije. Knjiga 9, Beograd.
- Republički zavod za statistiku. 2013. Popis stanovništva, domaćinstava i stanova u 2011. godini. In Dnevni migranti. Knjiga 11. Beograd.
- Zavod za statistiku. 1966. Popis stanovništva, domaćinstava i stanova 1961, In Migraciona obeležja – rezultati za naselja. Knjiga XII, Beograd.

# HOMOTOPY PERTURBATIONS METHOD: THEORETICAL ASPECTS & APPLICATIONS

STOJANOVIĆ VLADICA<sup>1</sup> \*, KEVKIĆ TIJANA<sup>1</sup>

Faculty of Natural Sciences and Mathematics, University of Priština, Kosovska Mitrovica, Serbia

## ABSTRACT

The application of the homotopy perturbation method (HPM) in two different research's area has been proposed in this paper. First, the HPM has been used for approximate solving of the well-known implicit equation for electrostatic surface potential of MOSFET transistor. The approximate analytical solution obtained in this case has relative simple mathematical form, and simultaneously high degree of accuracy. Next, HPM has been applied in determination of the invariant measures (IMs) of the non-linear dynamical systems with chaotic behavior. The convergence and efficiency of this method have been confirmed and illustrated in some characteristic examples of chaotic mappings.

**Keywords:** Homotopy perturbations, convergence, MOSFET modeling, invariant measures, chaotic maps.

## INTRODUCTION

The homotopy perturbation method (HPM) belongs to the general and powerful techniques for solving the nonlinear equations of various kinds. As a combination of the well-known homotopy method in topology and classic perturbation techniques, the HPM was first introduced in pioneer works of He (1999, 2000, 2003, 2006, 2008). After that, the extensive development and application of this method to various fields of science researches has been started. For instance, the HPM has been successfully applied for obtaining analytic or approximate solutions of non-linear differential and partial-differential equations (Biazar et al., 2009; El-Sayed et al., 2012; Gadallah & Elzaki, 2017), as well as Fredholm and Volterra integral equations (Hetmaniok et al., 2012, 2013; Dong et al., 2013). Furthermore, this method also has found significant application in solving many kinds of real based problems, mainly in the physical sciences (Zeb et al., 2014; Kevkić et al., 2017, 2018).

Let us emphasize that the HPM is increasingly being used also in scientific fields, such as, for example, environmental protection and epidemiology (Khan et al., 2014; Adamu et al., 2017). Thus, the wide variety of applications indicates to the flexibility and importance of this method. Finally, let us point out that HPM has been improving, developing and modifying, until to the present time. Consequently, today exist various solver techniques that are based, to a greater or lesser extent, on the basic HPM assumptions (Noor & Khan, 2012; Zhang et al., 2015; Tripathi & Mishra, 2016; Bota & Caruntu, 2017). Here is given a brief theoretical background about the HPM and some sufficient conditions to its convergence. Further, the HPM has been applied in two research's area, where still not observed its any significant application.

As a novel approach, the HPM technique firstly has been applied for solving of the implicit relation between the electrostatic

surface potential of an n-channel MOSFET transistor with terminal voltages. Approximate surface potential obtained in this way shows relative simple mathematical form, and at the same times a high degree of accuracy. Indeed, these properties of solution have crucial importance from the physical as well as design point of view. Further, the application of the HPM in determination of the invariant measures (IMs) of the non-linear dynamical systems with chaotic behavior has been investigated. For this purpose, the convergence and efficiency of the HPM has been confirmed and illustrated with some characteristic examples of chaotic mappings.

## METHODOLOGY OF THE HPM

For simple illustration of the basic concepts of HPM, we consider the following nonlinear equation:

$$\mathcal{N}[f(x)] = 0. \quad (1)$$

Here,  $f: \mathbb{R} \rightarrow \mathbb{R}$  is unknown function and  $\mathcal{N}(\cdot)$  is nonlinear operator defined on some functional domain  $\Omega$ . In solving Eq. (1) by using the HPM technique is assumed the introduction of *homotopy*  $\mathcal{H}: \Omega \times [0, 1] \rightarrow \mathbb{R}$  such that, for an arbitrary  $u \in \Omega$ :

$$\mathcal{H}[u, 0] = \mathcal{L}[u], \quad \mathcal{H}[u, 1] = \mathcal{N}[u], \quad (2)$$

where  $\mathcal{L}[u]$  is a linear operator, defined on the same domain  $\Omega$ . More precisely, if denote with  $p \in [0, 1]$  the so-called *embedding parameter*, then homotopy  $\mathcal{H}$  can be defined as a function

$$\mathcal{H}[u, p] = (1 - p) \mathcal{L}[u] + p \mathcal{N}[u], \quad (3)$$

which obviously satisfies the both of Eqs. (2). According to this, for the unknown function  $f(x)$ , we can form the so-called *homotopy equation*:

$$\mathcal{H}[f(x), p] = 0. \quad (4)$$

\* Corresponding author: vladica.stojanovic@pr.ac.rs

When  $p = 0$ , Eqs. (2)-(4) give the following linear equation:

$$\mathcal{L}[f(x)] = 0, \quad (5)$$

for which is assumed that has a unique solution  $f_0(x)$ , usually called *initial solution* or *initial approximation*. On the other hand, when  $p = 1$  the same Eqs. (2)-(4) obviously give the nonlinear Eq. (1).

The basic assumption of HPM is that general solution  $F(x, p)$  of the homotopy Eq. (4) can be expressed as the power series in  $p$ :

$$F(x, p) = \sum_{k=0}^{+\infty} p^k f_k(x). \quad (6)$$

From here, we get immediately  $F(x, 0) = f_0(x)$  as the initial solution of linear Eq. (5), i.e. as the solution of homotopy Eq. (4) when  $p = 0$ . On the other hand, the solution of the “main” Eq. (1), or equivalently Eq. (4) when  $p = 1$ , will be:

$$f(x) = \lim_{p \rightarrow 1^-} F(x, p) = \sum_{k=0}^{\infty} f_k(x). \quad (7)$$

on the condition of convergence the series in Eq. (7). In this case, according to Abel theorem, immediately follows:

**Theorem 1.** *If series  $\sum_{k=0}^{\infty} f_k(x)$  converges, then function  $F(x, p)$  is continuous from the left at  $p = 1$ , i.e. Eq. (7) holds.*

Notice that, if the conditions of the previous theorem are fulfilled, then series  $\sum_{k=0}^{\infty} f_k(x)$  represents the solution of the homotopy Eq. (4) when  $p = 1$ , i.e., it is solution of the nonlinear Eq. (1). Moreover, the solution  $f(x)$  of Eq. (1) can be estimated by the so-called *HPM-approximations*:

$$\begin{aligned} \widehat{f}_0(x) &= f_0(x), \\ \widehat{f}_k(x) &= \widehat{f}_{k-1}(x) + f_k(x) = \sum_{j=1}^k f_j(x), \quad k = 1, 2, \dots \end{aligned} \quad (8)$$

Obviously, series  $\sum_{k=0}^{\infty} f_k(x)$  is a solution of Eq. (1) if and only if the series  $\{\widehat{f}_k(x)\}$  converges to the unknown function  $f(x)$ . Sufficient conditions for this convergence can be also given by the following statement, which is a special case of Banach fixed point theorem:

**Theorem 2.** *Let  $\Omega$  is Banach space with sup-norm  $\|\cdot\|$  and the series  $\{f_k(x)\}$  defined on  $\Omega$ . If for some  $\alpha \in (0, 1)$  and  $k \geq 1$  the inequality  $\|f_k\| \leq \alpha \|f_{k-1}\|$  holds, then series  $\{\widehat{f}_k(x)\}$ , defined by Eqs. (8), uniformly converges to the unique solution  $f(x)$  of Eq. (1).*

*Proof.* According to assumptions of the theorem and Eqs. (8), for an arbitrary  $k, m > 0$  we have that:

$$\begin{aligned} \|\widehat{f}_{k+m} - \widehat{f}_k\| &\leq \|\widehat{f}_{k+m} - \widehat{f}_{k+m-1}\| + \dots + \|\widehat{f}_{k+1} - \widehat{f}_k\| \\ &\leq \|f_{k+m}\| + \dots + \|f_{k+1}\| \\ &\leq (\alpha^m + \dots + \alpha) \|f_k\| \\ &\leq \alpha^{k+1} \frac{1 - \alpha^m}{1 - \alpha} \|f_0\|. \end{aligned}$$

Thus,  $\lim_{k, m \rightarrow \infty} \|\widehat{f}_{k+m} - \widehat{f}_k\| = 0$ , i.e.  $\{\widehat{f}_k(x)\}$  is a Cauchy sequence in Banach space  $\Omega$ . It implies that  $\{\widehat{f}_k(x)\}$  is uniformly convergent, and its limit is uniquely determined by Eq. (7).  $\square$

In following will be describe some practical applications of the aforementioned HPM methodology.

## MODELING SURFACE POTENTIAL IN MOSFET TRANSISTORS

The most of MOSFET transistor models are based on charge sheet approximation and the incrementally linear relationship between the inversion charge density and the surface potential (van Langevelde & Klaassen, 2000; Chen & Gildenblat, 2001). Their combination gives following implicit relation between the surface potential  $\psi_s$  and gate voltage  $V_G$ :

$$V_G - V_{FB} - \psi_s = \gamma \sqrt{\psi_s + u_T \exp\left(\frac{\psi_s - 2\phi_F - V_{ch}}{u_T}\right)}. \quad (9)$$

where  $V_{FB}$  is the flat band voltage,  $u_T$  is the thermal voltage,  $\phi_F$  is Fermi potential,  $V_{ch}$  is the channel potential and  $\gamma$  is the body factor defined by  $\sqrt{2q\epsilon_{Si}N_A/C_{ox}}$ . Here  $N_A$  is acceptor concentration in homogeneously doped channel and  $C_{ox} = \epsilon_{ox}/t_{ox}$  is the oxide capacitance per unit area,  $t_{ox}$  is the gate oxide capacitance per unit area, as  $\epsilon_{ox}$  is the oxide permittivity.

Eq. (9) makes the base of all so-called surface potential based (SPBM) MOSFET models which are the most accurate physically based MOSFET models. However, it is obvious that Eq. (9) can be solved with respect to  $\psi_s$  only numerically, what represent the main drawback of the SPBM from the design and physical point of view. Note that, after some elementary transformations, the Eq. (9) can be rearranged in the following, dimensionless form

$$A \exp\left(\frac{y - C}{u_T}\right) - y^2 + (2x + \gamma^2)y - x^2 = 0, \quad (10)$$

where  $A := \gamma^2 u_T$ ,  $x := V_G - V_{FB}$ ,  $C := 2\phi_F + V_{ch}$  and  $y := \psi_s(x)$  is an unknown function. To find the (approximative) solution of Eq. (10), we apply the HPM technique. Firstly, we construct the homotopy equation

$$(1 - p) \mathcal{L}[Y(x; p)] + p \mathcal{N}[Y(x; p)] = 0, \quad (11)$$

where  $p \in (0, 1)$  is the embedding parameter, as

$$\mathcal{L}[Y(x; p)] = Y(x; p) - f_0(x)$$

is a *linear part*, and

$$\mathcal{N}[Y(x; p)] = A \exp\left(\frac{Y(x; p) - C}{u_T}\right) - Y^2(x; p) + (2x + \gamma^2)Y(x; p) - x^2$$

is a *non-linear (“true”) part* of Eq. (10).

When  $p = 0$  the homotopy Eq. (11) obviously becomes  $\mathcal{L}[Y(x; 0)] = 0$ , with the unique initial solution  $Y(x; 0) = f_0(x)$ . Similarly, for  $p = 1$ , Eq. (11) becomes  $\mathcal{N}[Y(x; 1)] = 0$ , and it is equivalent to Eq. (10), with the “main” solution  $Y(x; 1) \equiv \psi_s(x)$ .

Now, according to aforementioned facts, solution of the homotopy Eq. (11) can be expressed as the power series in  $p$ :

$$Y(x; p) = \sum_{k=0}^{\infty} p^k f_k(x). \quad (12)$$

From here, we get  $f_0(x) := Y(x; 0)$  as the initial solution of the Eq. (11), obtained for  $p = 0$ . On the other hand, the “main” solution of the Eq. (11), obtained for  $p = 1$ , will be

$$\psi_s(x) \equiv Y(x; 1) = \lim_{p \rightarrow 1^-} Y(x; p) = \sum_{k=0}^{\infty} f_k(x). \quad (13)$$

Thus, it represents the solution of the Eq. (10), on the condition of convergence the series in (13).

Now, substituting Eq. (12) in the homotopy Eq. (11), and by using Taylor’s expansion of the exponential term, we obtain

$$(1-p) \sum_{k=1}^{\infty} p^k f_k(x) = p \left\{ A \sum_{j=0}^{\infty} \frac{1}{j! u_T^j} \left[ \sum_{k=0}^{\infty} p^k f_k(x) \right]^j - \left[ \sum_{k=0}^{\infty} p^k f_k(x) \right]^2 + B(x) \sum_{k=0}^{\infty} p^k f_k(x) - C(x) \right\}, \quad (14)$$

where we denoted  $B(x) := 2x + \gamma^2 + 1$  and  $C(x) := x^2 + f_0(x)$ . By equating expressions with the identical powers  $p^k$ ,  $k = 1, 2, \dots$  we obtain the explicit expression of the functions  $\{f_k(x)\}$ . They can be expressed, recursively, with the following recurrence relations:

$$\begin{aligned} f_1(x) &= A \exp\left(\frac{f_0(x)}{u_T}\right) - f_0(x)^2 + B(x)f_0(x) - C(x), \\ f_2(x) &= A \exp\left(\frac{f_0(x)}{u_T}\right) \cdot \frac{f_1(x)}{u_T} - 2f_0(x)f_1(x) + B(x)f_1(x), \\ f_3(x) &= A \exp\left(\frac{f_0(x)}{u_T}\right) \cdot \left[ \frac{f_2(x)}{u_T} + \frac{f_1(x)^2}{2u_T^2} \right] - [2f_0(x)f_2(x) \\ &\quad + f_1(x)^2] + B(x)f_2(x), \\ &\vdots \end{aligned}$$

In the general case, by using the induction method, it can be easily shown that, for  $k \geq 2$  and  $m! \leq k < (m+1)!$ , hold the following equalities:

$$\begin{aligned} f_k(x) &= A \exp\left(\frac{f_0(x)}{u_T}\right) \cdot \sum_{j=1}^m \frac{1}{j! u_T^j} \sum_{i_1 + \dots + i_j = k-1} f_{i_1}(x) \cdots f_{i_j}(x) \\ &\quad - \sum_{j=0}^{k-1} f_j(x)f_{k-j-1}(x) + B(x)f_{k-1}(x). \end{aligned} \quad (15)$$

At last, the equalities above give the appropriate estimates of surface potential  $y = \psi_s(x)$ :

$$\begin{aligned} \widehat{\psi}_s^{(0)}(x) &= f_0(x), \\ \widehat{\psi}_s^{(k)}(x) &= \widehat{\psi}_s^{(k-1)}(x) + f_k(x) = \sum_{j=1}^k f_j(x), \quad k = 1, 2, \dots \end{aligned}$$

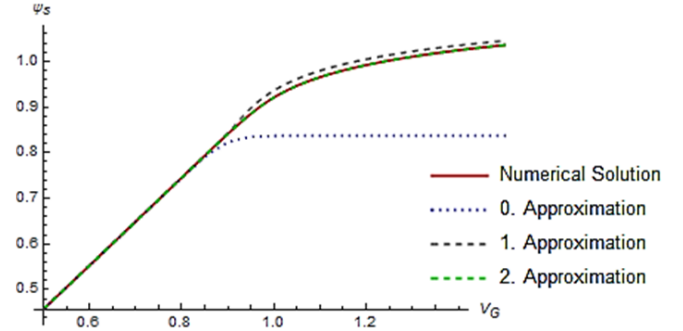


**Figure 1.** The HPM-approximations of the surface potential  $\psi_s(V_G)$ .

Fig.1 shows the surface potential versus gate voltage  $V_G$ . The convergences of the HPM-approximations are illustrated, along with the numerically obtained solution of Eq. (9). For initial solution was used the *the interpolation function*:

$$f_0(x) = \psi_{wi}(x) - u_T \log \left[ 1 + \exp \left( \frac{\psi_{wi}(x) - 2\phi_F - V_{ch}}{x} \right) \right], \quad (16)$$

where

$$\psi_{s_{wi}}(x) = \left( -\frac{\gamma}{2} + \sqrt{x + \frac{\gamma^2}{4}} \right)^2 \quad (17)$$

is an approximation of the surface potential  $\psi_s$  in the so-called *weak inversion region* (i.e. when  $\psi_s < 2\phi_F + V_{ch}$ ). As it easily can be seen, already for  $k \geq 2$ , the HPM-approximations  $\{\widehat{\psi}_s^{(k)}(x)\}$  give precise approximations of the surface potential  $\psi_s(x)$ .

## DETERMINATION OF INVARIANT MEASURES

In the researching of nonlinear chaotic dynamical models special attention is paid to determining their potential stochastic characteristics. Then, the precise analyses of the behavior of these models commonly needs the using of *the invariant (probabilistic) measures (IMs)*. One-dimensional nonlinear chaotic model is an usually defined by the operator  $T : A \rightarrow A$ , where  $A \subseteq \mathbb{R}$ . If chaotic map  $T(x)$  has a finite set of inverse branches  $T^{-1}(x) = \{g_1(x), \dots, g_\ell(x)\}$ , the determination of its IM is based on solving the well-known *Frobenius-Perron equation*:

$$f(x) = \sum_{y \in T^{-1}(x)} \frac{f(y)}{|T'(y)|}. \quad (18)$$

Here,  $f : \mathbb{R} \rightarrow \mathbb{R}$  is unknown probability density function which corresponds to appropriate IM, i.e. such that, for any Borel set  $B \subseteq \mathbb{R}$ , satisfies the following *T-invariant condition*:

$$\int_B f(x) dx = \int_B f \circ T(x) dx. \quad (19)$$

Since, as it is known, there no exists a general procedure to solve Frobenius-Perron Eq. (18) here is proposed one of the possible way of its solving, based on the HPM. For this purpose, we construct the following *homotopy equation*:

$$(1-p) \left[ F(x; p) - f_0(x) \right] + p \left[ F(x; p) - \sum_{y \in T^{-1}(x)} \frac{F(y; p)}{|T'(y)|} \right] = 0. \quad (20)$$

Here,  $p \in [0, 1]$  is embedding parameter and  $F(x, p)$  is solution of the homotopy Eq. (20) expressed as the power series given by Eq. (6). Thus, the solution of Frobenius-Perron Eq. (18) can be obtained in the same way as in Eq. (7), i.e. by substituting the power series from Eq. (6) in Eq. (20). After some computations, the following equations get ones:

$$\begin{aligned} f_1(x) &= \sum_{y \in T^{-1}(x)} \frac{f_0(y)}{|T'(y)|} - f_0(x), \\ f_k(x) &= \sum_{y \in T^{-1}(x)} \frac{f_{k-1}(y)}{|T'(y)|}, \quad k \geq 2. \end{aligned} \quad (21)$$

Using Eqs. (21), functions  $\{f_k(x)\}$  can be obtained recursively for an arbitrary  $k = 1, 2, \dots$ . The appropriate *HPM-approximations* of the unknown function  $f(x)$  are

$$\widehat{f}_k(x) := \sum_{j=0}^k f_j(x), \quad k = 0, 1, 2, \dots \quad (22)$$

and their convergence, under some sufficiently conditions, was proven in Stojanović et al. (2018). In the following, some examples of application of the HPM in determining IMs will be described.

**Example 3 ( $\Lambda$ -map).** On the closed unit interval  $[0, 1]$  consider the so-called *Lambda ( $\Lambda$ ) map* (Fig. 2, left panel):

$$T_a(x) = \begin{cases} \frac{x}{a}, & 0 \leq x < a, \\ \frac{1-x}{1-a}, & a \leq x \leq 1, \end{cases}$$

where  $a \in (0, 1)$  is a predefined parameter. In this case, we have:

$$|T'_a(x)| = \begin{cases} \frac{1}{a}, & 0 \leq x < a, \\ \frac{1}{1-a}, & a \leq x \leq 1, \end{cases}$$

and  $T_a^{-1}(x) = \{ax, 1 - (1-a)x\}$  is the set of inverse branches. Thus, the Frobenius-Perron equation is

$$f(x) = af(ax) + (1-a)f(1 - (1-a)x).$$

If we take, as an initial approximation  $f_0(x) \equiv 1$ , then the first of Eqs. (21) gives:

$$f_1(x) = af_0(ax) + (1-a)f_0(1 - (1-a)x) - f_0(x) \equiv 0.$$

After that, using the second of Eqs. (21), immediately follows  $f_k(x) \equiv 0$ , for any  $k \geq 2$ . In that way, the initial approximation  $f_0(x) \equiv 1$  is exact solution of the Frobenius-Perron Eq. (18), i.e. the invariant probability measure for this map is standard Lebesgue measure.

**Example 4 (Truncated  $\Lambda$ -map).** Consider again the closed unit interval  $[0, 1]$  and the following map (Fig. 2, right panel):

$$T_a(x) = \begin{cases} \frac{x}{a}, & 0 \leq x < a, \\ -x + a + 1, & a \leq x \leq 1, \end{cases}$$

where, in the same way as in the previous case,  $a \in (0, 1)$  is a predefined parameter. Here, we have:

$$|T'_a(x)| = \begin{cases} \frac{1}{a}, & 0 \leq x < a, \\ 1, & a \leq x \leq 1, \end{cases}$$

and the set of inverse branches is  $T_a^{-1}(x) = \{g_1(x), g_2(x)\}$ , where:

$$\begin{aligned} g_1(x) &= ax, \quad 0 \leq x \leq 1, \\ g_2(x) &= \begin{cases} 0, & 0 \leq x < a, \\ -x + a + 1, & a \leq x \leq 1, \end{cases} \end{aligned}$$

According to this, here the Frobenius-Perron Eq. (18) takes the following form:

$$f(x) = \begin{cases} af(g_1(x)), & 0 \leq x < a, \\ af(g_1(x)) + f(g_2(x)), & a \leq x \leq 1. \end{cases} \quad (23)$$

Now, if we take, as in previous example  $f_0(x) \equiv 1$  and apply Eqs. (21), we obtain:

$$f_1(x) = \begin{cases} af_0(g_1(x)) - f_0(x), & 0 \leq x < a, \\ af_0(g_1(x)) + f_0(g_2(x)) - f_0(x), & a \leq x \leq 1, \end{cases}$$

$$= \begin{cases} a - 1, & 0 \leq x < a, \\ a, & a \leq x \leq 1, \end{cases}$$

$$f_2(x) = \begin{cases} af_1(g_1(x)), & 0 \leq x < a, \\ af_1(g_1(x)) + f_1(g_2(x)), & a \leq x \leq 1, \end{cases}$$

$$= \begin{cases} a(a-1), & 0 \leq x < a, \\ a^2, & a \leq x \leq 1, \end{cases}$$

$$f_3(x) = \begin{cases} af_2(g_1(x)), & 0 \leq x < a, \\ af_2(g_1(x)) + f_2(g_2(x)), & a \leq x \leq 1, \end{cases}$$

$$= \begin{cases} a^2(a-1), & 0 \leq x < a, \\ a^3, & a \leq x \leq 1, \end{cases} \text{ etc.}$$

In general, using the induction method, it can be easily proven that equalities:

$$f_k(x) = \begin{cases} a^{k-1}(a-1), & 0 \leq x < a, \\ a^k, & a \leq x \leq 1, \end{cases}$$

hold for an arbitrary  $k \geq 1$ . According to thus obtained series  $\{f_k(x)\}$ , the solution of Frobenius-Perron equation in this case is as following:

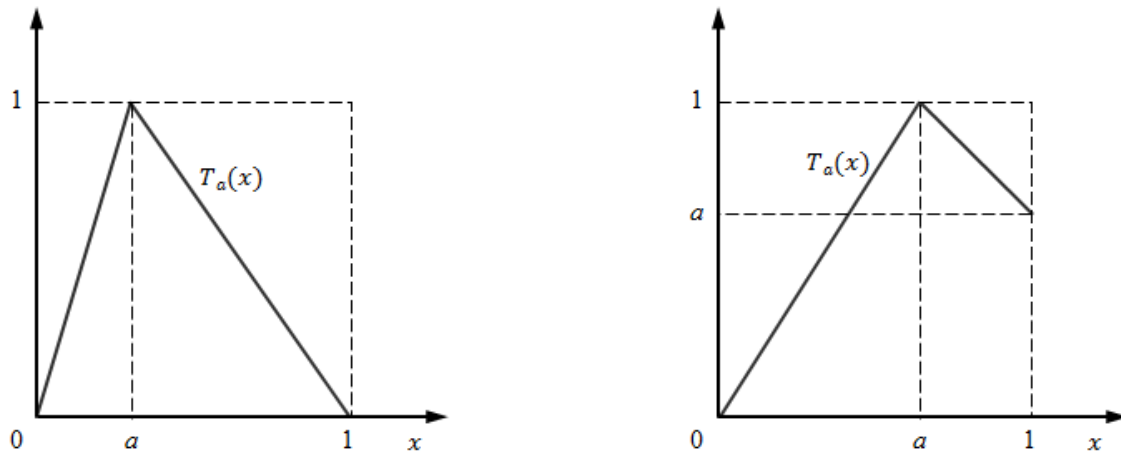


**Figure 2.** Graphs of the  $\Lambda$ -map (panel left) and the truncated  $\Lambda$ -map (panel right).

$$f(x) := \sum_{k=0}^{\infty} f_k(x) = \begin{cases} 1 + (a-1) \sum_{k=1}^{\infty} a^{k-1}, & 0 \leq x < a, \\ \sum_{k=0}^{\infty} a^k, & a \leq x \leq 1, \end{cases}$$

$$= \begin{cases} 0, & 0 \leq x < a, \\ \frac{1}{1-a}, & a \leq x \leq 1, \end{cases} \quad (24)$$

i.e. it is concentrated on the interval  $[a, 1]$ . It can be easily proved that the last expression in Eq. (24) represents the invariant probability density of truncated  $\Lambda$ -map, i.e. the exact solution of the Frobenius-Perron Eq. (23). Also, notice that, according to the well-known facts about geometric series, the above HPM procedure converges for arbitrary  $a \in (0, 1)$ .

## CONCLUSION

This paper describes the Homotopy perturbation method (HPM) representing the powerful technique for solving of nonlinear equations of various kinds. The HPM has been introduced in approximate solving of the well-known implicit relation between the electrostatic surface potential and terminal voltages in MOSFET transistor. As the second application of the HPM has been chosen the determination of the invariant measures (IMs) of the non-linear dynamical systems with chaotic behavior.

In the first case, the simple mathematical form and high degree of accuracy of obtained HPM approximate analytical solution lead to the improved surface potential based MOSFET model preferring for various circuit simulation programs. On the other hand, due to the second application of HPM procedure is confirmed that invariant measures of the chaotic mappings can be easily analytically determined. Two considered examples have been presented to elucidate the efficiency and implementation of the HPM in solving of various kind of research problems.

## REFERENCES

- Adamu, G., Bawa, M., Jiya, M., & Chado, U. 2017. A mathematical model for the dynamics of Zika virus via homotopy perturbation method. *Journal of Applied Sciences and Environmental Management*, 21(4), pp. 615–623. doi: 10.4314/jasem.v21i4.1
- Biazar, J., Badpeima, F., & Azimi, F. 2009. Application of the homotopy perturbation method to Zakharov–Kuznetsov equations. *Computers & Mathematics with Applications*, 58(11-12), pp. 2391–2394. doi: 10.1016/j.camwa.2009.03.102
- Bota, C. & Caruntu, B. 2017. Approximate analytical solutions of nonlinear differential equations using the Least Squares Homotopy Perturbation Method. *Journal of Mathematical Analysis and Applications*, 448, pp. 401–408. doi: 10.1016/j.jmaa.2016.11.031
- Chen, T. L. & Gildenblat, G. 2001. Analytical approximation for the MOSFET surface potential. *Solid-State Electronics*, 45, pp. 335–339. doi: 10.1016/s0038-1101(00)00283-5
- Dong, C., Chen, Z., & Jiang, W. 2013. A modified homotopy perturbation method for solving the nonlinear mixed Volterra–Fredholm integral equation. *Journal of Computational and Applied Mathematics*, 239(1), pp. 359–366. doi: 10.1016/j.cam.2012.09.003
- El-Sayed, A., Elsaid, A., El-Kalla, I., & Hammadb, D. 2012. A homotopy perturbation technique for solving partial differential equations of fractional order in finite domains. *Applied Mathematics and Computation*, 218(17). doi: 10.1016/j.amc.2012.01.057
- Gadallah, M. R. & Elzaki, T. M. 2017. An application of improvement of new homotopy perturbation method for solving third order nonlinear singular partial differential equations. *Universal Journal of Mathematics*, 2(1), pp. 110–124.
- He, J.-H. 1999. Homotopy perturbation technique. *Computer Methods in Applied Mechanics and Engineering*, 178(3-4), pp. 257–262. doi: 10.1016/s0045-7825(99)00018-3

- He, J.-H. 2000. A coupling method of a homotopy technique and a perturbation technique for non-linear problems. *International Journal of Non-Linear Mechanics*, 35(1), pp. 37–43. doi: 10.1016/s0020-7462(98)00085-7
- He, J.-H. 2003. Homotopy perturbation method: A new nonlinear analytical technique. *Applied Mathematics and Computation*, 135(1), pp. 73–79. doi: 10.1016/s0096-3003(01)00312-5
- He, J.-H. 2006. Homotopy perturbation method for solving boundary value problems. *Physics Letters A*, 350(1-2), pp. 87–88. doi: 10.1016/j.physleta.2005.10.005
- He, J.-H. 2008. Resent development of the homotopy perturbation method. *Topological Methods in Nonlinear Analysis*, 31(2), pp. 205–209.
- Hetmaniok, E., Nowak, I., Slota, D., & Witula, R. 2013. A study of the convergence of error estimation for the homotopy perturbation method for the Volterra-Fredholm integral equations. *Applied Mathematics Letters*, 26(1), pp. 165–169. doi: 10.1016/j.aml.2012.08.005
- Hetmaniok, E., Slota, D., & Witula, R. 2012. Convergence and error estimation of homotopy perturbation method for Fredholm and Volterra integral equations. *Applied Mathematics and Computation*, 218(21), pp. 10717–10725. doi: 10.1016/j.amc.2012.04.041
- Kevkić, T., Stojanović, V., & Petković, D. 2018. Solving Schrödinger equation for a particle in one-dimensional lattice: An homotopy perturbations approach. *Romanian Reports in Physics*, in press, pp. accepted manuscript.
- Kevkić, T., Stojanović, V., & Randjelović, D. 2017. Application of homotopy perturbation method in solving coupled Schrödinger and Poisson equation in accumulation layer. *Romanian Journal of Physics*, 62(9-10), pp. Article No. 122.
- Khan, M., Farasat Saddiq, S., Khan, S., Islam, S., & Ahmad, F. 2014. Application of homotopy perturbation method to an SIR epidemic model. *Journal of Applied Environmental and Biological Sciences*, 4, pp. 49–54.
- Noor, M. & Khan, W. 2012. New iterative methods for solving nonlinear equation by using homotopy perturbation method. *Applied Mathematics and Computation*, 219, pp. 3565–3574. doi: 10.1016/j.amc.2012.09.040
- Stojanović, V., Kevkić, T., Jelić, G., & Randjelović, D. 2018. Determination of invariant measures: An approach based on homotopy perturbations. *UPB Scientific Bulletin, Series A: Applied Mathematics and Physics*, 80(2), pp. 119–128.
- Tripathi, R. & Mishra, H. K. 2016. Homotopy perturbation method with Laplace transform (LT-HPM) for solving Lane-Emden type differential equations (LETDEs). New York: SpringerPlus. doi: 10.1186/s40064-016-3487-4
- van Langevelde, R. & Klaassen, F. 2000. An explicit surface-potential-based MOSFET model for circuit simulation. *Solid-State Electronics*, 44, pp. 409–418. doi: 10.1016/s0038-1101(99)00219-1
- Zeb, M., Haroon, T., & Siddiqui, A. 2014. Homotopy perturbation solution for flow of a third-grade fluid in helical screw rheometer. *UPB Scientific Bulletin, Series A: Applied Mathematics and Physics*, 76(4), pp. 179–190.
- Zhang, M.-F., Liu, Y.-Q., & Zhou, X.-S. 2015. Efficient homotopy perturbation method for fractional non-linear equations using Sumudu transform. *Thermal Science*, 19, pp. 1167–1171. doi: 10.2298/tsci1504167z

# INFINITESIMAL BENDING OF CURVES ON THE RULED SURFACES

MARIJA NAJDANOVIĆ<sup>1\*</sup>, LJUBICA VELIMIROVIĆ<sup>2</sup>

<sup>1</sup>Preschool Teacher Training College, Kruševac, Serbia

<sup>2</sup>Faculty of Sciences and Mathematics, University of Niš, Niš, Serbia

## ABSTRACT

In this paper we study infinitesimal bending of curves that lie on the ruled surfaces in Euclidean 3-dimensional space. We obtain an infinitesimal bending field under whose effect all bent curves remain on the same ruled surface as the initial curve. Specially, we consider infinitesimal bending of the curves which belong to the cylinder as well as to the hyperbolic paraboloid and find corresponding infinitesimal bending fields. We examine the variation of the curvature of a curve under infinitesimal bending on the hyperbolic paraboloid. Some examples are visualized using program packet *Mathematica*.

**Keywords:** Infinitesimal bending, Curve, Variation, Ruled surface, Cylinder, Hyperbolic paraboloid.

## INTRODUCTION

Infinitesimal bending of curves and surfaces is a special part of the surface bending theory which presents one of the main consisting parts of the global differential geometry. The problems of infinitesimal bending have physical applications (in the study of elasticity, for example) and have a long history.

Historically, the first result of the surface bending theory belongs to Cauchy. Later, bending theory was developed thanks to the works of leading mathematicians of the considered area like Blaschke, Cohn-Vossen, A. D. Alexandrov, A. V. Pogorelov, I. N. Vekua, V. T. Fomenko, I. Kh. Sabitov, I. I. Karatopraklieva, V. A. Alexandrov and many others.

Infinitesimal bending is determined by the stationary of arc length with appropriate precision. A concept of infinitesimal bending dealt first with infinitesimal bending of surfaces and then with the same problem in the theory of curves and manifolds.

Infinitesimal bending of surfaces and manifolds was widely studied in (Aleksandrov, 1936; Alexandrov, 2010; Efimov, 1948; Hinterleitner et al., 2008; Ivanova-Karatopraklieva & Sabitov, 1995; Kon-Fossen, 1959; Najdanović, 2014; Vekua, 1959; Velimirović, 2009). Infinitesimal bending of curves was considered in (Efimov, 1948; Najdanovic, 2015; Najdanovic & Velimirovic, 2017a,b; Rancic et al., 2009; Velimirović, 2001a,b, 2009; Velimirović et al., 2010; Yano et al., 1946).

First we shall give some basic facts, definitions and theorems according to (Velimirović, 2001a & Velimirović, 2009).

Let us consider continuous regular curve  $C \subset \mathcal{R}^3$ , given with the equation

$$C : \mathbf{r} = \mathbf{r}(u), \quad u \in I \subseteq \mathcal{R} \quad (1)$$

included in a family of the curves

$$C_\epsilon : \tilde{\mathbf{r}}(u, \epsilon) = \mathbf{r}_\epsilon(u) = \mathbf{r}(u) + \epsilon \mathbf{z}(u), \quad u \in I, \quad \epsilon \in (-1, 1), \quad (2)$$

where  $u$  is a real parameter and we get  $C$  for  $\epsilon = 0$  ( $C = C_0$ ).

**Definition 1.** Family of curves  $C_\epsilon$  is **infinitesimal bending of a curve**  $C$  if

$$ds_\epsilon^2 - ds^2 = o(\epsilon),$$

where  $\mathbf{z} = \mathbf{z}(u)$ ,  $\mathbf{z} \in C^1$  is **infinitesimal bending field** of the curve  $C$ .

**Theorem 2.** (Efimov, 1948) *Necessary and sufficient condition for  $\mathbf{z}(u)$  to be an infinitesimal bending field of a curve  $C$  is to be*

$$d\mathbf{r} \cdot d\mathbf{z} = 0, \quad (3)$$

where  $\cdot$  stands for the scalar product in  $\mathcal{R}^3$ .  $\square$

The next theorem is related to determination of the infinitesimal bending field of a curve  $C$ .

**Theorem 3.** (Velimirović, 2001a) *Infinitesimal bending field for the curve  $C$  (1) is*

$$\mathbf{z}(u) = \int [p(u)\mathbf{n}_1(u) + q(u)\mathbf{n}_2(u)] du, \quad (4)$$

where  $p(u)$  and  $q(u)$ , are arbitrary integrable functions and vectors  $\mathbf{n}_1(u)$  and  $\mathbf{n}_2(u)$  are respectively unit principal normal and binormal vector fields of the curve  $C$ .  $\square$

As

$$\mathbf{n}_1 = \frac{(\dot{\mathbf{r}} \cdot \dot{\mathbf{r}})\ddot{\mathbf{r}} - (\dot{\mathbf{r}} \cdot \ddot{\mathbf{r}})\dot{\mathbf{r}}}{\|\dot{\mathbf{r}}\| \|\ddot{\mathbf{r}}\|}, \quad \mathbf{n}_2 = \frac{\dot{\mathbf{r}} \times \ddot{\mathbf{r}}}{\|\dot{\mathbf{r}} \times \ddot{\mathbf{r}}\|},$$

infinitesimal bending field can be written in the form

$$\mathbf{z}(t) = \int [p(t) \frac{(\dot{\mathbf{r}} \cdot \dot{\mathbf{r}})\ddot{\mathbf{r}} - (\dot{\mathbf{r}} \cdot \ddot{\mathbf{r}})\dot{\mathbf{r}}}{\|\dot{\mathbf{r}}\| \|\ddot{\mathbf{r}}\|} + q(t) \frac{\dot{\mathbf{r}} \times \ddot{\mathbf{r}}}{\|\dot{\mathbf{r}} \times \ddot{\mathbf{r}}\|}] dt$$

\* Corresponding author: marijamath@yahoo.com

where  $p(t), q(t)$  are arbitrary integrable functions, or in the form

$$\mathbf{z}(t) = \int [P_1(t)\dot{\mathbf{r}} + P_2(t)\ddot{\mathbf{r}} + Q(t)(\dot{\mathbf{r}} \times \ddot{\mathbf{r}})]dt \quad (5)$$

where  $P_i(t)$ ,  $i = 1, 2$ ,  $Q(t)$  are arbitrary integrable functions, too.

An interesting problem is the infinitesimal bending of a plane curve which stays in the plane after bending. This problem was considered in the paper (Velimirović, 2001a). It was found corresponding infinitesimal bending field, i. e. it was proved the next theorem.

**Theorem 4.** *Infinitesimal bending field that plane curve*

$$K : \rho = \rho(\theta) \quad (6)$$

*under infinitesimal bending includes in a family of planes curves*

$$K_\epsilon : \rho_\epsilon = \rho_\epsilon(\theta), \quad \epsilon \in (-1, 1), \quad (7)$$

is

$$\mathbf{z}(\theta) = \rho(\theta) \sin \theta \mathbf{i} - \rho(\theta) \cos \theta \mathbf{j}, \quad (8)$$

where  $\mathbf{i}$  and  $\mathbf{j}$  are unit vectors in the direction of Cartesian axes. ■

Also, in the same paper it was proved that the area of the region determined by a plane curve being infinitesimally bent staying plane is stationary.

An interesting question considered in the paper (Velimirović et al., 2010) is about infinitesimal bending of a spherical curve but so that all bent curves are on the same sphere. It was proved that there isn't infinitesimal bending of a spherical curve belonging to the sphere.

In this paper we confront the question: Is it possible to infinitesimally bend a curve  $C$  which lies on the ruled surface  $S$ , but so that all bent curves of the family  $C_\epsilon$  stay on  $S$ ? The answer is affirmative and in the sequel we shall give an explicit formula for such an infinitesimal bending field.

## DETERMINATION OF INFINITESIMAL BENDING FIELD

**Theorem 5.** *Let a ruled surface  $S$  be given by*

$$S : \mathbf{r} = \mathbf{r}(u, v) = \rho(u) + v \mathbf{e}(u) \quad (u \in \mathcal{I}, v \in \mathcal{R}, \|\mathbf{e}(u)\| = 1), \quad (9)$$

*with a directrix  $\rho = \rho(u)$  and generatrices in the direction of the vector  $\mathbf{e}(u)$ , and let a curve*

$$C : \mathbf{r} = \mathbf{r}(t) = \mathbf{r}(u(t), v(t)) \quad (10)$$

*be on the surface  $S$ . Then infinitesimal bending field which given curve leaves on the surface  $S$  is*

$$\mathbf{z}(t) = c \mathbf{e}(u(t)) e^{-\int \frac{u^2(\rho_u \cdot \mathbf{e}_u + v\|\mathbf{e}_u\|^2)}{u\rho_u \cdot \mathbf{e} + v} dt}, \quad (11)$$

where  $u\rho_u \cdot \mathbf{e} + v \neq 0$  and  $c$  is a constant.

**Proof.** Let

$$C : \mathbf{r} = \mathbf{r}(t) = \rho(u(t)) + v(t) \mathbf{e}(u(t))$$

be a curve on the surface  $S$  and

$$C_\epsilon : \mathbf{r}_\epsilon(t) = \rho(u(t)) + v(t) \mathbf{e}(u(t)) + \epsilon \mathbf{z}(t)$$

be an infinitesimal bending of the curve  $C$  determined with the field  $\mathbf{z}$ . As the family of the curves  $C_\epsilon$ ,  $\epsilon \in (-1, 1)$  belongs to the surface  $S$ , the field  $\mathbf{z}$  must be in the form

$$\mathbf{z}(t) = \mathbf{e}(u(t)) z_1(t), \quad (12)$$

where  $z_1(t)$  is a real continuous differentiable function.

Having in mind that  $\mathbf{z}$  is an infinitesimal bending field, the condition (3) must be satisfied, i. e.

$$\dot{\mathbf{r}} \cdot \dot{\mathbf{z}} = 0, \quad (13)$$

i. e.

$$(\rho_u \dot{u} + \dot{v} \mathbf{e} + v \mathbf{e}_u \dot{u}) \cdot (\mathbf{e}_u \dot{u} z_1 + \mathbf{e} \dot{z}_1) = 0. \quad (14)$$

As it is valid  $\|\mathbf{e}\| = 1$ , we conclude that must be satisfied  $\mathbf{e} \cdot \dot{\mathbf{e}} = 0$  ( $\mathbf{e} \perp \dot{\mathbf{e}} \Leftrightarrow \dot{\mathbf{e}} \cdot \mathbf{e} + \mathbf{e} \cdot \dot{\mathbf{e}} = 0 \Leftrightarrow (\mathbf{e} \cdot \mathbf{e})' = 0 \Leftrightarrow \|\mathbf{e}\|^2' = 0 \Leftrightarrow \|\mathbf{e}\| = \text{const}$ ). Using this fact, we obtain homogenous linear differential equation

$$z_1 \dot{u}^2 (\rho_u \cdot \mathbf{e}_u + v\|\mathbf{e}_u\|^2) + \dot{z}_1 (\dot{u} \rho_u \cdot \mathbf{e} + \dot{v}) = 0, \quad (15)$$

whose solution is

$$z_1(t) = c e^{-\int \frac{u^2(\rho_u \cdot \mathbf{e}_u + v\|\mathbf{e}_u\|^2)}{u\rho_u \cdot \mathbf{e} + v} dt}, \quad (16)$$

$c$  is a constant and  $\dot{u} \rho_u \cdot \mathbf{e} + \dot{v} \neq 0$ . Putting (16) into (12), we obtain (11). ■

Let us note that if the directrix  $C : \rho = \rho(u)$  is at the same time the striction line of the ruled surface  $S$ , then it is valid

$$\dot{\mathbf{e}} \cdot \dot{\rho} = 0$$

(see Gray (1998)), therefore  $\mathbf{e}(u)$  is the field of the infinitesimal bending of curve  $C$  which that curve includes in a family of curves on the ruled surface  $S$ ,

$$C_\epsilon : \tilde{\rho}(u, \epsilon) = \rho_\epsilon(u) = \rho(u) + \epsilon \mathbf{e}(u).$$

In addition, each curve of the family  $C_\epsilon$  is "parallel" to the curve  $C$ , i. e. the cut of the each generatrix between  $C$  and  $C_\epsilon$  is of the same length. Indeed,

$$\|\tilde{\rho}(u_1, \epsilon) - \rho(u_1)\| = \|\epsilon \mathbf{e}(u_1)\| = \epsilon = \|\epsilon \mathbf{e}(u_2)\| = \|\tilde{\rho}(u_2, \epsilon) - \rho(u_2)\|,$$

due to  $\|\mathbf{e}(u_1)\| = \|\mathbf{e}(u_2)\| = 1$ . Note that for the directrix of the ruled surface can be taken every curve on the surface which is cut or touched by the generatrices, and therefore, the directrix can be the striction line, if there is one.

The ruled surfaces are not the only surfaces on which it is possible to infinitesimally bend curves. We will show that in the following example.

**Example 6.** Let  $S$  be the rotation surface in  $\mathcal{R}^3$  of class  $C^\infty$ , given as the graph of the function

$$F(x, y) = \begin{cases} e^{\frac{-1}{(r^2-1)^2}}, & r > 1 \\ 0, & 0 \leq r \leq 1 \end{cases} \quad x^2 + y^2 = r^2.$$

Note that  $S$  is not a ruled surface (in fact it is not ruled in any open neighborhood of any point of the unit circle  $(\cos \theta, \sin \theta, 0)$ ). Consider the curve  $C \subset S$  given by

$$C : \mathbf{r}(t) = (t, o, f(t)),$$

where

$$f(t) = \begin{cases} e^{\frac{-1}{(t^2-1)^2}}, & |t| > 1 \\ 0, & |t| \leq 1 \end{cases}$$

Let

$$g(t) = \begin{cases} 0, & |t| \geq 1 \\ e^{\frac{-1}{(t^2-1)^2}}, & |t| < 1 \end{cases}$$

Then the family of curves given by

$$C_\epsilon : \mathbf{r}_\epsilon = (t, \epsilon g(t), f(t))$$

belongs to the surface  $S$  and presents infinitesimal bending of the curve  $C$  determined with the field  $\mathbf{z} = (0, g(t), 0)$ .

## INFINITESIMAL BENDING OF CURVES ON THE CYLINDER

A cylinder is an example of the ruled surfaces. Let us find an infinitesimal bending field of a curve on the cylinder, that leaves the given curve on the cylinder after bending.

**Theorem 7.** Let the cylinder be given by the equation  $S : x^2 + y^2 = a^2$ . Let  $C : \mathbf{r}(t) : (\alpha, \beta) \rightarrow \mathcal{R}^3$  be a regular continuous curve on the cylinder  $S$  and  $\mathbf{z}(t)$  be a vector field of class  $C^1$  which given curve includes in the family of the curves  $C_\epsilon : \mathbf{r}_\epsilon = \mathbf{r}(t) + \epsilon \mathbf{z}(t)$ ,  $\epsilon \in (-1, 1)$ , on the cylinder  $S$ , under infinitesimal bending.

a) If the curve  $C$  is in the plane  $z = \text{const}$ , then infinitesimal bending field is  $\mathbf{z}(t) = z_3(t)\mathbf{k}$ , where  $\mathbf{k} = (0, 0, 1)$  and  $z_3(t)$  is an arbitrary real function of class  $C^1$ .

b) Otherwise, infinitesimal bending field is a constant vector  $\mathbf{z} = c\mathbf{k}$ , where  $c$  is a real constant. Bending is rigid and reduces to the translation along  $z$ -axis.

**Proof.** The parametric equation of the cylinder of height  $h$  and of semi-axis  $a$  is

$$\mathbf{r}(u, v) = (a \cos u, a \sin u, v), \quad u \in [0, 2\pi], \quad v \in [0, h]. \quad (17)$$

Let

$$\mathbf{r}(t) = \mathbf{r}(u(t), v(t)) = (a \cos u(t), a \sin u(t), v(t)), \quad t \in (\alpha, \beta) \quad (18)$$

be the curve which lies on the cylinder (17). Infinitesimal bending will be

$$\begin{aligned} \mathbf{r}_\epsilon(t) &= \mathbf{r}(t) + \epsilon \mathbf{z}(t) \\ &= (a \cos u(t) + \epsilon z_1(t), a \sin u(t) + \epsilon z_2(t), v(t) + \epsilon z_3(t)), \end{aligned} \quad (19)$$

where  $\mathbf{z}(t) = (z_1(t), z_2(t), z_3(t))$  and  $z_1(t), z_2(t), z_3(t)$  are real continuous differentiable functions. As the curves  $\mathbf{r}_\epsilon$  must be on the surface (17), it must be valid

$$(a \cos u(t) + \epsilon z_1(t))^2 + (a \sin u(t) + \epsilon z_2(t))^2 = a^2,$$

i.e. after recombination

$$2a(\cos u(t)z_1(t) + \sin u(t)z_2(t)) + \epsilon(z_1^2(t) + z_2^2(t)) = 0,$$

for each  $\epsilon \in (-1, 1) \setminus \{0\}$ . Therefore, it must be valid

$$\cos u(t)z_1(t) + \sin u(t)z_2(t) = 0 \quad (20)$$

and

$$z_1^2(t) + z_2^2(t) = 0. \quad (21)$$

From (21) we have  $z_1(t) = z_2(t) = 0$ , so that  $\mathbf{z}(t) = (0, 0, z_3(t))$ . As  $\mathbf{z}$  is infinitesimal bending field, it holds (13). Therefore,

$$(-a \sin u(t)\dot{u}(t), a \cos u(t)\dot{u}(t), \dot{v}(t)) \cdot (0, 0, \dot{z}_3(t)) = 0,$$

i.e.

$$\dot{v}(t)\dot{z}_3(t) = 0. \quad (22)$$

From here it is  $\dot{v}(t) = 0$  or  $\dot{z}_3(t) = 0$ . We distinguish two cases.

- When  $\dot{v}(t) = 0$ , we have  $v(t) = \text{const}$ , i.e. the curve  $\mathbf{r}(t)$  is in the plane  $z = \text{const}$ . Infinitesimal bending field in this case is  $\mathbf{z}(t) = (0, 0, z_3(t)) = z_3(t)\mathbf{k}$ .
- When  $\dot{z}_3(t) = 0$ , i.e.  $z_3(t) = \text{const}$ , we obtain infinitesimal bending field of an arbitrary curve on the cylinder in the form  $\mathbf{z} = (0, 0, c) = c\mathbf{k}$ ,  $c$  is a real constant. ■

**Example 8.** Let us consider some curves on the cylinder  $S : \mathbf{r}(u, v) = (3 \cos u, 3 \sin u, v)$  and their infinitesimal bending. These examples are visualized using the software package *Mathematica* (Gray, 1998).

For the circle  $C_1 : \mathbf{r}(t) = (3 \cos t, 3 \sin t, 0)$ , which is in the plane  $z = 0$ , we can take infinitesimal bending field  $\mathbf{z}(t) = t\mathbf{k}$ . On the figure Fig. (1) we can see the curve  $C_1$  and bent curves for  $\epsilon = 0.1, 0.3, 0.5, 0.9$ . Obviously, the curve  $C_1$  clefs under that infinitesimal bending and is included in a family of helices on the cylinder.

For the same circle  $C_1 : \mathbf{r}(t) = (3 \cos t, 3 \sin t, 0)$ , we can take  $\mathbf{z}(t) = t(2\pi - t)\mathbf{k}$ . As it is valid  $\mathbf{r}_\epsilon(t = 0) = \mathbf{r}_\epsilon(t = 2\pi)$ , the curve remains closed (Fig. (2)).

If we take the curve  $C_2 : \mathbf{r}(t) = (3 \cos t^3, 3 \sin t^3, t^3)$  and infinitesimal bending field  $\mathbf{z} = 4\mathbf{k}$ , we get only rigid motion, i.e. translation along the  $z$ -axis (Fig. (3)).

## INFINITESIMAL BENDING OF CURVES ON THE HYPERBOLIC PARABOLOID

A hyperbolic paraboloid is an example of doubly ruled surfaces. In the sequel we will find infinitesimal bending field of an arbitrary curve belonging to this surface.

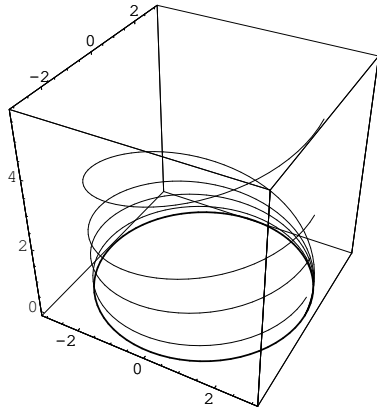


**Figure 1.** Infinitesimal bending of the circle  $C_1$  on the cylinder.

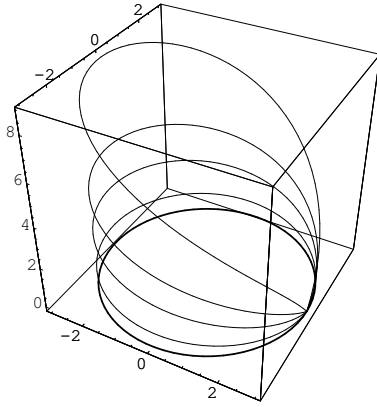


**Figure 2.** Infinitesimal bending of the circle  $C_1$  on the cylinder.

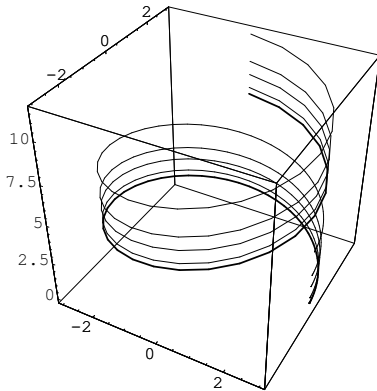


**Figure 3.** Trivial infinitesimal bending of the circle  $C_2$  on the cylinder.

**Theorem 9.** Let a hyperbolic paraboloid be given by the equation  $S : \mathbf{r}(u, v) = (u, v, uv)$  and continuous regular curve on it by  $C : \mathbf{r}(t) = \mathbf{r}(u(t), v(t))$ . Let  $\mathbf{z}(t)$  be a vector field of class  $C^1$  which given curve under infinitesimal bending includes in the family of the curves  $C_\epsilon : \mathbf{r}_\epsilon = \mathbf{r}(t) + \epsilon \mathbf{z}(t)$ ,  $\epsilon \in (-1, 1)$ , on the hyperbolic paraboloid  $S$ . Then the equations

$$\mathbf{z}(t) = ce^{-\int \frac{(uv)' \dot{u}}{\dot{v} + u(uv)'} dt} (0, 1, u(t)), \quad (23)$$

$\dot{v} + u(uv)' \neq 0$ , and

$$\mathbf{z}(t) = ce^{-\int \frac{(uv)' \dot{v}}{\dot{u} + v(uv)'} dt} (1, 0, v(t)), \quad (24)$$

$\dot{u} + v(uv)' \neq 0$ , determine the field  $\mathbf{z}(t)$ .  $c$  is an arbitrary constant.

**Proof.** Let

$$\begin{aligned} \mathbf{r}_\epsilon(t) &= \mathbf{r}(t) + \epsilon \mathbf{z}(t) \\ &= (u(t) + \epsilon z_1(t), v(t) + \epsilon z_2(t), u(t)v(t) + \epsilon z_3(t)) \end{aligned} \quad (25)$$

be an infinitesimal bending of  $C$  determined by the field  $\mathbf{z}(t) = (z_1(t), z_2(t), z_3(t))$ ,  $z_1, z_2, z_3$  are real continuous differentiable functions. As the curves (25) are on the surface  $S$ , it must be satisfied the next condition

$$(u(t) + \epsilon z_1(t))(v(t) + \epsilon z_2(t)) = u(t)v(t) + \epsilon z_3(t), \quad \forall \epsilon \in (-1, 1).$$

By dividing with  $\epsilon \neq 0$  we obtain

$$z_1(t)v(t) + z_2(t)u(t) - z_3(t) + \epsilon z_1(t)z_2(t) = 0. \quad (26)$$

Since the condition (26) must be valid for each  $\epsilon \in (-1, 1) \setminus \{0\}$ , it must be

$$z_1(t)v(t) + z_2(t)u(t) - z_3(t) = 0 \quad (27)$$

and

$$z_1(t)z_2(t) = 0. \quad (28)$$

From (28) we get  $z_1(t) = 0$  or  $z_2(t) = 0$ . We distinguish two cases.

- Let be valid  $z_1(t) = 0$ . The equation (27) reduces to  $z_2(t)u(t) = z_3(t)$ . From here we have

$$\mathbf{z}(t) = (0, z_2(t), u(t)z_2(t)). \quad (29)$$

Since  $\mathbf{z}(t)$  is an infinitesimal bending field, it holds (13). By substituting  $\dot{\mathbf{r}} = (\dot{u}, \dot{v}, \dot{u}v + u\dot{v})$  and  $\dot{\mathbf{z}} = (0, \dot{z}_2, \dot{u}z_2 + uz_2')$ , in the equation (13) we obtain

$$(\dot{v} + (uv)')u\dot{z}_2 + (uv)'\dot{u}z_2 = 0. \quad (30)$$

Solving the homogenous linear differential equation (30) by  $z_2$ , we obtain

$$z_2(t) = ce^{-\int \frac{(uv)' \dot{u}}{\dot{v} + u(uv)'} dt}, \quad \dot{v} + u(uv)' \neq 0. \quad (31)$$

From here and from (29) we get (23).

- Analogically we solve the case  $z_2(t) = 0$  and get (24).

It is easy to show that the fields (23) and (24) present infinitesimal bending fields of the curve  $C$  which that curve leaves on the hyperbolic paraboloid  $S$ , after bending. ■

**Example 10.** Let the curve  $C_3 : \mathbf{r}(t) = (t, t, t^2)$ ,  $t \in (a, b) \subseteq \mathcal{R}$ , be given on the surface  $S : \mathbf{r}(u, v) = (u, v, uv)$ . According to Theorem 9, after the necessary calculations, we obtain that infinitesimal bending fields of the curve  $C_3$  which given curve leaves on the surface  $S$ , for  $c = 1$ , have the next form

$$\mathbf{z}_1(t) = \left(0, \frac{1}{\sqrt{1+2t^2}}, \frac{t}{\sqrt{1+2t^2}}\right)$$

and

$$\mathbf{z}_2(t) = \left( \frac{1}{\sqrt{1+2t^2}}, 0, \frac{t}{\sqrt{1+2t^2}} \right).$$

The resulting deformations are shown in Fig. (4). We can see the curve  $C_3$  and bent curves  $C_{3\epsilon}$  for  $\epsilon = \pm 0.25, \pm 0.5, \pm 0.75, \pm 1$  under the field  $\mathbf{z}_1$ .

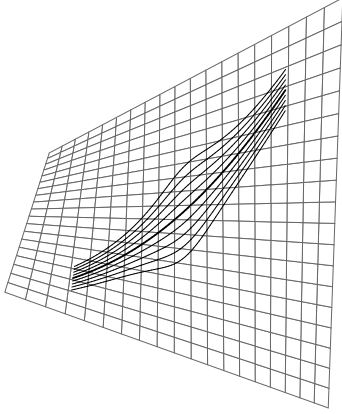


**Figure 4.** Infinitesimal bending of the curve  $C_3$  on the hyperbolic paraboloid.

*Example 11.* For the curve  $C_4 : \mathbf{r}(t) = (t, t^2, t^3)$  the corresponding infinitesimal bending fields are

$$\mathbf{z}_1(t) = \left( 0, \frac{1}{\sqrt{2+3t^2}}, \frac{t}{\sqrt{2+3t^2}} \right)$$

and

$$\mathbf{z}_2(t) = \left( \frac{1}{\sqrt{1+3t^4}}, 0, \frac{t^2}{\sqrt{1+3t^4}} \right).$$

Graphical presentation of the family of bent curves  $C_{4\epsilon}$  under the field  $\mathbf{z}_2$  is given in Fig. (5).

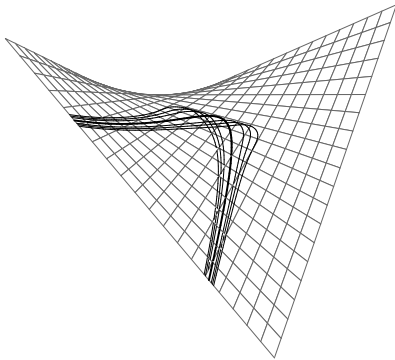


**Figure 5.** Infinitesimal bending of the curve  $C_4$  on the hyperbolic paraboloid.

## VARIATION OF THE CURVATURE OF CURVES ON THE HYPERBOLIC PARABOLOID

Under infinitesimal bending, geometric magnitudes describing a curve are changing and this change is determined by the variation. We define the variation according to (Vekua (1959)).

**Definition 12.** Let  $\mathcal{A} = \mathcal{A}(u)$  be the magnitude that characterizes a geometric property on the curve  $C$  and  $\mathcal{A}_\epsilon = \mathcal{A}_\epsilon(u)$  the corresponding magnitude on the curve  $C_\epsilon$  being infinitesimal bending of the curve  $C$ ,

$$\Delta \mathcal{A} = \mathcal{A}_\epsilon - \mathcal{A} = \epsilon \delta \mathcal{A} + \epsilon^2 \delta^2 \mathcal{A} + \dots \epsilon^n \delta^n \mathcal{A} + \dots \quad (32)$$

Coefficients  $\delta \mathcal{A}, \delta^2 \mathcal{A}, \dots, \delta^n \mathcal{A}, \dots$  are **the first, the second, ..., the  $n$ th variation** of the geometric magnitude  $\mathcal{A}$ , respectively under infinitesimal bending  $C_\epsilon$  of the curve  $C$ .

Obviously, for the first variation is effective

$$\delta \mathcal{A} = \frac{d}{d\epsilon} \mathcal{A}_\epsilon(u) \Big|_{\epsilon=0}, \quad (33)$$

i. e.

$$\delta \mathcal{A} = \lim_{\epsilon \rightarrow 0} \frac{\Delta \mathcal{A}}{\epsilon} = \lim_{\epsilon \rightarrow 0} \frac{\mathcal{A}_\epsilon(u) - \mathcal{A}(u)}{\epsilon}. \quad (34)$$

Infinitesimal bending is a kind of deformation under which the coefficients of the first fundamental form don't get the variations of the first order, i. e. these variations are zero. The magnitudes expressed by the coefficients of the first fundamental form and derivatives of these coefficients also have no variation of the first order (for example Cristoffel's symbols, area of a region on the surface and other). However, coefficients of the second fundamental form have, generally speaking, variations different from zero.

Let us examine the variation of the curvature  $K$  of a curve

$$C : \mathbf{r}(t) = \mathbf{r}(u(t), v(t)) \quad (35)$$

on the hyperbolic paraboloid

$$S : \mathbf{r}(u, v) = (u, v, uv). \quad (36)$$

The curve  $C$  infinitesimally bends on  $S$  under infinitesimal bending field (23). The curvature of the curves

$$C_\epsilon : \mathbf{r}_\epsilon = \mathbf{r}(t) + \epsilon \mathbf{z}(t) \quad (37)$$

is given by the formula

$$K_\epsilon = \frac{\|\mathbf{r}_\epsilon \times \dot{\mathbf{r}}_\epsilon\|}{\|\mathbf{r}_\epsilon\|^3}. \quad (38)$$

By direct calculation we get

$$\|\mathbf{r}_\epsilon \times \dot{\mathbf{r}}_\epsilon\|^2 = \|\dot{\mathbf{r}} \times \ddot{\mathbf{r}}\|^2 + 2\epsilon P_1(t) + \epsilon^2 P_2(t) + \epsilon^3 P_3(t) + \epsilon^4 P_4(t),$$

where

$$\begin{aligned} P_1(t) &= (\dot{v}(uv)'' - \ddot{v}(uv)')A(t) + (\dot{u}(uv)'' - \ddot{u}(uv)')C(t) \\ &\quad + (\dot{u}\ddot{v} - \ddot{u}\dot{v})D(t); \\ P_2(t) &= 2(\dot{v}(uv)'' - \ddot{v}(uv)')B(t) + A^2(t) + C^2(t) + D^2(t); \\ P_3(t) &= 2A(t)B(t); \quad P_4(t) = B^2(t); \\ A(t) &= (\ddot{u}\dot{v} - \dot{u}\ddot{v})z_2 + (4\dot{u}\dot{v} + \ddot{u}\dot{v})\dot{z}_2 - \dot{u}\dot{v}\ddot{z}_2; \\ B(t) &= \ddot{u}z_2\dot{z}_2 + 2\dot{u}\dot{z}_2^2 - \dot{u}z_2\ddot{z}_2; \\ C(t) &= (2\dot{u}^2 - u\ddot{u})\dot{z}_2 + u\dot{u}\ddot{z}_2; \quad D(t) = \dot{u}\dot{z}_2 - \ddot{u}z_2; \end{aligned} \quad (39)$$

The function  $z_2(t)$  is determined by Eq. (31). Also,

$$\|\dot{\mathbf{r}}_\epsilon\|^2 = \|\dot{\mathbf{r}}\|^2 + \epsilon^2[(\dot{u}z_2 + uz_2')^2 + \dot{z}_2'^2]. \quad (40)$$

It is valid

$$\lim_{\epsilon \rightarrow 0} \frac{K_\epsilon^2 - K^2}{\epsilon} = \frac{d}{d\epsilon} K_\epsilon^2 \Big|_{\epsilon=0} = \frac{2P_1(t)}{\|\dot{\mathbf{r}}\|^6}, \quad (41)$$

and also,

$$\lim_{\epsilon \rightarrow 0} \frac{K_\epsilon^2 - K^2}{\epsilon} = \lim_{\epsilon \rightarrow 0} \frac{K_\epsilon - K}{\epsilon} \cdot (K_\epsilon + K) = \delta K \cdot 2K, \quad (42)$$

where  $\delta K$  is the variation of the curvature  $K$  of curve (35). By comparing (41) and (42), using  $K \neq 0$  we obtain

$$\delta K = \frac{P_1(t)}{K\|\dot{\mathbf{r}}\|^6}. \quad (43)$$

Let us verify the case  $K = 0$ . From (41) and (42) we conclude  $P_1(t) = 0$ . Now it is

$$\delta K = \lim_{\epsilon \rightarrow 0} \frac{K_\epsilon}{\epsilon} = \frac{\sqrt{\epsilon^2 P_2(t) + \epsilon^3 P_3(t) + \epsilon^4 P_4(t)}}{\epsilon[\sqrt{\|\dot{\mathbf{r}}\|^2 + \epsilon^2((\dot{u}z_2 + uz_2')^2 + \dot{z}_2'^2)}]^3}$$

i. e.

$$\delta K = \frac{\sqrt{P_2(t)}}{\|\dot{\mathbf{r}}\|^3}. \quad (44)$$

Therefore, it holds

**Theorem 13.** *The first variation of the curvature  $K$  of curve (35) on the hyperbolic paraboloid (36) under infinitesimal bending (23) doesn't have to be zero and it is given by Eq. (43) for  $K \neq 0$ , i. e. (44), for  $K = 0$ , where  $P_1$  and  $P_2$  are the functions given in (39).*

## ACKNOWLEDGEMENT

The second author was supported by the research project 174012 of the Serbian Ministry of Science.

## REFERENCES

- Aleksandrov, A. D. 1936. 0 beskonechno malyh izgibaniyah neregulyarnyh poverhnostei. Matem. sbornik, 1(43), pp. 307–321.
- Alexandrov, V. A. 2010. New manifestations of the Darboux's rotation and translation fields of a surface. New Zealand Journal of Mathematics, 40, pp. 59–65.
- Efimov, N. 1948. Kachestvennyye voprosy teorii deformatsii poverhnostei. UMN. 3. 2, pp. 47–158.

- Gray, A. 1998. Modern differential geometry of curves and surfaces with Mathematica. CRC Press. 2nd ed.
- Hinterleitner, I., Mikeš, J., & Stránská, J. 2008. Infinitesimal F-planar transformations. Russian Mathematics, 52(4), pp. 13–18. doi:10.3103/s1066369x08040026
- Ivanova-Karatopraklieva, I. & Sabitov, I. K. 1995. Bending of surfaces. Part II. Journal of Mathematical Sciences, 74(3), pp. 997–1043. doi:10.1007/bf02362831
- Kon-Fossen, S. E. 1959. Nekotorye voprosy differ. geometrii v celom. Moskva: Fizmatgiz.
- Najdanovic, M. 2015. Infinitesimal bending influence on the Willmore energy of curves. Filomat, 29(10), pp. 2411–2419. doi:10.2298/fil1510411n
- Najdanovic, M. & Velimirovic, L. 2017a. Second order infinitesimal bending of curves. Filomat, 31(13), pp. 4127–4137. doi:10.2298/fil1713127n
- Najdanović, M. S. 2014. Infinitesimal bending influence on the volume change. Applied Mathematics and Computation, 243, pp. 801–808. doi:10.1016/j.amc.2014.06.032
- Najdanovic, M. S. & Velimirovic, L. S. 2017b. On the Willmore energy of curves under second order infinitesimal bending. Miskolc Mathematical Notes, 17(2), pp. 979–987. doi:10.18514/mmn.2017.2133
- Rancic, S., Velimirovic, L., & Zlatanovic, M. 2009. Curvebend graphical tool for presentation of infinitesimal bending of curves. Filomat, 23(2), pp. 108–116. doi:10.2298/fil0902108r
- Vekua, I. 1959. Obobschennyye analiticheskie funktsii. Moskva.
- Velimirović, L. 2001a. Change of geometric magnitudes under infinitesimal bending. Facta universitatis - series: Mechanics, Automatic Control and Robotics, 3(11), pp. 135–148.
- Velimirović, L. 2001b. Infinitesimal bending of curves. Matematički bilten Skopje, Makedonija, 25(LI), pp. 25–36.
- Velimirović, L., Ćirić, M., & Zlatanović, M. 2010. Bending of spherical curves. In: Proceedings of 25th International Scientific Conference MoNGeometrija, SUGIG, pp. 657–667.
- Velimirović, L. S. 2009. Infinitesimal bending. University of Niš - Faculty of Sciences and Mathematics.
- Yano, K., Takano, K., & Tomonaga, Y. 1946. On the infinitesimal deformations of curves in the spaces with linear connection. Proceedings of the Japan Academy, 22(10), pp. 294–309. doi:10.3792/pja/1195572193

# TEMPORAL AND SPATIAL VARIATIONS OF AMBIENT DOSE EQUIVALENT RATE IN URBAN AND RURAL SITES

LJILJANA GULAN<sup>1\*</sup>

<sup>1</sup>Faculty of Natural Sciences and Mathematics, University of Priština, Kosovska Mitrovica, Serbia

## ABSTRACT

This study deals with the results of measuring the ambient dose equivalent rates conducted in test field. The impacts of temporal and weather variations (wind, precipitation, moisture, temperature) as well as spatial characteristics (rural and urban sites) on the ambient dose equivalent rate were analyzed. Mean ambient dose equivalent rate in rural site (142 nSv/h) is higher than in urban site (128 nSv/h). The reason is difference in altitude and also the difference in the local geology. Although an increasing of temperature, decreasing the moisture in air, and slowing down the wind speed during the observed period showed tendency of stability the ambient dose equivalent rate, no correlation was found between ambient dose equivalent rate and any parameter.

**Keywords:** Ambient dose equivalent rate, Variation.

## INTRODUCTION

Background radiation, which is registered under normal conditions, originates from cosmic radiation, natural and anthropogenic radionuclides in the soil, air and ground surface (UNSCEAR, 2000). It is characteristic for a certain area, because it depends on the geology of a terrain and an altitude. Cosmic radiation consists mainly of protons and radiations which appear in proton interactions with atoms in atmosphere. At sea level contribution to the dose equivalent relates to muons (over 70%), electrons and photons (~15%), neutrons (10%), protons and charged pions (1-2%). Contribution to external dose rate from directly ionizing and photon component is 32 nSv/h, and 7.8 nSv/h from neutron component (UNSCEAR, 2008); contribution from radionuclides in air (<sup>7</sup>Be and <sup>22</sup>Na) to the dose rate is below 1 nSv/h, and average contribution from radon and decay products outdoors is 2.5 nSv/h (Bossey et al., 2017).

It is known that the dose rate from photon and ionizing component varied with latitude, but the variation is small. The dose rate is about 10% lower at the geomagnetic equator than at high latitudes; the variability due to the solar cycle is also estimated to be about 10% (UNSCEAR, 2008). The ionizing component strongly depends on altitude; a variation of absorbed dose rate in air by a factor of 4 was measured in China for the same latitude, but different altitude (Wang, 2002). The cosmic ray dose rate at elevations above sea level was estimated according to the following equation (Bouville & Lowder, 2002):

$$E_1(z) = E_1(0)[0.21 \cdot e^{-1.649z} + 0.79 \cdot e^{0.4528z}] \quad (1)$$

where  $E_1(0)$  is the dose rate at sea level and  $z$  is the altitude in kilometres.

The production of cosmogenic radionuclides is greatest in the upper stratosphere and it is dependent not only on altitude but also on latitude.

Naturally occurring radionuclides of terrestrial origin are present in all environmental media, but in various degrees. These radionuclides with half-lives comparable to the age of the earth as well as their decay products exist in sufficient amount and can contribute to population exposure. Natural radiation in soil and on the ground surface originates from <sup>40</sup>K and radionuclides in series <sup>238</sup>U, <sup>235</sup>U and <sup>232</sup>Th, and anthropogenic radiation appears after nuclear weapon tests and nuclear accidents. This terrestrial component gives important contribution to the dose rate. The contribution of <sup>137</sup>Cs to the ambient dose equivalent rate is more significant in areas affected by the Chernobyl accident. The worldwide average contribution to external dose rate from terrestrial gamma radiation outdoors is estimated to 70 µSv/y (UNSCEAR, 2008).

The dose rate in air changes from place to place and over time, because the diversity of soil composition affects the dose variation more than cosmic radiation (Gulan & Spasović, 2017). The variation of terrestrial gamma radiation is usually greater than the variation of cosmic radiation. Therefore, it is important and desirable to get information on background radiation by measuring the gamma absorbed dose rate or ambient dose equivalent rate in the environment, where possible. This can serve as a useful database in the case of accidents.

Various meteorological conditions (temperature, wind, moisture, precipitation) can influence the variation in the values of the measured ambient dose equivalent rates. The maximum value of ambient dose equivalent rate in ground level air reaches at the end of summer and beginning of autumn, because of increased amount of autumn precipitation and difference in air and soil temperatures (Serbian Radiation Protection and Nuclear Safety Agency, 2016; Lebedyte et al.,

\* Corresponding author: ljiljana.gulan@pr.ac.rs

2003). It was observed that ambient dose equivalent rate increased during heavy rain which appeared after long drought, but when rain stopped, it decreased slightly (Lebedyte et al., 2003).

Soil receives heat from Sun and indirectly heats the air thus raising the temperature of the lower layers of the atmosphere. Moisture (humidity) is very changeable component of the atmosphere. The speed and direction of the wind are unstable due to turbulence. The wind draws air from the soil due to the Magnus effect above the uneven soil surface. Metrological conditions forming turbulent air mixing can influence the variation in ambient dose equivalent rate due to radon decay products for 6-17% (Lebedyte et al., 2003).

The higher levels of background radiation are associated with volcanic rock masses (granite), and lower levels with sedimentary rocks (Stojanovska et al., 2016; Abba et al., 2017) and Quaternary geological background (Sanusi et al., 2014).

The aim of this study was to measure the ambient dose equivalent rates of test field in the rural and urban sites of the town Kruševac, and then analyze the spatial and temporal variations according to the preliminary results of the radiation levels.

## EXPERIMENTAL

### Materials and methods

Radiation measuring instruments calibrated in terms of ambient dose equivalent have been widely used for the purpose of radiation protection. In this study the Geiger counter RADEX model RD1503<sup>+</sup> was used for measurements of ambient dose equivalent rate in air. The measurement with this detector is based on four averaged measurements which have been made within 40 seconds. RADEX model RD1503<sup>+</sup> operates in the interval of ambient dose equivalent rates from 0.05 to 9.99  $\mu\text{Sv/h}$  and in the temperature range from -18 °C to 65 °C. Measurement uncertainty for gamma radiation is  $\pm 15\%$  (RADEX, 2017; Gulan & Spasović, 2017). The natural radiation of terrestrial origin, as well as radiation from radionuclides in the air (decay products of radon, Be-7 and Na-22 in the atmosphere) is measured by RADEX.

Two measuring points, located at a relative distance of 20 km and different in altitudes, were selected in order to determine the spatial and temporal variations of ambient dose equivalent rates, as well as the influence of weather on the measuring values. The rural site is located at 304 m above sea level, and the urban site is 137 m above sea level. The geological units labeled as Quaternary and Neogene are mostly lowland landscapes. The Quaternary and Neogene unit often covers the rocks derived from nearby igneous and metamorphic rock, *i.e.* Jastrebac and Kopaonik mountains (Vučković et al., 2016). The measurements of ambient dose equivalent rate were carried out at 1 m above the ground in the

period from 07.10.2017-21.10.2017. Some authors reported diurnal variations of ambient dose equivalent rate: the maximums are at 3-6 a.m., and minimums are at 3-6 p.m., (Lebedyte et al., 2003). For this reason the measurements were conducted between 1 and 2 p.m. every day at the same time, in order to get reliable diurnal values.

Since meteorological conditions can have a significant impact on the ambient dose equivalent rate measurements, parameters such as wind speed, temperature, moisture, precipitation were noted during measurements.

## RESULTS AND DISCUSSION

Ambient dose equivalent rate, the values of wind speed, moisture, temperature during 15 days of measurements in test field (rural and urban sites) are presented in Table 1 and Table 2, respectively. The measurement of ambient dose equivalent rate range in an interval from 0.125  $\mu\text{Sv/h}$  (09.10.; 15.10.) to 0.17  $\mu\text{Sv/h}$  (08.10.) in rural site (Table 1). An increasing of temperature from 5 °C to 12 °C affects the increase of dose equivalent value. Ambient dose equivalent rate range from 0.110  $\mu\text{Sv/h}$  (10.10.) to 0.143  $\mu\text{Sv/h}$  (07.10.) in urban site (Table 2).

It was raining on the first day of measurements, but in the other days it was sunny, without precipitation. After rain the soil pores are filled with water which impedes exhalation. It is evident from Table 1 and Table 2 that humidity influences variation in value of the ambient dose equivalent rate in the first three days of measurement. Radon exhalation from soil depends on precipitation amounts and also diffusion coefficient increase with temperature (Lebedyte et al., 2003).

**Table 1.** Ambient dose equivalent rate (ADER), the values of wind speed, moisture, temperature during 15 days in rural site

Date	ADER ( $\mu\text{Sv/h}$ )	Wind (km/h)	Moisture (%)	Temperature (°C)
07.10.	0.153	26	99	5
08.10.	0.170	15	97	12
09.10.	0.125	13	84	14
10.10.	0.145	8	53	17
11.10.	0.128	16	58	17
12.10.	0.133	8	56	18
13.10.	0.133	11	59	19
14.10.	0.143	12	60	18
15.10.	0.125	5	57	16
16.10.	0.140	2	66	21
17.10.	0.148	3	42	25
18.10.	0.150	6	37	27
19.10.	0.153	3	34	26
20.10.	0.155	0	42	24
21.10.	0.133	4	74	23

**Table 2.** Ambient dose equivalent rate (ADER), the values of wind speed, moisture, temperature during 15 days in urban site

Date	ADER ( $\mu\text{Sv/h}$ )	Wind (km/h)	Moisture (%)	Temperature ( $^{\circ}\text{C}$ )
07.10.	0.143	27	99	4
08.10.	0.120	16	97	12
09.10.	0.123	13	84	14
10.10.	0.110	8	53	17
11.10.	0.113	14	58	17
12.10.	0.125	8	56	18
13.10.	0.133	11	59	19
14.10.	0.125	12	60	21
15.10.	0.123	9	57	22
16.10.	0.138	3	57	23
17.10.	0.138	2	49	26
18.10.	0.138	10	37	27
19.10.	0.138	3	33	26
20.10.	0.128	12	42	26
21.10.	0.123	5	74	24

The high humidity with wind speed of 27 km/h during first days affects diurnal changes in the values of dose rates. These values decrease as humidity decreases in the coming days; somehow stable values of ambient dose equivalent rates are established. This was due to a gradual (from day to day) decrease of the wind speed and an increase in air temperature, which influence slightly increasing the dose equivalent rate.

Descriptive statistics of ambient dose equivalent rate for both, rural and urban site is presented in Table 3. Mean ambient dose equivalent rate in rural site (142 nSv/h) is higher than in urban site (128 nSv/h). Similar value for median, low values of standard deviation and skewness indicate normal distribution of results.

**Table 3.** Descriptive statistics of ambient dose equivalent rate measurements in rural and urban sites

Parameters	Rural site	Urban site
Minimum	125	110
Maximum	170	143
Mean	142	128
Median	143	125
Standard Deviation	12.9	9.7
Skewness	0.45	-0.18
Kurtosis	-0.20	-0.82

Apparently from Fig. 1, diurnal ambient dose equivalent rate for certain period is higher in the rural than in the urban site. In addition to the difference in altitude which may be reason of such results, the difference can also be due to the environment itself, including the composition of soil and

geological features, since rural site is located on the slope of the mountain Jastrebac.

A weak correlation was found between measurements in rural and urban sites; Pearson coefficient,  $r$  was 0.3. There is no correlation between ambient dose equivalent rate and any noted parameter (wind speed, moisture, temperature).

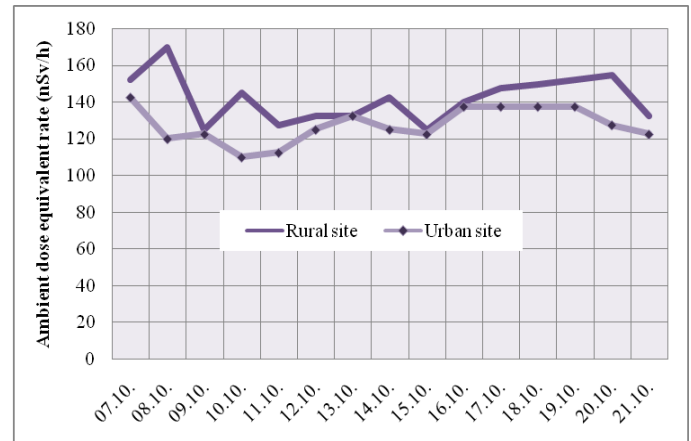


**Figure 1.** Values of ambient dose equivalent rates in test field during fifteen days of October 2017.

Obtained results are in good agreement with values of ambient dose equivalent rate measured in Republic of Serbia in 2015, which varied from 81 to 142 nSv/h (Serbian Radiation Protection and Nuclear Safety Agency, 2016). The range of ambient dose equivalent rate from this study (110-170 nSv/h) is comparable with other results obtained for specific sites of lead, cink and phosphate ores in Raška (70-150 nSv/h) and Bosilegrad (78-123 nSv/h) (Todorović et al., 2012).

In this study background radiation levels were preliminary registered in test field by measuring the ambient dose equivalent rates. The influences of weather conditions and spatial characteristics on obtained results were analyzed.

## CONCLUSION

Preliminary measurements of the ambient dose equivalent rates in test field showed that the mean value of the ambient dose equivalent rate during fifteen days in the urban site was always lower than in rural site. The reasons are the joint influences of weather variations in temperature, humidity, wind speed, precipitation, since these parameters are interrelated and interdependent and the exact influence of each parameter is not possible to determine. Also, the higher altitude of the rural site in comparison with urban, and the geographical location near hilly terrain may have impact on measured values of ambient dose equivalent rates.

The moisture influences variation in value of the ambient dose equivalent rate. Although an increasing of temperature, decreasing the moisture in air, and slowing down the wind speed during the observed period showed tendency of stability

the ambient dose equivalent rate, no correlation was found between ambient dose equivalent rate and any parameter (wind speed, moisture, temperature).

## ACKNOWLEDGMENTS

The paper is a part of the research done within the project no. III41028 supported by the Ministry of Education, Science and Technology Development of the Republic of Serbia and the project no. IJ01-17 supported by the Faculty of Natural Sciences and Mathematics, University of Priština, Kosovska Mitrovica. The author is grateful to Mrs. Danijela Aleksić for field work.

## REFERENCES

- Abba, H.T., Hassan, W.M.S.W., Saleh, M.A., Aliyu, A.S., & Ramli, A.T. 2017. Terrestrial gamma radiation dose (TGRD) levels in northern zone of Jos Plateau, Nigeria: Statistical relationship between dose rates and geological formations. *Radiation Physics and Chemistry*, 140, pp. 167-172. doi:10.1016/j.radphyschem.2017.01.023
- Bossew, P., Cinelli, G., Hernández-Ceballos, M., Cernohlawek, N., Gruber, V., Dehandschutter, B., . . . de Cort, M. 2017. Estimating the terrestrial gamma dose rate by decomposition of the ambient dose equivalent rate. *Journal of Environmental Radioactivity*, 166, pp. 296-308. doi:10.1016/j.jenvrad.2016.02.013
- Bouville, A. & Lowder W.M. 1988. Human population exposure to the cosmic radiation. *Radiation Protection Dosimetry*, 24, pp. 293-299. doi:10.1093/oxfordjournals.rpd.a080290
- Gulan, Lj., & Spasović, L. 2017. Outdoor and Indoor Ambient Dose Equivalent Rates in Berane Town, Montenegro. In RAD5 Proceeding of Fifth International Conference on radiation and applications in various fields of research. RAD Association. doi:10.21175/radproc.2017.28
- Lebedyte, M., Butkus, D., & Morkūnas, G. 2002. Variations of the ambient dose equivalent rate in the ground level air. *Journal of Environmental Radioactivity*, 64(1), pp. 45-57. doi:10.1016/s0265-931x(02)00057-7
- RADEX. 2017. Radiation Detector RD1503+. Retrieved from: <https://www.quarta-rad.ru/en/catalog/dozimetradiometr-radon/dozimetr-radex-rd1503/>.
- Sanusi, M.S.M., Ramli, A.T., Gabdo, H.T., Garba, N.N., Heryanshah, A., Wagiran, H., & Said, M.N. 2014. Isodose mapping of terrestrial gamma radiation dose rate of Selangor state, Kuala Lumpur and Putrajaya, Malaysia. *Journal of Environmental Radioactivity*, 135, pp. 67-74. doi:10.1016/j.jenvrad.2014.04.004
- Serbian Radiation Protection and Nuclear Safety Agency. 2016. Annual Report of population exposure to ionizing radiation in 2015. Belgrade, Republic of Serbia. in Serbian.
- Stojanovska, Z., Boev, B., Zunic, Z.S., Ivanova, K., Ristova, M., Tsenova, M., . . . Bossew, P. 2016. Variation of indoor radon concentration and ambient dose equivalent rate in different outdoor and indoor environments. *Radiation and Environmental Biophysics*, 55(2), pp. 171-183. doi:10.1007/s00411-016-0640-y
- Todorović, D.J., Janković, M.M., Nikolić, J.D., & Kosutić, D.D. 2012. Radioactivity of mining sites of lead, zinc and phosphate ores in Serbia. *Journal of Environmental Science and Health, Part A*, 47(6), pp. 812-817. doi:10.1080/10934529.2012.664992
- United Nations Scientific Committee on the Effects of Atomic Radiation (UNSCEAR). 2000. Sources and effects of ionizing radiation: Report to General Assembly with Scientific Annexes. New York.
- United Nations Scientific Committee on the Effects of Atomic Radiation (UNSCEAR). 2010. Sources and effects of ionizing radiation. Annex B: Exposure of the public and workers from various sources of radiation. New York.
- Vuckovic, B., Gulan, Lj., Milenkovic, B., Stajic, J.M., & Milic, G. 2016. Indoor radon and thoron concentrations in some towns of central and South Serbia. *Journal of Environmental Management*, 183, pp. 938-944. doi:10.1016/j.jenvman.2016.09.053
- Wang, Z. 2002. Natural radiation environment in China. *International Congress Series*, 1225, pp. 39-46. PII: S0531-5131(01)00548-9

# INFLUENCE OF METEOROLOGICAL PARAMETERS ON THE OPERATION OF A GRID - CONNECTED PV SOLAR PLANT

DRAGANA D. MILOSAVLJEVIĆ<sup>1\*</sup>

<sup>1</sup>Faculty of Science and Mathematics, University of Niš, Niš, Serbia

## ABSTRACT

Elementary description and information on a grid-connected photovoltaic solar power plant (PV plant) of 2 kW<sub>p</sub> installed in Niš and the influence of meteorological parameters on its operation are given in this paper. Besides, experimental results of the calculation of the energy efficiency, electrical energy generated and output power of this PV plant operating in the real climate conditions in 2017 are presented. The results regarding climate parameters and characteristic performance parameter of 2 kW<sub>p</sub> PV plant in Niš in 2017 are discussed and it was found that in 2017 annual energy efficiency of this PV plant was 10.63% and it decreased with the ambient temperature increasing.

**Keywords:** Solar radiation, Photovoltaic conversion, Photovoltaic solar power plant, Energy efficiency, Ambient temperature.

## INTRODUCTION

Right from the beginning the solar power, especially photovoltaic (PV), presents one of the most dominant renewable energy in the world. Solar energy, in particular, photovoltaic (PV) arrays, can fulfill all the electricity needs of mankind. PV systems have been used to supply electrical energy to the millions of people that do not have access to networks (Tobnaghi & Vafaei, 2016). Electric power supply to remoter households or villages is substantially application of PVs for many incoming years. Over the past two decades, installed off-grid and/or on-grid PV systems have shown their great potential (Pavlović et al., 2013). Number of installed PV systems has rapidly increased. Over recent years worldwide investment in the research of the PV conversion of solar radiation into electricity aiming at the production of high quality, cheap solar modules and other PV systems components has been increasing. Worldwide more and more companies, research and development centers and organizations are competing in research, promotion and production of the PV systems (Pavlović et al., 2015). Up to date worldwide several thousands of PV systems power of 1 kW to several hundreds of megawatts have been installed. The performance and operation of a PV system are dependent upon many site-specific factors such as geographical position, season, cloudiness, air pollution and especially ambient temperature (Shravanth et al., 2016). In this study the operation of a grid-connected PV plant installed at the Faculty of Science and Mathematics (FSM) in Niš, Republic of Serbia, were investigated, in particular with respect to the temperature effect. The findings of this study are expected to be useful information for energy yield prediction and loss analysis of the PV systems, especially in moderate continental climate regions.

## PHOTOVOLTAIC SOLAR POWER PLANT IN NIŠ

In October, 2012 on the roof of the FSM in Niš a grid-connected PV plant power of 2 kW<sub>p</sub>, was installed (Fig.1). The main components of this plant are solar modules, inverter, DC and AC distribution boxes and network connector. This PV plant consists of 10 solar modules made of monocrystalline silicon, single power of 200 W. Solar modules are fixed on the metal bracket, inclined at 32° towards the South, mounted on the roof of the Faculty and serial interconnected in a string. By appropriate conductors solar modules are connected to DC distribution box, single phase inverter power of 2 kW, AC distribution box and the city electrical network. At the output of AC distribution box there is AC voltage 230V, 50Hz (Milosavljević et al., 2015).



**Figure 1.** Solar modules inclined at 32° towards the South on the roof of the building in Niš.

For the remote diagnostics, monitoring and data acquisition of this PV plant, as central communication interface, *Sunny WEBBox* is used which is by *Bluetooth*- connected to the inverter

\* Corresponding author: dragana82nis@yahoo.com

and by sensor *Sunny SensorBox* oriented towards the South and tilted at the angle of 32° on the roof of the building.

Data on PV plant are each 5 minutes recorded in *WEBBox* where their acquisition is performed. This device enables continuous recording of the electrical parameters of PV plant into the internal memory. Additionally, numeric amounts of the electrical parameters of PV plant are directly recorded on *SD* memory card or by *FTP* server (Milosavljević et al., 2015; Milosavljević et al., 2016).

Inverter and additional equipment for the functioning and monitoring of PV plant are placed in the Solar Energy Laboratory, inside the Faculty (Fig.2).



**Figure 2.** Part of the PV plant inside the Laboratory.

The solar radiation intensity, solar energy, wind speed and the ambient temperature in Niš were measured by *Sunny SensorBox*. The *Sunny SensorBox* is connected with *Sunny WEBBox* through *SMA Power Injector with Bluetooth*. In combination with *Sunny WebBox*, it provides a continuous target-actual comparison of system performance (Milosavljević et al., 2015; Milosavljević et al., 2016).

## EXPERIMENT

Variations in the climate, ambient temperature and solar irradiation from month-to-month affect on the performance parameters and operation of PV plant. Therefore, it is very substantially to define which characteristic performance parameters are suitable for which system evaluations based on their weather and climate dependence (Pantić et al., 2016). One of the major causes for the decreased performance of modules is overheating. The efficiency of a solar cell declines by about 0.5% for every 1 degree Celsius increase in temperature. The most important parameter considered for the performance evaluation of the PV solar plant is the photovoltaic effective

conversion efficiency in operative conditions, which affects the electrical energy generation and thus the most valuable product of the component (Hamrouni et al., 2008).

The conversion efficiency of a photovoltaic solar cell or modul is the percentage of the solar energy exposing on a PV system that is converted into usable electricity. Energy efficiency of PV plant indicates a ratio of the electricity generated by PV plant at certain point of time and the solar energy falling on the solar modules at the same point of time (Milosavljević et al., 2015; Milosavljević et al., 2016).

Monthly energy efficiency of PV plant is calculated by means of the Eq. (1) (Chioncel et al., 2010; Attari. et al., 2016; <https://www.nrel.gov/docs/fy05osti/37358.pdf>; [http://www.irena.org/DocumentDownloads/events/2013/March/Palau/4\\_System\\_Design\\_Guidelines.pdf](http://www.irena.org/DocumentDownloads/events/2013/March/Palau/4_System_Design_Guidelines.pdf)):

$$\eta_M = \frac{\sum_{i=1}^n (E_D)_i}{S \cdot \sum_{i=1}^n (G_{opt})_i} \quad (1)$$

where  $n$  – is a number of days in a month,  $E_D$  – is a total amount of electricity generated by PV plant and transmitted to the network grid during the day (Wh),  $G_{opt}$  – is a total amount of energy of the global solar irradiation falling during the day on square meter of solar modules of PV plant (Wh/m<sup>2</sup>) and  $S$  – is a total solar modules surface (PV array area) (m<sup>2</sup>).

This experiment was performed in the Solar Energy Laboratory at the FSM in Niš. Experimental energy efficiency of PV plant is calculated by entering into the Eq. (1) measurement data of the daily amount of electrical energy produced by PV plant and measurement data of solar energy falling during the day on PV array area.

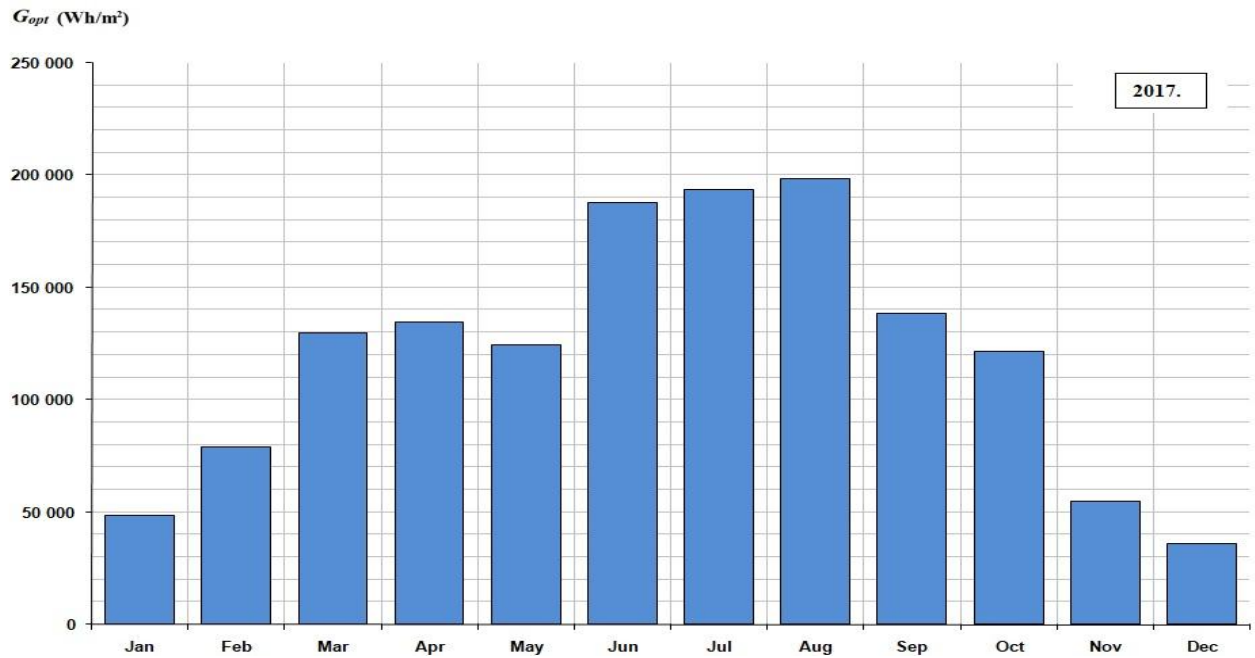
## RESULTS AND DISCUSSION

In this section the experimental measurement data of meteorological parameters and some characteristic performance parameter of the 2 kW<sub>p</sub> PV plant at FSM in Niš for the measured period from January 1, 2017 to January 1, 2018 are analyzed and discussed.

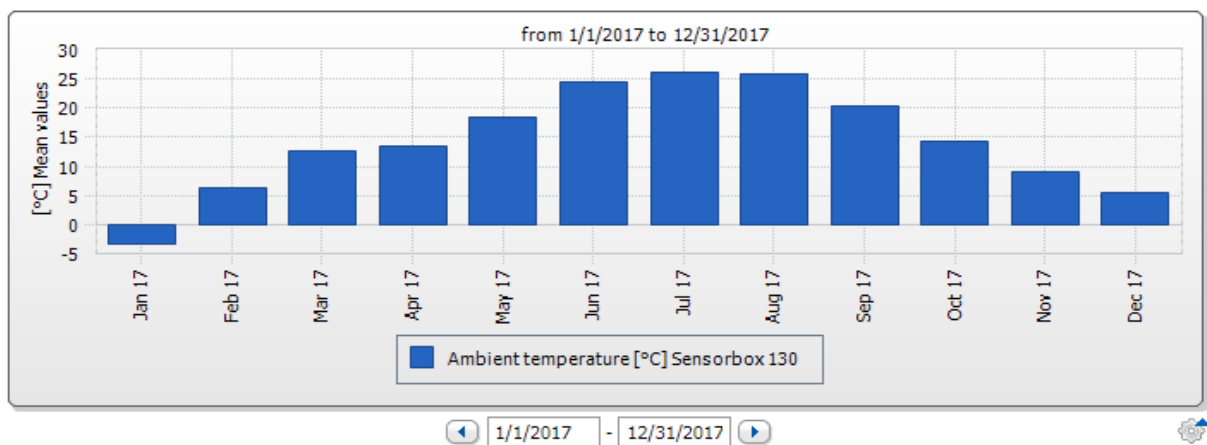
The change of the energy of solar radiation ( $G_{opt}$ ) falling on a square meter of the surface oriented southward, at the angle of 32° in relation to the horizontal surface, is presented in Figure 3.

Figure 3. shows that in 2017 montly values of the energy of solar radiation ( $G_{opt}$ ) falling on square meter of the surface inclined at 32° towards the South range from 35,67 kWh/m<sup>2</sup> (in December) to 198,33 kWh/m<sup>2</sup> (in August). It should be noted that from 20 to 27 May 2017, the device did not register solar radiation so that there were no measurements for that period.

The change of the average monthly values of ambient temperature  $T_{amb}$  (°C) and wind speed  $v$  (m/s), measured in Niš, in 2017 are presented in Figures 4 and 5, respectively.



**Figure 3.** The change of the energy of solar radiation ( $G_{opt}$ ) falling on a square meter of the surface oriented southward, at the angle of  $32^\circ$  in relation to the horizontal surface.



**Figure 4.** The change of the average monthly values of ambient temperature  $T_{amb}$  ( $^{\circ}\text{C}$ ), measured in Niš, in 2017.

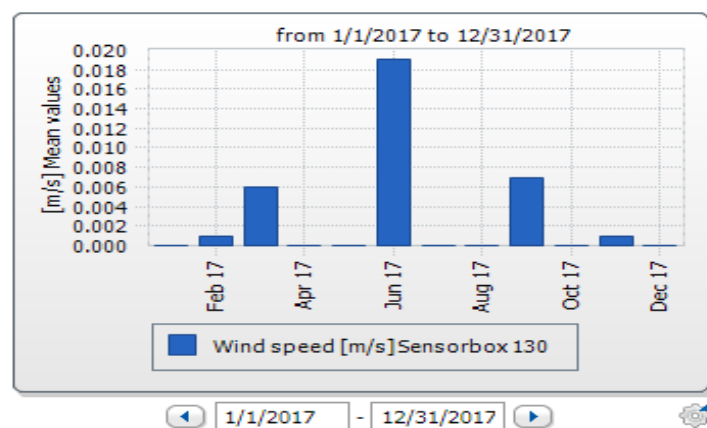


**Figure 5.** The change of the average monthly values of wind speed  $v$  ( $\text{m/s}$ ), measured in Niš, in 2017.

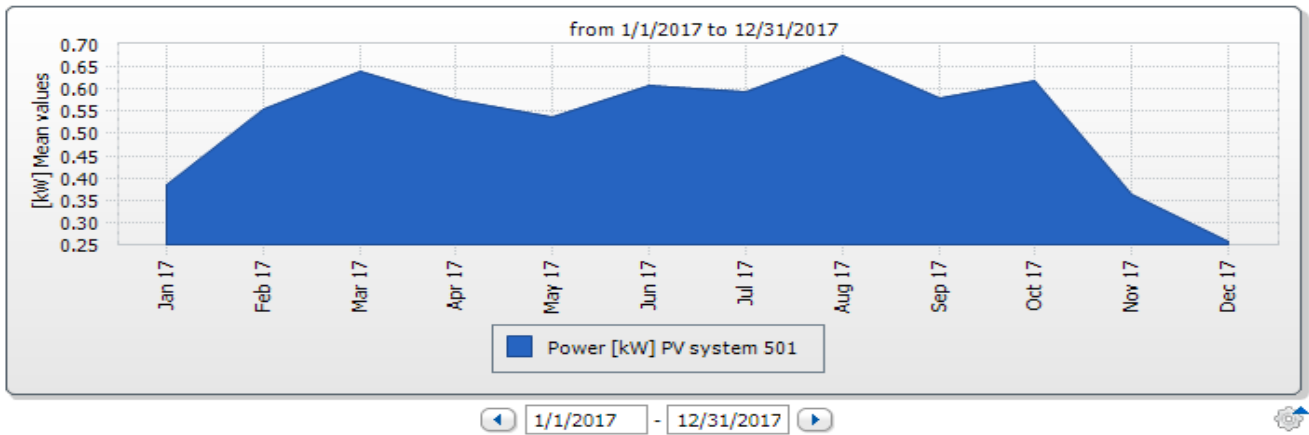


**Figure 6.** The change of the mean values of output power of PV solar plant of 2 kW<sub>p</sub>.

In 2017 average monthly values of the ambient temperature  $T_{amb}$  varied from the lowest value of -3.358°C in January to the highest value of 26.076°C in July. The average annual value of the ambient temperature is 14°C. In the same period average monthly values of the wind speed  $v$  range from 0.00 m/s to 0.019 m/s.

The change of the mean values of output power of PV solar plant of 2 kW<sub>p</sub> is presented in Figure 6.

Figure 6. shows that in 2017 average monthly values of the output power of PV plant of 2 kW<sub>p</sub>, varied from 0.258 kW (in December) to 0.675 kW (in August). The output power of solar modules strongly depends on solar irradiation falling upon their PV array area (Ayompe et al., 2011).

( $G_{opt}$ ) received by PV array area during the 2017, is presented in Figure 8.

The major changed by temperature was output voltage which reduces with the increased solar module temperatures. Decrease in output voltage affects the output power of solar module can not be generated effectively even there has increases of the output current. Furthermore, the efficient operation of solar modules and therefore PV plant also decreases with the increasing of solar module temperatures (Shiva & Sudhakar, 2015; Jahn & Nasse, 2004; Eltawil & Zhao, 2010).

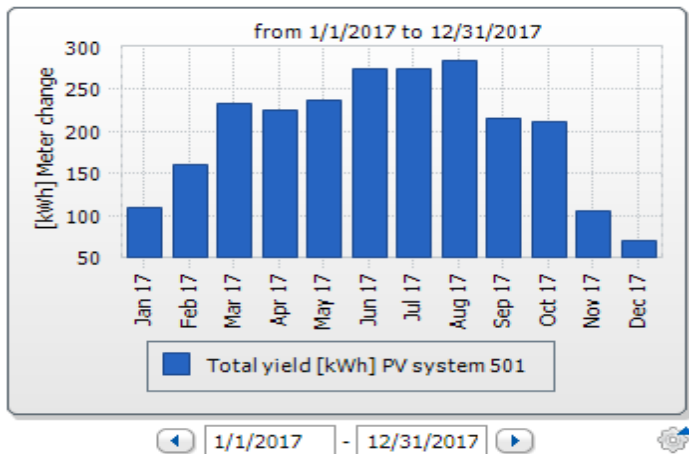


**Figure 7.** Total monthly amount of the electrical energy produced by PV plant of 2 kW<sub>p</sub> in 2017.

Total monthly amount of the electrical energy produced by PV plant of 2 kW<sub>p</sub> in 2017 is shown in Figure 7.

Figure 7. shows that the total monthly amounts of the electrical energy produced by PV plant of 2 kW<sub>p</sub> in 2017 varied from 69.415 kWh to 284.994 kWh.

Graphics of the changes in the experimental values for the total monthly amount of the electricity produced by PV plant ( $E$ ) depending on the measured monthly values of the solar energy

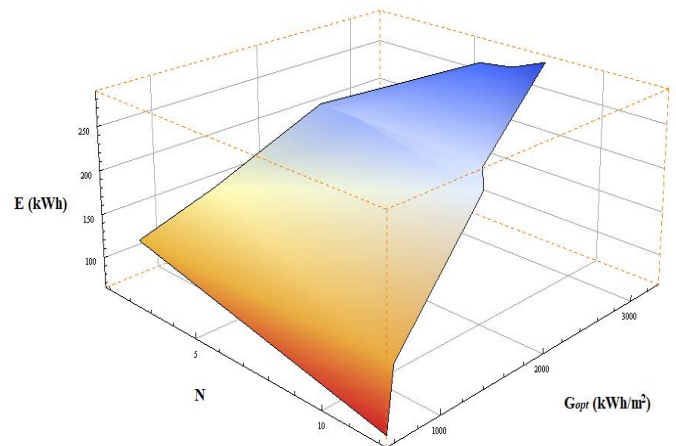


**Figure 8.** Graphics of the changes in the experimental values for the total monthly amount of the electricity produced by PV plant ( $E$ ) depending on the measured monthly values of the solar energy ( $G_{opt}$ ) received by PV array area during the 2017 ( $N$  is a number of the month in the year).

Graphics of the change of the monthly energy efficiency ( $\eta_M$ ) of PV solar plant of 2 kW<sub>p</sub> during the measured period is presented in Figure 9.

Figure 9. shows that the experimentally determined monthly values of the energy efficiency ( $\eta_M$ ) of PV plant varied from 8.53% (in July) to 13.74% (in January), in 2017. The temperature of solar module is increased with increase in solar

radiation level, as it starts increase above its rated temperature the efficiency goes on reducing. Consequently, the energy efficiency of PV plant is the lowest in the summer months.

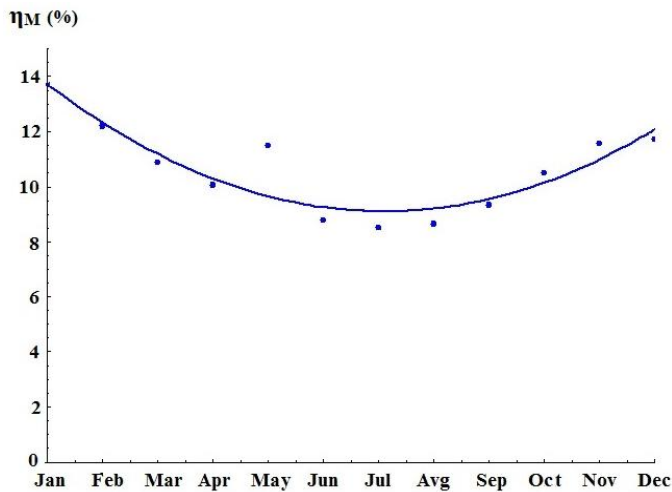


**Figure 9.** Graphics of the change of the monthly energy efficiency ( $\eta_M$ ) of PV solar plant of 2 kW<sub>p</sub> during the measured period.

Graphics of the monthly energy efficiency ( $\eta_M$ ) of PV plant depending on the measured ambient temperature ( $T_{amb}$ ), in 2017, is given in Figure 10.

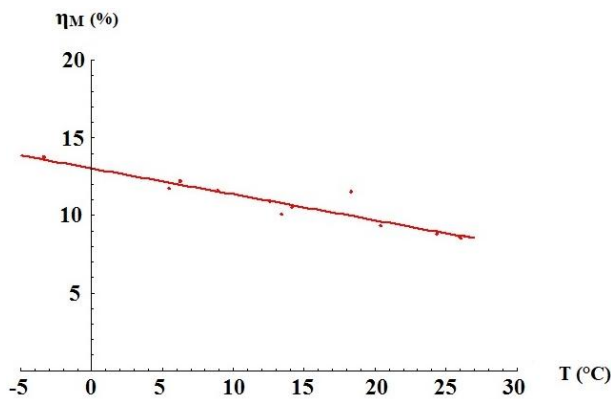


**Figure 10.** Graphics of the monthly energy efficiency ( $\eta_M$ ) of PV plant depending on the measured ambient temperature ( $T_{amb}$ ), in 2017.

Energy efficiency of PV plant linearly decreases with increasing the ambient temperature, as shown in Figure 10. Dependence of the energy efficiency of PV plant on the ambient temperature was obtained by a simple linear regression, based on the method of least squares. In this case, the characteristic regression equation is:

$$\eta_M = 13.0347 - 0.166909T_{amb} \quad (2)$$

where  $\eta_M$  – is the experimental energy efficiency of PV plant and  $T_{amb}$  – is the ambient temperature for the territory of the town of Niš obtained by continuous measurements.

In the Eq. (2) regression coefficient – 0.166909 represents *slope* in a regression model and it responds to the monthl average change of the expected value of dependent variable  $\eta_M$  for the unit change of the independent variable  $T_{amb}$ . Based on the data presented in Figure 10. one can notice that energy efficiency decreases by 0.17% with the increase in the ambient temperature for 1°C.

Graphics of the changes in the experimental values for the energy efficiency ( $\eta_M$ ) of PV plant depending on the measured values of the ambient temperature ( $T_{amb}$ ), and solar energy ( $G_{opt}$ ) received by its PV array area, is given in Figure 11.

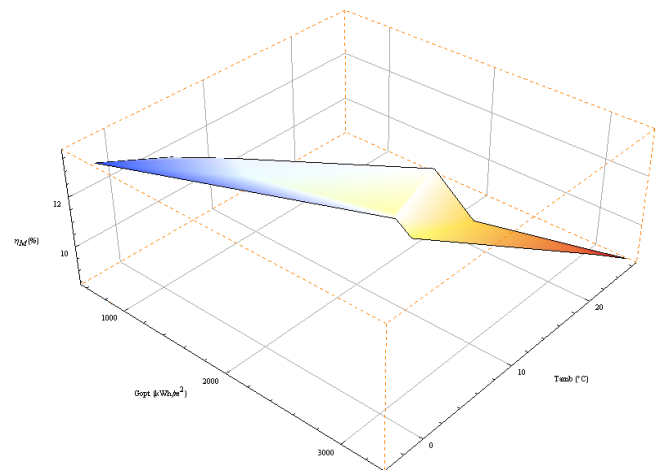


**Figure 11.** Graphics of the changes in the experimental values for the energy efficiency ( $\eta_M$ ) of PV plant depending on the measured values of the ambient temperature ( $T_{amb}$ ), and solar energy ( $G_{opt}$ ) received by its PV array area

The ambient and solar module temperature potential are conditioned by the solar radiation. High solar radiation induces the high ambient temperature. The solar module temperature increasing was due to higher insolation heating, low wind speed with the consequent low heat transferred from the module to the ambient. Accordingly, the energy efficiency ( $\eta_M$ ) of PV plant of 2 kW<sub>p</sub> decreased with the ambient temperature increasing, as can be seen in Figure 11.

## CONCLUSION

Based on the presented results for the measured period from January 1, 2017 to January 1, 2018 it can be concluded that variations in climate, solar radiation and ambient temperature influence on the performance parameters and PV plant operating. The total energy of solar radiation reaching a square meter of the plane oriented southward, at the angle of 32° in relation to the horizontal plane, for the whole measuremet period, was 1445,189 kWh/m<sup>2</sup> and PV plant has received of 23975.76 kWh/m<sup>2</sup> of solar radiation. PV plant of 2 kW<sub>p</sub> has generated 2400.01 kWh of electrical energy and its annual energy efficiency was 10.63%.

The ambient temperature is a very important factor in terms of solar module temperature. As the solar irradiation increased, temperature of solar module has also increased which is directly effect to solar module and therefore PV plant electrical efficiency to decrease. The ambient temperature increasing affects on the increasing of thermal vibration of cristal lattice atom of materials used to produce solar cells, which in turn impedes directed movement of free carriers of charging resultin in open circuit voltage decrease and solar cells power degradation. In this case, energy efficiency of PV plant of 2 kW<sub>p</sub> in Niš decreases by 0.17% for each 1°C increase in the ambient temperature.

## ACKNOWLEDGMENTS

This study was carried out in the framework of the project TR 33009 approved by the Ministry of Education and Science of the Republic of Serbia.

## REFERENCES

- Attari, K., Elyakoubi, A., & Asselman, A. 2016. Performance analysis and investigation of a grid-connected photovoltaic installation in Morocco. *Energy Reports*, 2, pp. 261-266. doi:10.1016/j.egy.2016.10.004
- Ayompe, L.M., Duffy, A., McCormack, S.J., & Conlon, M. 2011. Measured performance of a 1.72kW rooftop grid connected photovoltaic system in Ireland. *Energy Conversion and Management*, 52(2), pp. 816-825. doi:10.1016/j.enconman.2010.08.007
- Chioncel, C.P., & et al., 2010. Yield factors of a photovoltaic plant. *Acta Technica Corviniensis - Bulletin of Engineering*, . pp. 63-66.
- Eltawil, M.A., & Zhao, Z. 2010. Grid-connected photovoltaic power systems: Technical and potential problems: A review. *Renewable and Sustainable Energy Reviews*, 14(1), pp. 112-129. doi:10.1016/j.rser.2009.07.015
- Hamrouni, N., Jraidi, M., & Chérif, A. 2008. Solar radiation and ambient temperature effects on the performances of a PV pumping system. *Revue des Energies Renouvelables*, . 11 (1), pp. 95 – 106.
- Retrieved from: <https://www.nrel.gov/docs/fy05osti/37358.pdf>.
- Retrieved from: [http://www.irena.org/DocumentDownloads/events/2013/March/Palau/4\\_System\\_Design\\_Guidelines.pdf](http://www.irena.org/DocumentDownloads/events/2013/March/Palau/4_System_Design_Guidelines.pdf).
- Jahn, U., & Nasse, W. 2004. Operational performance of grid-connected PV systems on buildings in Germany. *Progress in Photovoltaics: Research and Applications*, 12(6), pp. 441-448. doi:10.1002/pip.550
- Milosavljević, D.D., Pavlović, T.M., & Piršl, D.S. 2015. Performance analysis of A grid-connected solar PV plant in Niš, Republic of Serbia. *Renewable and Sustainable Energy Reviews*, 44, pp. 423-435. doi:10.1016/j.rser.2014.12.031
- Milosavljević, D.D., Pavlović, T.M., Mirjanić, D.L., & Divnić, D. 2016. Photovoltaic solar plants in the Republic of Srpska - current state and perspectives. *Renewable and Sustainable Energy Reviews*, 62, pp. 546-560. doi:10.1016/j.rser.2016.04.077
- Pantic, L.S., Pavlović, T.M., Milosavljević, D.D., Radonjic, I.S., Radovic, M.K., & Sazhko, G. 2016. The assessment of different models to predict solar module temperature, output power and efficiency for Nis, Serbia. *Energy*, 109, pp. 38-48. doi:10.1016/j.energy.2016.04.090
- Pavlović, T.M., Tripanagnostopoulos, Y., Mirjanić, D.L., & Milosavljević, D.D. 2015. Solar Energy in Serbia, Greece and the Republic of Srpska. In *Monographs.Banja Luka: Academy of Sciences and Arts of the Republic of Srpska - Department of Natural-mathematical and Technical Sciences. Vol. XXVI, Vol. 26, ISBN:978-99938-21-70-0*.
- Pavlović, T., Milosavljević, D., Radonjić, I., Pantić, L., Radivojević, A., & Pavlović, M. 2013. Possibility of electricity generation using PV solar plants in Serbia. *Renewable and Sustainable Energy Reviews*, 20, pp. 201-218. doi:10.1016/j.rser.2012.11.070
- Shiva, K.B., & Sudhakar, K. 2015. Performance evaluation of 10 MW grid connected solar photovoltaic power plant in India. *Energy Reports*, 1, pp. 184-192. doi:10.1016/j.egy.2015.10.001
- Shravanth, V.M., Srinivasan, J., & Ramasesha, S.K. 2016. Performance of solar photovoltaic installations: Effect of seasonal variations. *Solar Energy*, 131, pp. 39-46. doi:10.1016/j.solener.2016.02.013
- Tobnaghi, D.M., & Vafaei, R. 2016. The impacts of grid-connected photovoltaic system on distribution networks - A review. *ARNP Journal of Engineering and Applied Sciences*, 11 (5), pp. 3564-3570.

CIP - Каталогизација у публикацији  
Народна библиотека Србије, Београд

5

**The UNIVERSITY thought.** Publication in natural sciences / editor in chief Nebojša Živić. - Vol. 3, no. 1 (1996)- . - Kosovska Mitrovica : University of Priština, 1996- (Kosovska Mitrovica : Art studio KM). - 29 cm

Polugodišnje. - Prekid u izlaženju od 1999-2015. god. - Je наставак: Универзитетска мисао. Природне науке = ISSN 0354-3951  
ISSN 1450-7226 = The University thought. Publication in natural sciences  
COBISS.SR-ID 138095623

#### Available Online

This journal is available online. Please visit <http://www.utnsjournal.pr.ac.rs> or <http://www.utnsjournal.com> to search and download published articles.